2008

Carbon conversion during bubbling fluidized bed gasification of biomass

Kevin Jay Timmer
Iowa State University

Carbon conversion during bubbling fluidized bed gasification of biomass

By

Kevin Jay Timmer

A dissertation submitted to the graduate faculty

in partial fulfillment of the requirements for the degree of

DOCTOR OF PHILOSOPHY

Co-majors: Mechanical Engineering; Biorenewable Resources and Technology

Program of Study Committee:
Robert C. Brown, Major Professor
Steven J. Hoff
Song-Charng Kong
Greg M. Maxwell
Brent H. Shanks

Iowa State University

Ames, Iowa

2008

TABLE OF CONTENTS

LIST OF FIGURES

LIST OF TABLES

NOMENCLATURE

a_s	surface area of the char per unit mass
A	pre-exponential factor
A_{fb}	cross-sectional area of the freeboard of the reactor
A_p	pre-exponential constant for primary pyrolysis
A_{pipe}	inner cross sectional area of the outlet pipe
A_{probe}	cross sectional area of the probe tip
A_s	pre-exponential constant for secondary pyrolysis
$A_{s,i}$	total surface area of particles in size interval i
$A_{s,particle}$	surface area of a char particle
AVS	apparent volume shrinkage
CEMs	continuous emission monitors
$\bar{d}_p$	hydrodynamic weighted average diameter
d_{pi}	average particle diameter for sieve interval i
dt	differential time
D	diameter of char particle
E	activation energy
ER	equivalence ratio
f	pyrolytic fixed carbon fraction
fc	fixed carbon
f_v	volatile mass fraction
F	pyrolytic fixed carbon feed rate
F(D,t)	instantaneous feed rate of char per unit size
F_i	mass feed rate of char into the reactor in size interval i
$\bar{h}_b$	enthalpy per mol of the biomass at STP

$\bar{h}_{pg}$	enthalpy per mol of producer gas at STP
k	reaction rate constant
k_e	carbon elutriation rate constant
k_r	gas-solid carbon chemical reaction rate constant
k_t	total fixed carbon removal rate constant
LHV	lower heating value
$m_{b,dry}$	mass of dry biomass injected into the reactor
$\dot{m}_{b,dry}$	dry biomass feed rate
$m_{C,b}$	mass of carbon entering the reactor with the biomass
$\dot{m}_{C,b}$	mass flow rate of biomass carbon into the reactor
$m_{C,e}$	mass of carbon elutriated as char
$m_{C,i}$	mass of gaseous carbon leaving the reactor with gas species i
$m_{C,gas}$	total mass of gaseous carbon emitted by the reactor during burnout
$m_{C,PMC}$	mass of carbon in the coarse particulate matter
$m_{C,PMF}$	mass of carbon in the fine particulate matter
$m_{C,thimble}$	mass of carbon collected in the thimble filter
m_i	mass of char in size interval i
$m_{particle}$	mass of a char particle
$M_{C,i}$	molecular weight of carbon in carbonaceous gas species i
n	number of size intervals in the population balance model
$n_{i,ave}$	average volume fraction of carbonaceous gas species i
$n_{N_2,a}$	volume fraction of N_2 in dry air at STP
$n_{N_2,pg}$	volume fraction of N_2 in dry producer gas at STP
$n_{N_2,p}$	average N_2 concentration in the products during Δt
Q_a	volumetric flow rate of fluidization air at STP
Q_{pg}	volumetric flow rate of producer gas at STP

Q_{probe}	volumetric flow rate in the isokinetic sample system
R	universal gas constant
R_e	pyrolytic fixed carbon elutriation rate
R_r	pyrolytic fixed carbon chemical reaction rate
R_t	total fixed carbon removal rate
STP	standard temperature and pressure
t	time
t_{ss}	time to reach steady state
T	temperature
T_{STP}	standard temperature
TDH(C)	transport disengagement height for coarse particles
TDH(F)	transport disengagement height for fine particles
U	superficial gas velocity
U_{fb}	superficial gas velocity in the freeboard of the reactor
U_{mf}	minimum fluidization velocity
$V_{particle}$	volume of a spherical char particle
V_{pg}	average producer gas velocity in the outlet pipe
W_{char}	mass of char in the reactor
W_C	mass of carbon in the reactor
x_i	mass fraction for sieve interval i
Δt	discrete time step
η_{cg}	cold gas efficiency
η_{fc}	pyrolytic fixed carbon conversion efficiency
η_{tc}	total carbon conversion efficiency
ρ	char density
ρ_b	biomass density

ρ_{CVC}	constant volume char density
ρ_{CM}	measured char density
$\bar{\upsilon}_{IG}$	molar specific volume for an ideal gas at STP
τ_p	time constant for decay of primary pyrolysis products
τ_s	time constant for decay of secondary pyrolysis products
$\lambda(D,t)$	instantaneous mass distribution of char

ACKNOWLEDGEMENTS

First and foremost, I thank and give praise to the sovereign God, the creator, sustainer, and redeemer of all things. The God who loves us and by his grace calls us to the meaning filled work of unfolding the mysteries of his creation for his glory and for the betterment of our neighbors and the rest of creation.

I also thank my family. I thank my immediate family: Karen my wife and our three daughters Ana, Sarah, and Katy. They are precious gifts which shower me with love, prayers, understanding, sacrifice, and support. I am also indebted to our extended family of parents and siblings for their prayers and encouragement. And to our church family at Trinity Christian Reformed Church in Ames for their friendship, love, prayers, and acts of kindness. They opened themselves to us and treated us like family, transforming a bearable situation into a blessing.

I owe much to Dr. Robert Brown and to his colleague Jerod Smeenk. I value their friendship and the opportunity to share in their accumulated wisdom. Dr. Brown unselfishly committed himself to me and my situation. He faithfully and insightfully guided me along a direct path toward successful conclusion of this project. Jerod's patient, day-to-day instruction and organized and well maintained laboratory environment enabled me to complete my work in a timely fashion.

My work also benefitted from diligent, competent, and responsible help in the laboratory. Fellow graduate student Nathan Nelson and laboratory associate Nicholas Sikes were always willing to help tackle equipment problems. Undergraduate assistants Karl Broer, Harrison Bucy, Mark Wright, and Nick Howard were assets in the lab, investing themselves in my research and success beyond what their wage required.

I am indebted to many others at ISU including Diane Love and the rest of the CSET staff for their support during my research and during these last months as I have worked at wrapping things up. I am thankful for the Biorenewable Resources and Technology interdepartmental graduate program and its supporting staff. The BRT programmed allowed me to take a broad spectrum of courses which was an ideal fit for me and my academic needs. I am also grateful to the members of my committee for their time and careful consideration.

I also want to thank Dordt College, Sioux Center, Iowa for granting me a leave of absence from my teaching position and for partially funding this adventure. I am indebted to my colleagues in the Dordt College Engineering Department. They have willingly made many sacrifices to accommodate me working on this project.

In addition to the support I received from Dordt College I am also grateful for financial assistance from other sources. This dissertation is based upon work supported by the Natural Resources Conservation Service, U. S. Department of Agriculture, under Agreement No. NRCS 68-3-475-3151; the U. S. Department of Energy, under Agreement No. DE-FC36-01G011091; and the ISU Foundation under the Bergles Professorship in Thermal Sciences at Iowa State University. Any opinions, findings, conclusions, or recommendations expressed herein are those of the author and do not necessarily reflect the views of the sponsors.

ABSTRACT

Gasification is one means of transforming biomass so that it can be more easily utilized as a renewable source of thermal energy, transportation fuel, and chemicals. Under typical gasification conditions it is not uncommon that a portion of the carbon entering with the biomass leaves the reactor unconverted as char. Understanding and improving carbon conversion during biomass gasification in an atmospheric bubbling fluidized bed reactor is the focus of this study.

To better understand the intricacies of biomass gasification a carbon conversion analytic methodology was developed. The methodology is based on a mass balance of the fixed carbon entering and leaving the gasifier. It allows fixed carbon leaving the reactor by elutriation to be distinguished from that which has been chemically converted. Carbon conversion analysis was applied to several steady state gasification experiments in a laboratory scale bubbling fluidized bed reactor utilizing ground seed corn as the feedstock. The impact on the gasification of ground seed corn was investigated for variations in the equivalence ratio, the gasification temperature, the superficial gas velocity, the biomass particle size, and the concentration of H_2O entering the reactor. Insights gleaned from these experiments suggest that carbon conversion during gasification of ground seed corn in a bubbling fluidized bed is limited by elutriation of char comminuted by either fragmentation or chemically assisted attrition. Consequently, increased carbon conversion was realized with reductions in the superficial gas velocity through the reactor.

1. INTRODUCTION

The goal of this research is to understand the mechanism of carbon conversion during bubbling fluidized bed gasification of biomass. To achieve this goal a carbon conversion analysis methodology is developed and applied to several gasification experiments which utilize ground seed corn as biomass. By focusing on the flow of fixed carbon into and out of the reactor the methodology assists in deciphering the complexities of biomass gasification.

Increasingly over the last twenty-five years there has been renewed interest in using biomass as a source for thermal energy, transportation fuel, and chemicals. Biomass can be converted to these various products by a number of means. Gasification represents one of these methods. Gasification is a thermochemical process which converts the organic material in biomass into a gas by subjecting it to elevated temperatures in an oxygen lean combustion environment. Under typical gasification conditions it is not uncommon that a portion of the carbon entering with the biomass leaves the reactor unconverted as a porous solid termed char. The presence of unconverted carbon in the exit stream of the gasifier is undesirable for a number of reasons. Understanding and improving carbon conversion during biomass gasification in bubbling fluidized bed reactors is focus of this study.

The basic concepts of fluidized bed gasification of biomass are introduced and a thermodynamic equilibrium analysis of the process is performed. The equilibrium analysis shows that carbon conversion is not limited thermodynamically at typical gasification conditions. To lay a foundation for further investigation a comprehensive picture of char and its processing in the reactor is constructed based on current literature. The carbon conversion efficiency during gasification is determined by the relative flow of solid carbon entering and leaving the reactor. Therefore, an analysis method based on a solid carbon mass flow balance through the reactor is developed to help sort through the complexities of biomass gasification and their implications for carbon conversion. This carbon conversion analysis technique allows solid carbon leaving the reactor due to chemical conversion to be distinguished from that leaving by elutriation. The technique is applied to several steady state gasification experiments. The experiments use ground seed corn as the feedstock and assess the influence of several key operating parameters on carbon conversion during fluidized bed gasification.

2. BACKGROUND

Gasification is a thermochemical process which converts biomass into a gas by subjecting it to elevated temperatures in an oxygen lean combustion environment. The thermal energy required to drive the gasification reactions can be provided from outside the gasifier but is often generated by combusting a portion of the biomass.

As biomass is heated in a fuel rich environment it goes through several stages of thermochemical conversion. Initially, as biomass temperatures increase moisture in the material is driven off. The biomass temperature can rise above 100°C only after drying is complete. At elevated temperatures a portion of the biomass begins to break down into volatile gases, which are released. Depending on the type of biomass, devolatilization may begin at temperatures as low as 225°C [1]. The devolatilization process is often referred to as pyrolysis although technically pyrolysis can only take place in an inert environment. The volatile gases include carbon monoxide (CO), carbon dioxide (CO_2), hydrogen (H_2), steam (H_2O), light hydrocarbons (such as methane (CH_4)) and condensable hydrocarbons, sometimes referred to as tar. The quantity of volatile gases released from the material depends on the composition of the biomass, the heating rate during pyrolysis, the final temperature and the time spent at that temperature as well as other factors. Typically, volatile material comprises 65 – 85% of the dry weight of plant based biomass as determined by a standard proximate analysis. Pyrolysis of biomass in a gasifier leaves behind a highly porous solid called char. Although rich in carbon, char also contains significant quantities of inorganic material, collectively called ash, and small amounts of hydrogen and oxygen. At sufficiently high temperatures the solid carbon (C_s) in the char can undergo the following gas-solid reactions:

Equation 1	$C_s + ½\ O_2 \Leftrightarrow CO$	Carbon-oxygen reaction
Equation 2	$C_s + CO_2 \Leftrightarrow 2CO$	Boudouard reaction
Equation 3	$C_s + H_2O \Leftrightarrow H_2 + CO$	Steam gasification
Equation 4	$C_s + 2H_2 \Leftrightarrow CH_4$	Hydrogenation reaction

The inorganic ash is all that remains after gasification and oxidation of the carbon in the char are complete.

Gasifier designs are diverse but most can be categorized as either updraft, downdraft, entrained flow, or fluidized bed. An introduction to updraft, downdraft, and entrained flow gasifiers is given in Reference [1]. Fluidized bed gasifiers are the subject of this work and are briefly described below.

A fluidized bed consists of a bed of particles that is fluidized by passing a sufficient amount of gas or liquid up through the particles. When the bed is fluidized the friction force caused by the gas flowing up between the particles in the bed balances the weight of the bed and the particles are suspended. The superficial gas velocity is defined as the volume flow rate of gas through the reactor divided by its cross sectional area. The minimum fluidization velocity, U_{mf}, is the minimum superficial gas velocity which still causes fluidization. This condition is referred to as minimum fluidization. A fluidized bed of solids behaves like a fluid in many respects. As flow is increased beyond that required to suspend the particles, the bed begins to bubble, churn, and mixed quite violently, resembling a boiling liquid. Operated at these conditions fluidized beds can have high rates of heat and mass transfer and are therefore utilized in many industries [2].

Fluidized bed gasifiers are typically blown by air, oxygen, steam, carbon dioxide, or some combination of these gases. Fluidized bed gasifiers are often further classified as bubbling, circulating, or turbulent based on the degree of entrainment of bed media in the gas downstream of the bed. Reference [3] provides a detailed introduction to the various types of gasifiers. Bubbling fluidized bed gasification is the focus of this study, although many of the insights gained may be applicable to the other technologies as well. The gas flow rate in a bubbling bed reactor, operated at typical gasification conditions, is often sufficient to cause violent mixing and splashing in the bed but, by definition, bed media is rarely carried out of the unit if sufficient freeboard is provided.

A bubbling fluidized bed gasifier is illustrated in Figure 1. As shown, the gasifier can be divided into three basic sections: plenum, bed, and freeboard. During operation a splash zone develops above the bed making it difficult to delineate a precise separation between the bed and the freeboard. The splash zone is often considered to be part of the freeboard. The

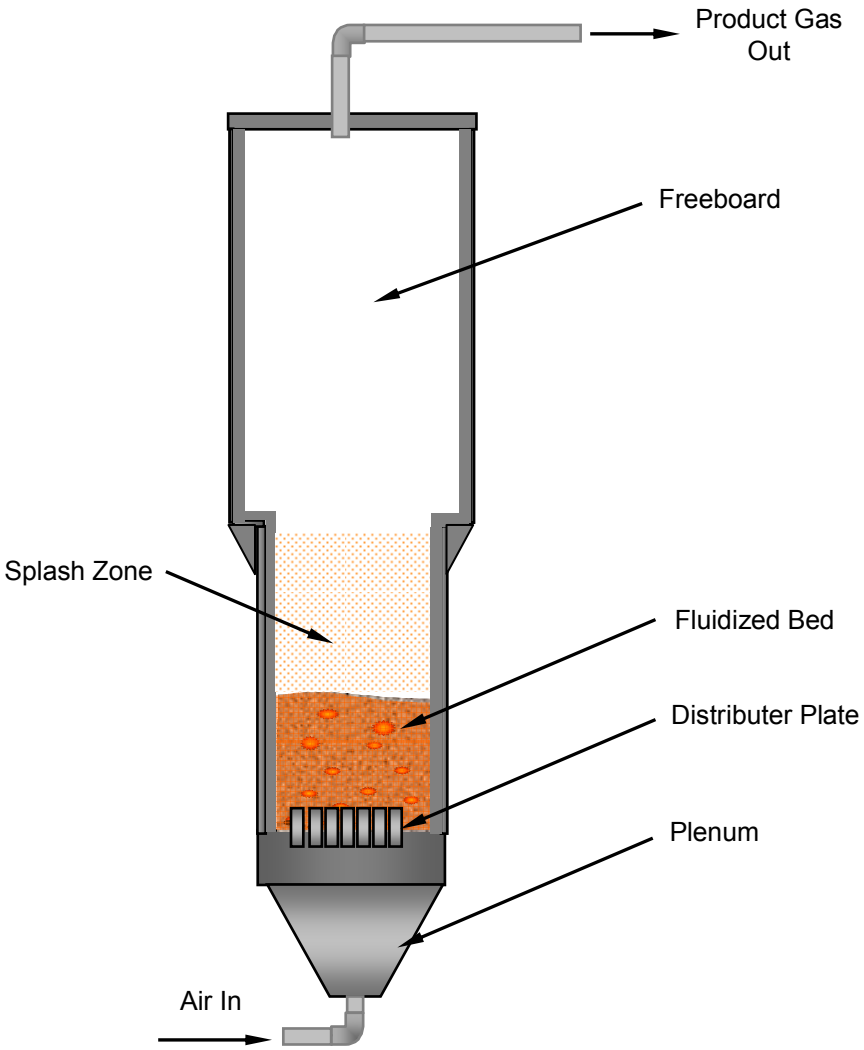

Figure 1. Fluidized bubbling bed gasifier

bed can consist of almost any particulate material that will fluidize (see Reference [4] for a classification of particles and their corresponding fluidization characteristics), but silica based sand is often used in biomass gasification. The freeboard section of a bubbling bed gasifier often has a larger diameter than the bed section, as shown in Figure 1, to decrease the average gas velocity, encouraging disengagement of any entrained particles.

Biomass can be fed at any point along the height of the reactor but is often introduced into the bed. Upon entering the hot gasifier bed the biomass undergoes very rapid drying and devolatilization. The remaining material, char, is subject to fragmentation, attrition, oxidation, and gasification, reducing the size of the char particles until they are small enough to be carried out of the reactor by the gas flow.

The production of char is undesirable in most gasification applications. Unconverted carbon that escapes the reactor as char represents a wasted resource and therefore a source of inefficiency. Additionally, many applications downstream of the gasifier are not able to accommodate particulate laden gas feeds and therefore require filtration equipment to remove the char. Once removed from the gas stream, char often becomes a waste stream that must be disposed of properly. Therefore, improving the carbon conversion can simultaneously improve the economics of gasification, reduces the size of filtration equipment, and decrease disposal demands. These factors, and no doubt others, motivate reducing the amount of char generated, or conversely, increasing the carbon conversion that takes place in the gasifier. The definition of what constitutes converted carbon varies in the literature. Some authors consider condensable hydrocarbons, referred to as tar, as converted while others do not. The focus of this study is on the formation and conversion of char carbon during gasification of biomass and therefore the carbon in tar is considered to be converted. The total carbon conversion efficiency is therefore defined as the percent of the carbon entering with the fuel that is converted to a carbonaceous gas, vapor, or aerosol. It is often easier to quantify the amount of carbon that leaves the reactor unconverted as a solid rather than trying to quantify carbonaceous vapors and aerosols. For this reason the total carbon conversion is calculated as:

Equation 5 $$\eta_{tc} = \frac{\left(m_{C,b} - m_{C,e}\right)}{m_{C,b}}$$

where

$m_{C,b}$ = mass of carbon entering with the biomass
$m_{C,e}$ = mass of carbon elutriated as char

Understanding and improving carbon conversion during biomass gasification in an atmospheric pressure, bubbling fluidized bed, while maintaining or improving the chemical quality of the produced gas, is the primary goal of this research.

Biomass gasification is fundamentally a thermochemical transformation. As such, the products of biomass gasification will reach thermodynamic equilibrium concentrations if given sufficient time at operating conditions. Therefore, equilibrium thermodynamics was used to determine the theoretical maximum carbon conversion achievable at typical biomass gasification conditions and to better understand what factors most significantly affect this maximum.

2.1. Equilibrium Carbon Conversion

Thermodynamic equilibrium calculations for biomass gasification have been performed by several authors [5-11]. This study used the thermodynamic equilibrium software STANJAN [12]. Given the molar fractions of C, H, O, and N entering with the biomass and air, STANJAN calculates the equilibrium concentrations of the resulting products, including solid carbon, based on the minimization of the Gibbs free energy for the specified temperature. Results from STANJAN calculations were compared to equilibrium values generated by Desrosiers [11] and were in good agreement.

The equilibrium carbon conversion on a percent basis is calculated using STANJAN results for gasification of generic biomass ($CH_{1.4}O_{0.6}$) at four temperatures and is shown in Figure 2 as a function of the equivalence ratio (ER). The equivalence ratio is defined as the ratio of the actual oxygen-to-fuel ratio divided by the stoichiometric oxygen-to-fuel ratio for theoretical combustion:

Equation 6
$$ER = \frac{\left(\text{Mass of } O_2 / \text{Mass of Fuel}\right)_{\text{actual}}}{\left(\text{Mass of } O_2 / \text{Mass of Fuel}\right)_{\text{stoichiometric}}}$$

By this definition an ER < 1.0 means that less oxygen than is required to completely oxidize the fuel is provided. As shown in the figure thermodynamic equilibrium predicts increased carbon conversion with increasing temperature and equivalence ratio. It is interesting to note that at lower temperatures and/or equivalence ratios the theoretical maximum carbon conversion is significantly less than 100%. However, at typical gasification conditions (ER = 0.2 – 0.35, T = 700°C - 900°C) complete carbon conversion is thermodynamically possible.

STANJAN was also used to assess the impact on the carbon conversion of changing the amount of water and carbon dioxide entering the gasifier. Figure 3 illustrates these affects for a constant equivalence ratio of 0.3 and gasification temperature of 630°C. Clearly thermodynamic equilibrium predicts improved carbon conversion with increases in either the water or carbon dioxide inlet concentrations but the affect is more dramatic in the case of water. The thermodynamic equilibrium constant for steam gasification (Equation 3) is larger than for CO_2 gasification (Equation 2) at 630°C. Therefore, for a given increase in concentration, H_2O will affect a larger change in the carbon conversion than will CO_2. This is consistent with the trends shown in Figure 3.

Summarizing, thermodynamic equilibrium calculations predict solid carbon in the products of biomass gasification at low temperatures and ER values but at typical gasification conditions (ER = 0.2 – 0.35, T = 700°C - 900°C), solid carbon is not an equilibrium product. The calculations also suggest that actual gasification of solid carbon might be improved with increases in: the equivalence ratio, the gasification temperature, the amount of water entering the gasifier, or the amount of carbon dioxide fed to the gasifier. In the next section the behavior predicted by thermodynamics is compared to published experimental data.

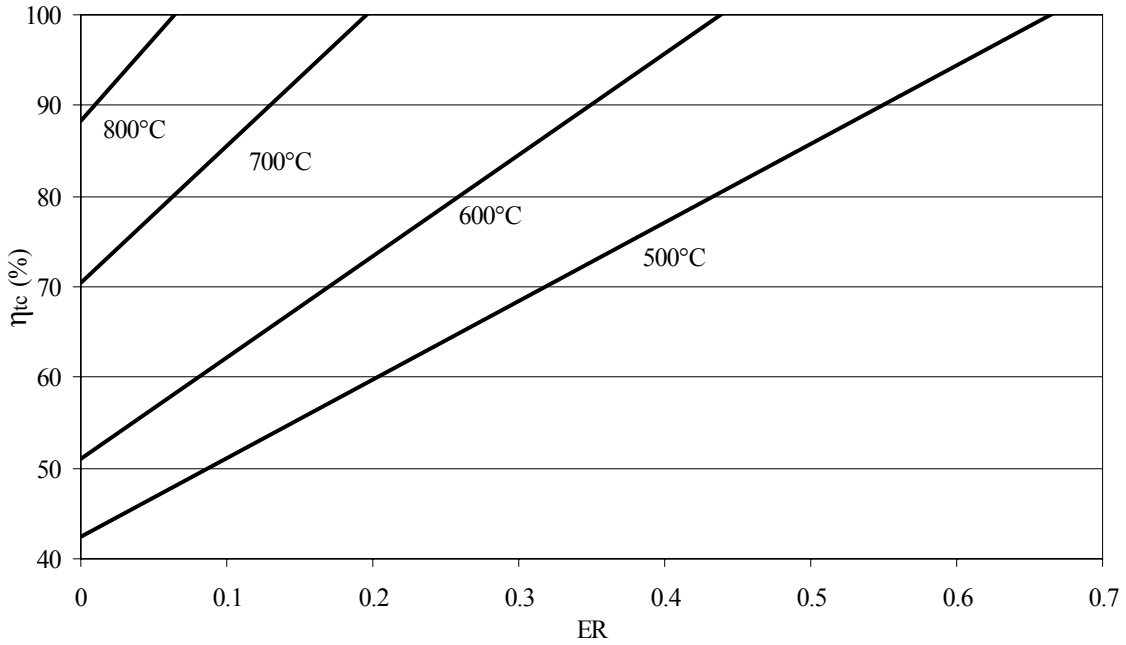

Figure 2. Equilibrium carbon conversion as a function of temperature and equivalence ratio for $CH_{1.4}O_{0.6}$ biomass with 12 wt% moisture on a dry basis, gasified in air

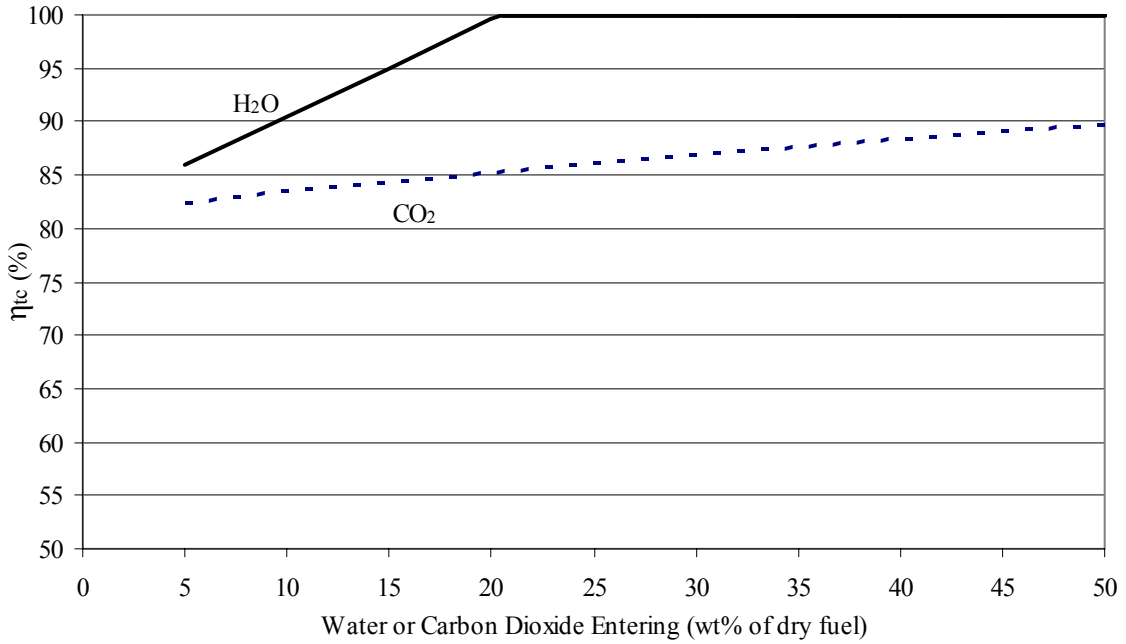

Figure 3. Equilibrium carbon conversion as a function of wt% of H_2O or CO_2 entering the reactor during gasification of $CH_{1.4}O_{0.6}$ biomass at T = 630°C and ER = 0.3

2.2. Non-equilibrium Gasification

Thermodynamic equilibrium calculations are useful for identifying trends in gasification behavior but the products of real biomass gasification fall short of reaching equilibrium. Table 1 makes this point by comparing experimental data [13] to STANJAN equilibrium calculations for the gasification of switchgrass in air. As shown in the table, thermodynamic equilibrium predicts lower N_2 concentrations then measured experimentally. The calculated N_2 concentration is lower in part because at equilibrium all of the solid carbon and tar vapor is converted to gas, while experimentally, solid carbon and tar remain unconverted in the product stream. With less carbon in the gas phase the relative concentration of N_2 is higher.

The predicted quantity of CO is higher, while CO_2 is somewhat lower than the measured values. This difference is once again substantially attributed to the presence of solid carbon and tar in the reactor exit stream. Given sufficient time at the reaction conditions the tar would be cracked to lighter molecules and the solid carbon in the experimental gas stream would be gasified according to Equation 2 and Equation 3. Both reaction produce CO and reaction Equation 2 consumes CO_2, consistent with the observed differences between equilibrium and experimental concentrations.

Table 1. Comparison of switchgrass gasification products to STANJAN thermodynamic equilibrium calculations, experimental data from Reference [13]

Product Stream Constituent	Equilibrium (% vol/vol dry)	700 °C, ER = 0.30 (% vol/vol dry)[a]
N_2	39.2	48.2
H_2	24.4	10.4
CO_2	13.0	15.2
CO	23.2	17.1
CH_4	0.3	5.4
C_2H_4	0.0	1.8
C_s	0.0	1.9
Tar	0.0	1.1[b]

[a] C_s and Tar are given as wt % of the dry product stream

[b] estimated from similar experiments

The lower than predicted experimental H_2 concentrations are significantly explained by the high concentration of CH_4 present in the product stream of the gasifier. Given sufficient time at 700°C CH_4 will dissociate as Equation 4 proceeds in the reverse direction. Hydrogenation to form methane, the forward reaction of Equation 4, is exothermic and is favored at lower temperatures. At 700°C the dissociation of CH_4 happens very slowly. Therefore methane is very stable at these temperatures and the quantity present in the gasification product stream is often considered to be comparable to that released from the biomass during devolatilization [7, 14].

Even though thermodynamic equilibrium is unable to accurately predict the products of actual biomass gasification, it is useful for identifying potential ways of improving carbon conversion. These means of improving carbon conversion, namely: increasing ER, the gasification temperature, or the quantity of H_2O or CO_2 entering the gasifier, are considered in light of published experimental data in the following discussion.

2.2.1. Carbon conversion as a function of equivalence ratio

Thermodynamic equilibrium calculations predict significant increases in the carbon conversion with increases in the equivalence ratio as shown in Figure 2. Experimental work [7, 14-20] supports this trend but carbon conversion is lower than predicted. Published η_{tc} vs. ER data for air or air/steam blown bubbling and circulating fluidized beds [7, 14-18] is presented in Figure 4. There is considerable scatter in the data due to variations in biomass type and operating conditions within and between the data sets as well as experimental uncertainty in the measurements themselves. However, it is clear that experimental carbon conversion values are below equilibrium predictions. The experimentally measured carbon conversions are not reaching equilibrium because the gasification reactions (Equation 2 and Equation 3) happen too slowly for the products to reach equilibrium before exiting the reactor. By contrast the carbon-oxygen reaction (Equation 1), which is five orders of magnitude faster than the gasification reactions, has sufficient time to react, causing noticeable improvements in η_{tc} for modest changes in ER as shown in Figure 4.

As Figure 4 demonstrates, increasing the equivalence ratio is a proven path to higher carbon conversion. However, the quality of the produced gas is negatively impacted by

increases in ER. Using thermodynamic equilibrium calculations, Desrosiers [11] predicts that the lower heating value (LHV) of the produced gas will decrease with increases in the equivalence ratio for biomass gasification in air. Dilution by N_2 combined with further oxidation of the combustible gases as the ER increases are responsible for this decrease. Published experimental data [15, 16, 21] support this conclusion as can be seen in Figure 5. The cold gas efficiency is one means of evaluating the effectiveness of the gasification process. It is calculated by dividing the enthalpy content of the produced gas at standard conditions (which implies that the condensable hydrocarbons have been removed) by the enthalpy entering with the biomass:

Equation 7 $$\eta_{cg} = \frac{\overline{h}_{pg}}{\overline{h}_{b}}$$

where

$\overline{h}_{pg}$ = enthalpy per mol of producer gas at standard conditions

$\overline{h}_{b}$ = enthalpy per mol of the biomass at standard conditions

Gasifying with air Li *et al.* [7] showed that thermodynamic equilibrium predicts a maximum cold gas efficiency at equivalence ratios between 0.18 and 0.25, depending on the gasification temperature. However, experimentally the authors saw the cold gas efficiency peak between ER values of 0.25 – 0.35 [7]. A maximum in cold gas efficiency is expected because at low ER values some solid carbon is present at equilibrium. As the ER is increased the solid carbon is transformed to CO gas. The chemical energy added to the product gas by the additional CO is large enough to offset the diluting effect of the increased N_2 volume realized with increased ER, resulting in a net increase in the cold gas efficiency. However, once all the solid carbon has been converted, N_2 dilution combined with progressive oxidation of the product gas stream erode the chemical energy content of the gas, leading to lower cold gas efficiencies. Experimentally the cold gas efficiency peak has been shown to occur at higher ER values than predicted by thermodynamic equilibrium [7]. This shift is due to the presence of tar, a non-equilibrium product, and solid carbon at higher ER values than predicted by equilibrium. The on-going conversion of tar and solid carbon into energetic gas species tends to delay the measured occurrence of the cold gas efficiency peak to higher ER values. The maximum thermodynamic cold gas efficiency occurs at the

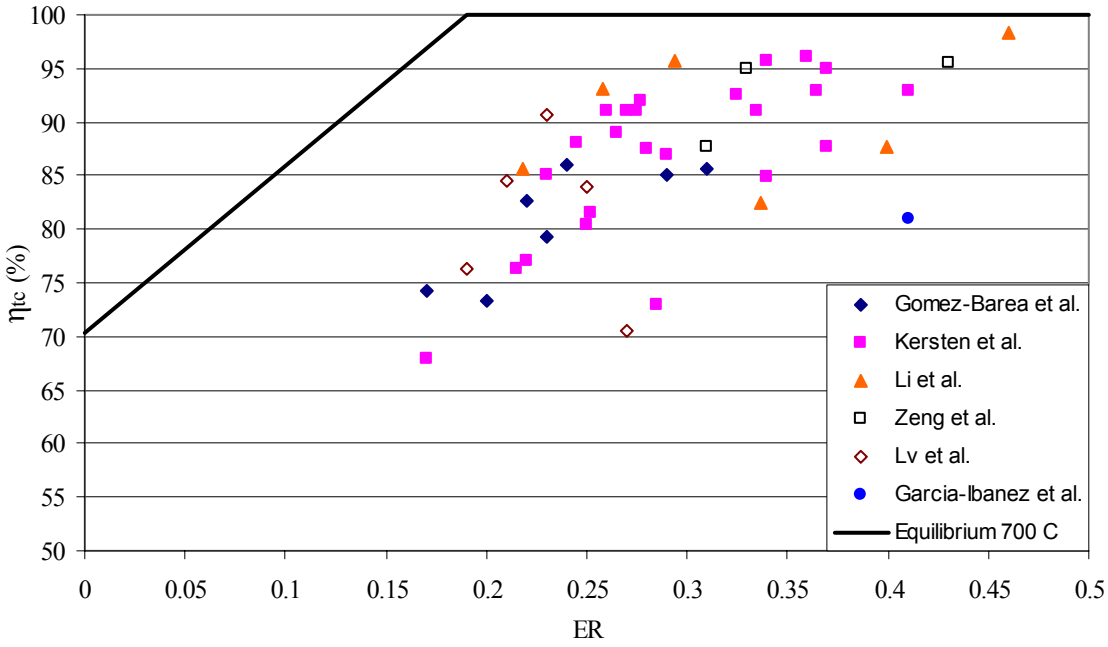

Figure 4. Carbon conversion as a function of the equivalence ratio for published experimental gasification data [7, 14-18]

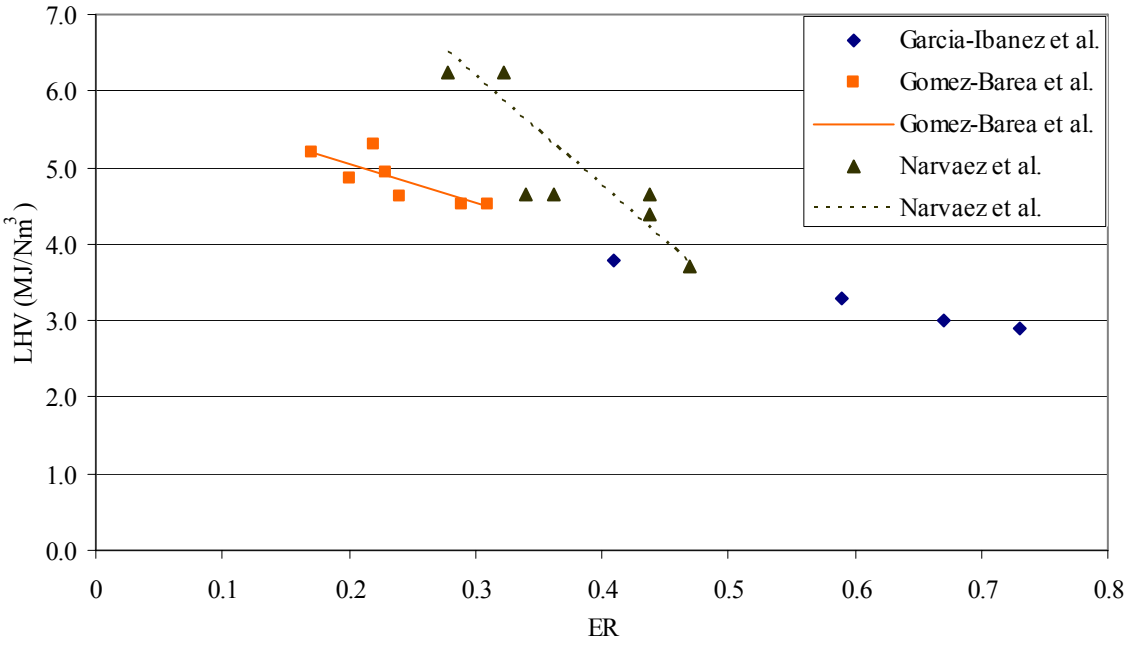

Figure 5. LHV of producer gas as a function of the equivalence ratio for published experimental gasification data [15, 16, 21]

equivalence ratio where solid carbon is completely consumed. By contrast, tar and solid carbon remain in the product gas stream of actual gasification at ER values well beyond the measured peak in cold gas efficiency. At equivalence ratios above the measured optimum the diluting affect of nitrogen, which enters with the gasification air, offsets any additional gain in carbon conversion.

Clearly, if maximizing the cold gas efficiency or the LHV of the produced gas is the objective of the gasification process than increasing the ER beyond a certain value may be undesirable even if carbon conversion is improved. There may, however, be some applications in which the total enthalpy, chemical as well as sensible, of the produced gas is recovered. In these situations it may be desirable to operate at higher equivalence ratios, which would tend to increase the carbon conversion and decrease the tar concentration, while the total energy content of the gas remained essentially the same.

2.2.2. Carbon conversion as a function of temperature

Although thermodynamic equilibrium predicts a dramatic increase in carbon conversion with temperature (see Figure 2), experimental gasification data [7, 13, 14, 16, 18, 19, 22-26] for a variety of biomass fuels and gasification conditions do not show this same strong trend. Figure 6 displays a portion of this data [7, 13, 14, 16, 18, 23, 24] which reports carbon conversion consistent with the definition that is used in this document and for air or air/steam blown bubbling or circulating fluidized beds with ER values below 0.4. Despite the scatter in the data it is clear that over the temperature range shown, carbon conversion for the gasification process as a whole is a surprisingly weak function of temperature.

A chemical reaction rate's dependence on temperature is accounted for through the use of a reaction rate constant, k(T), which is generally assumed to follow the Arrhenius equation:

Equation 8 $$k(T) = A \cdot \exp(-E/RT)$$

where

k = reaction rate constant
A = pre-exponential factor
E = activation energy

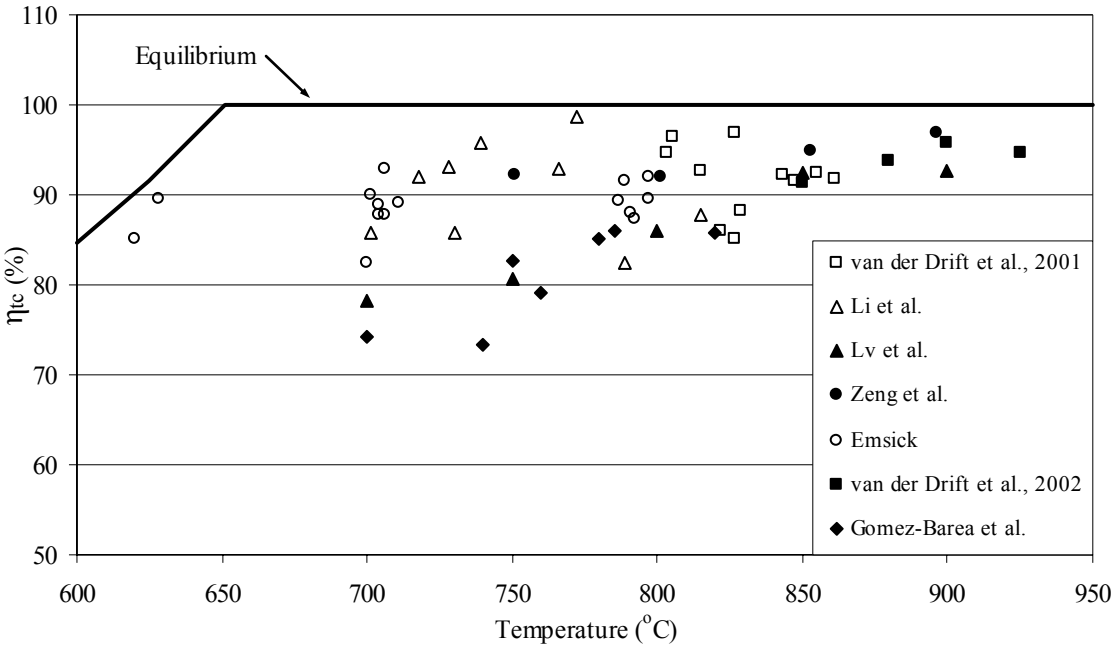

Figure 6. Comparison between equilibrium and experimental carbon conversion as a function of temperature during biomass gasification [7, 13, 14, 16, 18, 23, 24]

R = gas constant
T = absolute temperature

Therefore if carbon conversion is being limited by chemical reaction rates then an exponential dependence on temperature is expected. The temperature dependence illustrated in Figure 6 suggests that carbon conversion is not limited by chemical kinetics.

2.2.3. Carbon conversion as a function of water input

The role of water or steam in the gasification of biomass has received significant research attention [7, 11, 17, 18, 21, 22, 25-37]. Experimental conditions, while analyzing the effects of the quantity of water entering the gasifier, are quite varied between data sets, making direct comparison between results difficult. A partial list of methodologies include gasifying with: only steam; a mixture of steam and air; a mixture of steam and oxygen; feeding fuel with a range of moisture content; and injecting steam, saturated or superheated into the reactor. With this wide diversity of methods it is not surprising that there is little agreement between data sets.

Two driving forces for exploring steam in gasification are steam reforming of tars and enhancement of H_2 concentrations in the producer gas as a result of the water-gas shift reaction (Equation 12). Because of this focus few authors report the response of carbon conversion to changes in the steam concentration in the gasifier. However, Gil *et al.* [26] found that increasing moisture in a steam/O_2 blown circulating fluidized bed gasifier from a molar ratio (H_2O/O_2) of 2 up to a value of 3 only slightly decreased the char yield as shown by comparing the two curves in Figure 7. The lack of significant improvement is particularly clear when the scatter in the data is considered. The weak influence of water concentration on the gasification of biomass is supported by the work of others. Kersten *et al.* [17] give carbon conversion results for a circulating fluidized bed as a function of the H/C ratio. Their carbon conversion measurements, which do not consider tar as being converted, are reproduced in Figure 8. The H/C ratio takes into account the hydrogen that enters with the biomass, biomass moisture, and any added steam. The authors [17] conclude that little or no improvement in the carbon conversion occurs with the addition of steam to the reactor. Assuming that the mass fraction of carbon in the char remains relatively constant over the data set Figure 7, the decreasing char yield corresponds to increasing carbon conversion. The figure plots char yield as a function of the (H_2O+O_2)/biomass (kg/kg dry ash free (daf)) ratio. Moving to the right on this graph corresponds to increases in the amount of H_2O in the reactor but also to increases in the ER. The char yield is shown to significantly decrease as the (H_2O+O_2)/biomass ratio is increased. Given the weak dependence of char yield on the H_2O/O_2 molar ratio demonstrated by comparing the two curves of Figure 7 and shown in Figure 8, the decrease in char yield with higher (H_2O+O_2)/biomass ratios is likely due to the increase in the O_2 concentration rather than the H_2O. Decreased char yield, which corresponds to an increase in the carbon conversion, with increases in O_2 concentration, which corresponds to increased ER values, is demonstrated in Figure 4.

While steam's impact on the carbon conversion seems weak, there is general agreement that increasing moisture levels above low initial concentrations in the gasifier decreases the tar concentration in the producer gas [21, 22, 26, 32].

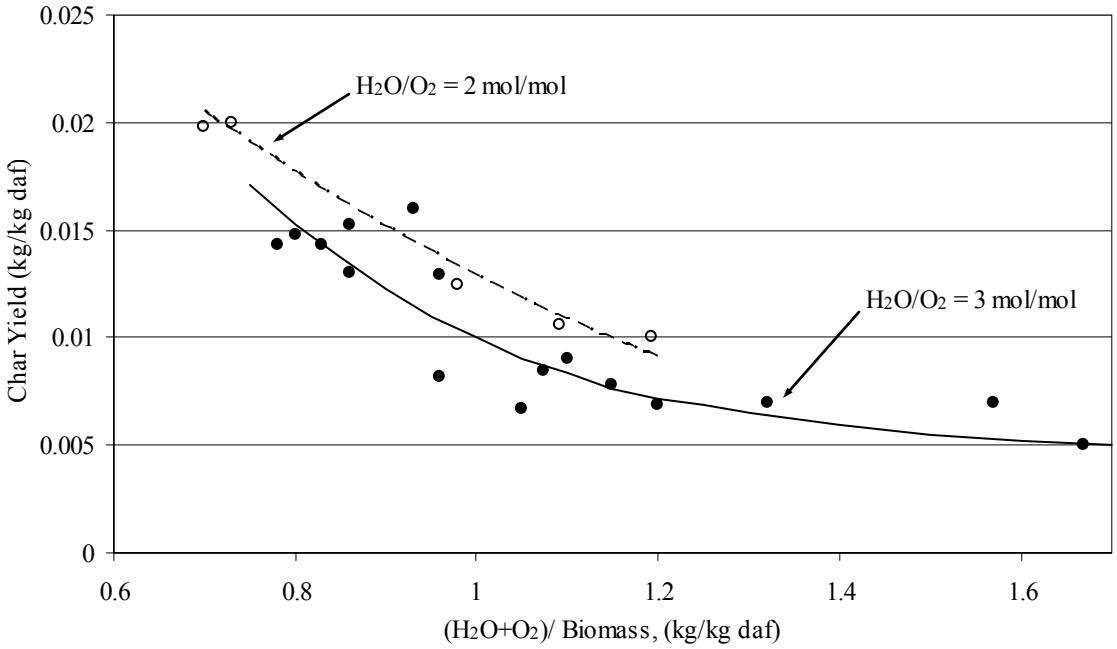

Figure 7. Char yield as a function of (H_2O+O_2)/Biomass ratio during gasification [26]

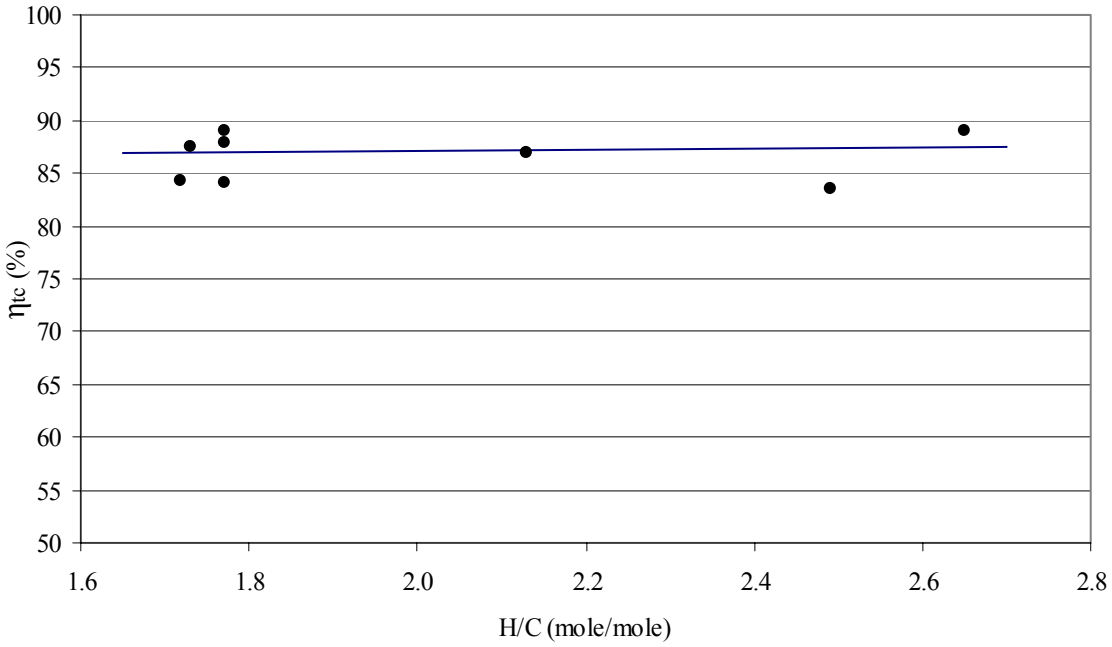

Figure 8. Carbon conversion as a function of the H/C ratio during biomass gasification in a circulating fluidized bed [17]

2.2.4. Carbon conversion as a function of carbon dioxide concentration

Thermodynamic equilibrium predicts increased carbon conversion with increases in the carbon dioxide concentration as shown in Figure 3. Experimental work [30, 35-37] suggests that, while CO_2 can act as a gasification reactant to reduce char, it is 4 – 100 times slower than gasification with water at typical gasification temperatures. This coupled with the fact that any un-reacted carbon dioxide acts as a diluent to the producer gas, has led most researchers to conclude that steam gasification holds more promise for improving carbon conversion than does carbon dioxide gasification. Published data showing carbon conversion as a function of the CO_2 concentration entering the gasifier was not found.

2.2.5. Summary

These comparisons have shown that the products of typical bubbling and circulating fluidized bed biomass gasification are not at thermodynamic equilibrium when blown with air, air/steam, or steam/O_2. Thermodynamic equilibrium gasification calculations gave some direction to potential avenues of increased carbon conversion but it is clear from experimentation that increased carbon conversion is more difficult to achieve than implied by thermodynamics. In particular, it was noted that although increasing the ER may lead to significant increases in the carbon conversion, it also decreases the quality of the produced gas as ER values rise beyond an optimum level. The experimental η_{tc} vs. gasification temperature data revealed that the overall carbon conversion process in the gasifier is not limited by chemical kinetics, depending only weakly on temperature. Evidence that increasing the water concentrations in the gasifier may yield improved carbon conversion was also given but the potential gains appear small. Finally, it was reported that carbon dioxide gasification, which is slower than steam gasification at typical operating conditions, has not been considered a viable means of improving carbon conversion.

While many authors report carbon conversion response to varied operating conditions, few explore underlying explanations for the behavior. Therefore a better understanding of what is actually limiting carbon conversion in biomass gasification may facilitate efforts to improve it. To that end, the following section unfolds the details of biomass gasification as they are currently understood to occur in a bubbling fluidized bed gasifier.

2.3. Chemical Conversion and Transport of Char through a Fluidized Gasifier

The following discussion, based on current literature, tracks a typical biomass particle as it makes its way through the fluidized bed gasification process, a process that is complex and not well understood. The discussion begins with a description of the relevant characteristics of the biomass and finishes with the ultimate fate of the biomass material.

2.3.1. Biomass composition

The composition of the biomass is critical to understanding its behavior in gasification. There are primarily three means of assessing biomass composition of interest for gasification: proximate analysis, ultimate analysis, and an organic compound analysis. Each analytical description of biomass approaches the material from a unique perspective and yields insights that are useful for understanding its gasification. Brown [1] provides tables that summarize the results of these characterizations for a number of biomass materials.

Proximate analysis partitions biomass into three mass fractions: volatile matter, fixed carbon, and ash. As dry biomass is heated it will begin to break down and evolve gases. Performed under ASTM prescribed conditions, the mass fraction of this evolved gas is labeled the volatile fraction of the material. The material that remains, the char, is then further analyzed to determine its carbon content, referred to as fixed carbon, and the balance is called ash. Biomass is often distinguished from other solid fuels like coal by its high volatile content (65 - 85 wt% for biomass compared to 20 – 40 wt% for coal).

An ultimate analysis reveals the mass fraction on a dry basis of individual elements present in a material. Although vegetative biomass varies, it is typically 40 – 50 wt% C, 35 – 45 wt% O, 4 – 6 wt% H, and 0.05 – 2 wt% N with the balance (0.1 – 22 wt%) being made up of a large number of elements often collectively referred to as ash [1].

Plant-based biomass can also be characterized based on its relative content of the organic structures: cellulose, hemicellulose, and lignin. Each of these compounds has unique gasification characteristics. Cellulose and hemicellulose gasify readily while lignin can be quite recalcitrant [33, 38].

2.3.2. Fluidized bed gasification

2.3.2.1. Bed temperature

Fluidized bed biomass gasification is typically performed at temperatures between 700°C – 900°C. At lower temperatures the gasification process is slowed, resulting in lower biomass processing rates for a given equipment size. At temperatures above approximately 700°C inorganic alkali metals, present in all vegetative biomass, begin to combine with the silica sand bed and form low melting temperature eutectics [39, 40]. As the alkali accumulates in the bed over time the eutectics cause the sand particles become sticky and adhere to each other, eventually resulting in agglomeration of the bed and loss of fluidization. Calcined crushed limestone added to the bed can increase the melting point of the eutectics allowing operation at higher temperatures for extended periods of time [39, 40]. However, unless the limestone concentration in the bed is maintained over time, its mitigating affects are eventually eroded and bed agglomeration results. While the addition of limestone to the bed enables operation at elevated temperatures, the risk of agglomeration prevents gasification above 900°C for extended periods without regular bed replacement.

2.3.2.2. Drying and devolatilization

Generally, biomass is stored in a hopper and is provided to the gasifier by a system of augers. Although they can be fed into the reactor any where along its length, biomass particles are often fed near the bottom of the hot (700°C - 900°C) fluidized bed in an effort to maximize their residence time in the bed. In this environment the biomass undergoes rapid drying and devolatilization. For small particles (< 1 mm) devolatilization is thought to be essentially complete in less than a second after entering the bed [29, 30, 41-43]. During this brief period in the history of the biomass particle a number of important events take place.

Biomass undergoes rapid drying and devolatilization after entering the bed as illustrated in Figure 9. This process separates biomass into two fractions: volatiles and char. The volatile fraction includes H_2, H_2O, CO, CO_2, CH_4, acetylene (C_2H_2), ethylene (C_2H_4), ethane (C_2H_6), propane (C_3H_8), and tar. The tar is composed of a large variety of condensable hydrocarbons that are generally present as vapors, but possibly also as aerosols, in the hot gas. Biomass has a high volatile matter content, generally between 65 – 87 wt% on a dry basis [1].

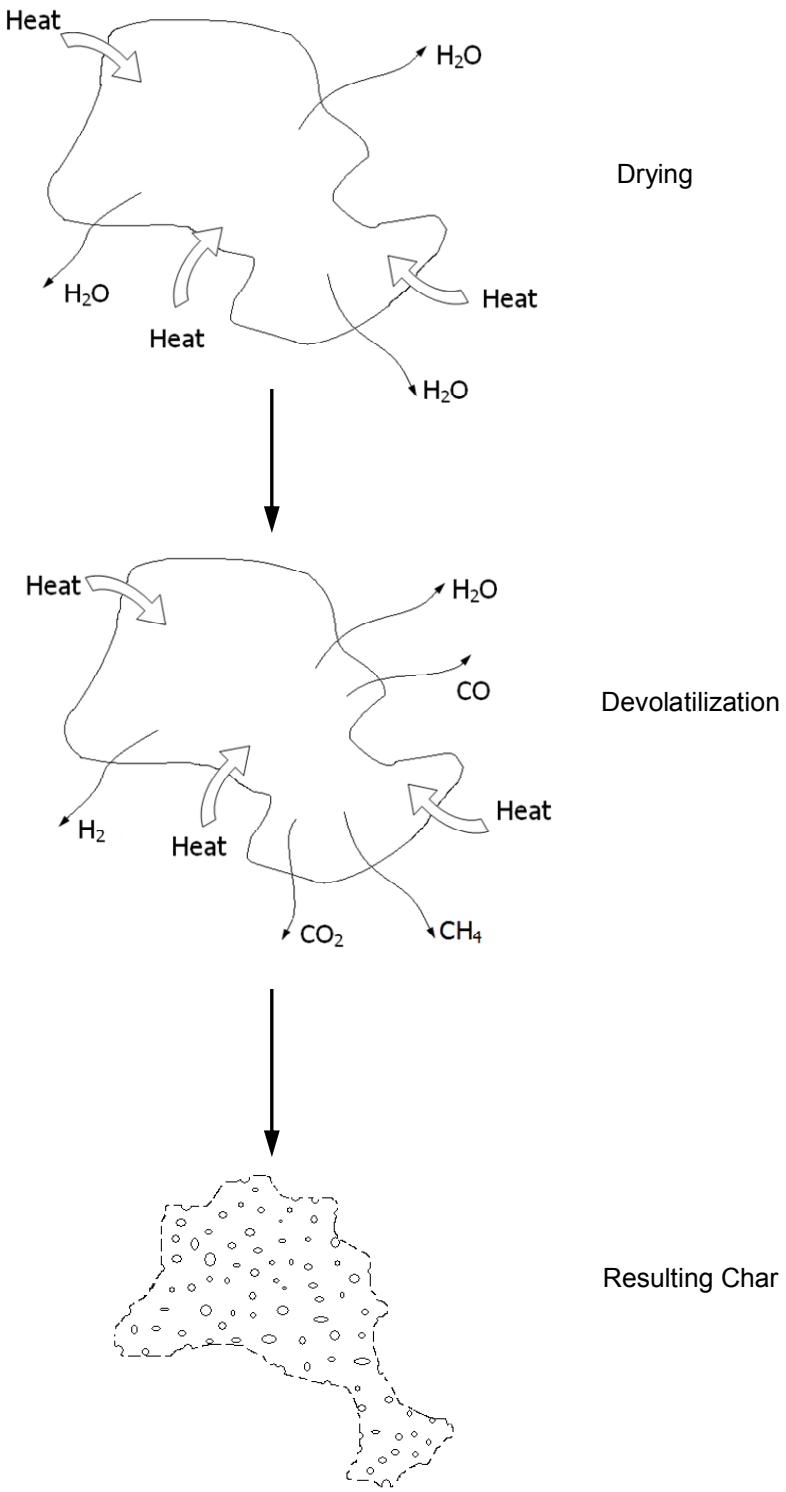

Figure 9. Drying and devolatilization of biomass particle

Consequently, biomass fuel particles lose a substantial amount of mass over a short time period. Pyrolysis, devolatilization in the presence of inert gas, research shows that the amount of mass lost to volatiles depends not only on the specific type of biomass but also on the heating rate and final temperature. Higher temperatures [29, 30, 41-48] and higher heating rates [44, 47-49] tend to increase the volatile fraction driven off [42, 47-49]. Increasing the volatile fraction effectively increases the carbon conversion. Scott *et al.* [42] claim that if the particle's residence time is significantly long compared to the time required to heat the particle to 500°C, the volatile fraction released essentially becomes a function of the final temperature only. Figure 10 is taken from Scott *et al*. [42]. It shows char yield, which is calculated as (1 – volatile release), as a function of temperature for maple wood sawdust. The decrease in char yield due to increased temperature is quite pronounced at lower temperatures, but as the figure illustrates and in agreement with other research on wood [43, 44], the affect is diminished at temperatures above 600°C.

At the completion of devolatilization the mass of the original biomass particle is divided into two fractions: volatiles and char. The fate of the volatiles during their residence time in the reactor is described in the following section while the fate of the char is discussed in the subsequent section.

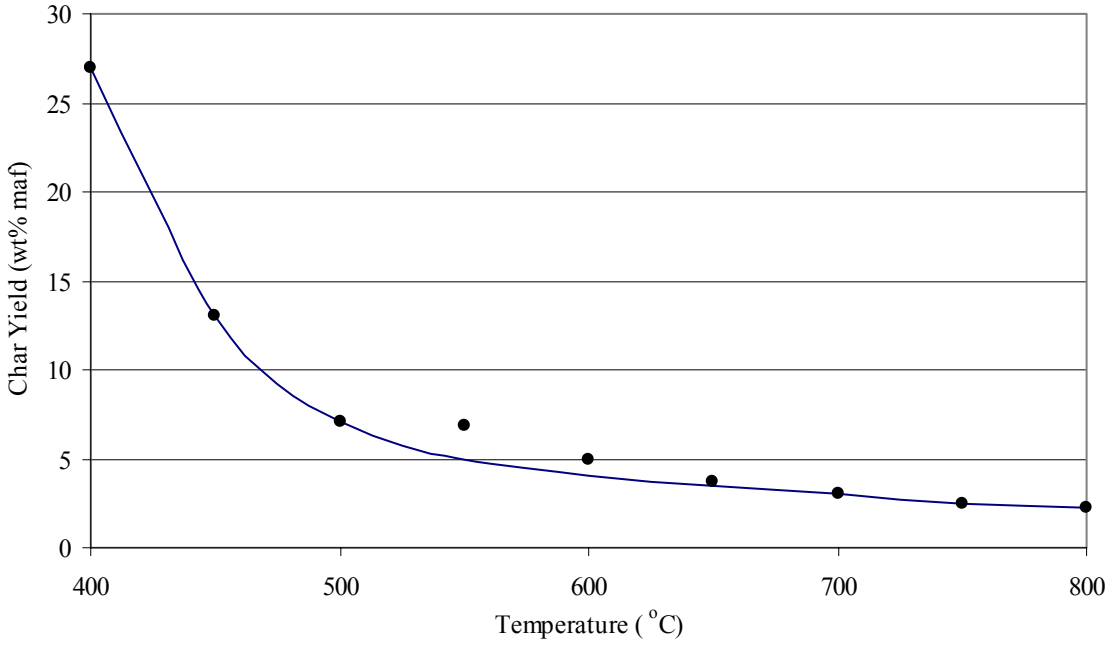

Figure 10. Char yield as a function of temperature for maple wood sawdust gasification [42]

2.3.2.3. Fate of volatiles

The volatile material released from the biomass during drying and devolatilization is a mixture of H_2, H_2O, CO, CO_2, CH_4, C_2H_2, C_2H_4, C_2H_6, C_3H_8, and larger, condensable hydrocarbons, collectively known as tar. The tar is often present in vapor form at gasification temperatures although high boiling point compounds may occur as aerosols. The quantity of tar generated during devolatilization depends on several factors including but not limited to: the pyrolysis temperature, the partial pressure of water vapor in the gas surrounding the particle, and whether the local environment is oxidative or reducing. The concentration of tar tends to decrease as the concentrations of either water [7, 21, 22, 26, 32, 45] or oxygen [7, 20, 21, 26, 32] increase or as the pyrolysis temperature increases [7, 20-22, 26, 32, 45, 49, 50] due to increased heat transfer to the particle and/or higher gasification temperatures.

As the volatiles are released from a single biomass particle they tend to form voids in the bed, which are referred to as bubbles. Because these bubbles are formed by the devolatilization of gas from within the particle as opposed to voids formed by the fluidizing gas as it passes through the bed, at least one author [51] has referred to them as endogenous bubbles. There is evidence that as biomass particles are continuously fed into the bed the endogenous bubbles coalesce, creating a volatile gas plume through the bed above the feed port [52-54]. Whether by pluming or by individual endogenous bubbles, a portion of the volatile gases may pass through the bed and into the freeboard largely without reaction, while the balance may experience significant contact with bed solids as well as with other gases present in the bed.

While in the bed volatiles can participate in homogeneous as well as heterogeneous reactions. When O_2 or air is the gasifying agent the devolatilization products can participate in the following exothermic, oxidative reactions:

Equation 9	$CO + ½\ O_2 \Leftrightarrow CO_2$	Carbon monoxide oxidation
Equation 10	$H_2 + ½\ O_2 \Leftrightarrow H_2O$	Hydrogen oxidation
Equation 11	$C_nH_x + n/2\ O_2 \Leftrightarrow n\ CO + x/2\ H_2$	Tar oxidation

The volatiles may also experience the following homogeneous gas-phase, exothermic reactions:

Equation 12	$CO + H_2O \Leftrightarrow CO_2 + H_2$	Water gas shift reaction
Equation 13	$CO + 3H_2 \Leftrightarrow CH_4 + H_2O$	Methanation reaction

CO_2 and H_2O can react with char and aerosols of tar in the heterogeneous gasification reactions (Equation 2 and Equation 3, respectively). These reactions are endothermic and are described in more detail as part of the char gasification discussion in Section 2.3.2.4.

In addition to oxidation tar vapor can undergo other chemical reactions. These are known as thermal cracking and steam reforming, depending on the relevant reaction taking place [21]. Thermal cracking is a process which reduces large hydrocarbon molecules to smaller ones by subjecting them to elevated temperatures. Steam reforming reduces the size of hydrocarbons by oxidizing carbons in the chain using water in a reaction similar to steam gasification (Equation 3) [21].

Tar is undesirable in most applications and steam is sometimes added to air gasification or is used to fluidize the bed in lieu of air to encourage the reforming reaction. Thermal cracking and steam reforming rates are enhanced as temperature is increased [7, 21, 22, 47, 49, 55].

2.3.2.4. Fate of the char

Biomass char

The solid portion of the biomass remaining after devolatilization is referred to as char. Biomass char is considerably less dense than its parent material, as might be expected given that approximately 80% of its mass is devolatilized. Although char is significantly less dense than the biomass it came from, it is denser than what would be anticipated as a result of pyrolysis. Apparently biomass particles shrink in volume as the volatiles are released [50, 56, 57]. This shrinkage is illustrated in Table 2 using data from several sources [17, 47, 57-59]. As noted in the table some data compares bulk densities while other sources have provided solid densities. The constant volume char density is the calculated char density assuming the

volume of the char particle to be the same as the biomass particle from which it was derived. The constant volume char density is calculated:

Equation 14 $$\rho_{CVC} = \rho_b (1 - f_v)$$

where

ρ_b = biomass density
f_v = volatile fraction

Some authors published the volatile fraction of the biomass used in their trials as shown in the table. In other cases the volatile fraction was not published and a value for a similar biomass material, as indicated in the table, is used to calculate the values in the table. The apparent volume shrinkage, AVS, listed in the table is an estimate of the percent reduction in

Table 2. Apparent biomass particle shrinkage during devolatilization [1, 17, 23, 47, 57-60]

Biomass Material	ρ_b (kg/m^3)	f_v (wt % dry)	ρ_{CVC} (kg/m^3)	ρ_{cm} (kg/m^3)	AVS (%)	Temperature (°C)
demolition wood[a]	1200	80.0[b]	240	300	25	851
black locust[c]	380	79.2	79	100	27	850
almond shells[d]	800	80.0	160	220	38	777
pine seed shells[e,f]	1200	77.1	275	490	78	850
wood chips[e,f]	550	79.3	114	170	49	850
olive husks[e,f]	1000	64.8	352	400	14	850
straw[g,h]	100	71.3[i]	29	50	72	1000
straw pellets[g,h]	300	71.3[i]	86	100	16	1000
olive waste[g,h]	1300	72.4[j]	359	400	11	1000
birch wood[g,h]	300	78.7[k]	64	100	56	1000

[a] from Kersten et al.
[b] from van der Drift et al.
[c] from Scala et al., 2000
[d] from Di Felice et al.
[e] from Scala et al., 2006
[f] devolatilization may not be complete due to large particles and short residence times
[g] from Zanzi et al.
[h] values compare bulk densities of biomass and char
[i] from Brown
[j] from Ollero et al.
[k] from Phyllis, database for biomass and waste, www.ecn.nl/phyllis, Energy Research Centre of the Netherlands

particle volume required to achieve the measured char densities. It is calculated according to:

Equation 15 $$AVS = \frac{(\rho_{cm} - \rho_{CVC})}{\rho_{CVC}}$$

where

ρ_{cm} = measured char density

As shown in the table the measured char densities are all higher than the calculated constant particle volume densities, giving rise to the apparent shrinkage values listed. For some of the entries in Table 2 the apparent shrinkage may be overestimated due to incomplete devolatilization of the char particles. These cases are identified in the table. It should also be noted that because density measurements are often made after the char has been collected a portion of the densification could be attributed to shrinkage of the char during cooling.

Biomass char owes its low density to its high porosity. Under high rates of heating, a large fraction of the developed pores have been observed to be macro pores (> 50 nm) [47, 58, 61-63]. These large pores are thought to originate from the longitudinal cell structure of the original plant material [58] as well as from micro pore (< 2 nm) coalescence during very rapid heating to high temperatures [61, 63]. Meso pores (2 – 50 nm) have sizes between the extremes of micro and macro pores. Rapid heating and high pyrolysis temperatures decrease the char yield because of increased volatile release from the particle, which can result in increased porosity and a corresponding decrease in char density [49, 64]. At lower temperatures and heating rates most biomass chars retain much of the overall structure found in the original biomass. However, at high devolatilization temperatures and high heating rates some biomass materials, woody biomass in particular, appear to undergo partial melting, resulting in a porous char material with a structure distinct from the biomass from which it was derived [61, 63]. Regardless of the degree of morphological change, most biomass char is very porous and is unable to withstand much physical stress. Therefore biomass char is said to be very friable, that is, easily broken apart.

Biomass char is very reactive when compared to coal char [11, 28, 49, 58, 65-67]. The reactivity of biomass char may depend on several factors including but not limited to: the alkali content of the biomass, the mobility of the alkali, the total porosity of the char, the size distribution of the pores, the elemental structure of the carbon in the char, the presence of residual volatiles in the char, the particle diameter, the heat transfer rate to the particle, and

the devolatilization temperature. The factors listed above are described in the discussion that follows.

First, vegetative biomass contains alkali metals such as potassium (K) and sodium (Na). Increased char reactivity due to the catalytic effect of these alkali has been demonstrated [11, 22, 47, 55, 60, 68-70]. Potassium oxide (K_2O) is often the most abundant alkali oxide in vegetation and the most catalytically active and therefore has received the most attention. Potassium oxide is reported to increase the reactivity of biomass and coal chars by as much as a factor of 100 [68, 71]. Further description of catalyzed oxidation and gasification reactions can be found in following paragraphs which describe char oxidation and gasification.

Secondly, biomass char is highly porous and consequently has a large surface area available for reaction. Table 3 lists biomass char surface areas as reported in the literature. Coal char surface areas are also listed for comparison. Despite the large variation in char preparation, in general, biomass yields char with larger surface area than does coal. Hurt *et al.* [72] observed an insensitivity in CO_2 gasification reactivity of coal chars to changes in micro pore surface area and concluded that most of the active carbon sites must be located in the macro pores. Fushimi *et al.* [33] arrived at a similar conclusion for biomass char. Therefore a char particle with greater macro pore surface area is expected to be more reactive than a similar char with fewer macro pores. Pyrolysis research [58, 61-63, 73] has also shown that increasing the heating rate and/or the pyrolysis temperature tends to not only increase the total surface area of the char, but also the fraction of the surface area existing as macro pores, and therefore the reactivity.

A third factor that influences the reactivity of the char depends on the elemental structure of the carbon in the char. Wornat *et al.* [74] and Henrich *et al.* [66] conclude that the disordered nature of the carbon structure in biomass, as compared to coal, leads to a large number of active carbon sites during pyrolysis, which in turn, contribute to the high combustion reactivities observed.

Fourthly, Guerrero *et al.* [62] reported higher concentrations of hydrogen and oxygen in biomass chars that have been exposed to high heating rates as compared to chars that have been prepared at lower heating rates. The authors believe that as the hydrogen and oxygen

atoms are removed during further reaction, additional active carbon sites are created leading to increased reactivity.

Table 3. Surface area of chars [61, 62, 70, 71]

Parent Material	Surface Area (m^2/g)	Measurement Method	Reference
pine wood	476	CO_2 adsorption isotherm	Cetin et al.
eucalyptus wood	589	CO_2 adsorption isotherm	Guerreo et al.
grapefruit skin	665	CO_2 adsorption isotherm	Marquez-Montesinos et al.
anthracite coal	279	CO_2 adsorption isotherm	McKee et al.
Pittsburgh coal hvA bit.	198	CO_2 adsorption isotherm	McKee et al.
Illinois no. 6 coal hvB bit.	280	CO_2 adsorption isotherm	McKee et al.
San Juan, subbit. coal	297	CO_2 adsorption isotherm	McKee et al.
lignite	695	CO_2 adsorption isotherm	McKee et al.

Finally, experiments show that smaller diameter biomass particles produce chars with higher reactivities than do larger particles [49, 64]. This trend is expected. Larger particles, in contrast to smaller ones, will experience, in the absence of fragmentation, lower heating rates per unit mass and will therefore devolatilize at lower average temperatures. It has already been noted above that decreased heating rates and lower pyrolysis temperatures lead to less reactive chars.

Although biomass char is more reactive on average than coal char, data of Wornat *et al* [75] show large variations in the reactivity from particle to particle, ranging from inert to diffusion controlled. This wide range was documented in char derived from both southern pine as well as switchgrass. The authors attribute the differences in reactivities to observed compositional and morphological variations in the char particles.

The elemental composition of char varies, reflecting the variations in parent materials and the environmental conditions in which it was derived. Often char is assumed to be the non-volatile fraction given by the proximate analysis, i.e. the fixed carbon plus the ash. This can be a reasonable approximation but actual heating rates, maximum temperatures, and residence times experienced in a gasifier can be substantially different than the test

conditions of the proximate analysis. These differences can affect the fraction of fixed carbon in char and encourage the retention of small quantities of oxygen and hydrogen in the char [17, 23, 62, 74].

During and after their formation the low density char particles may undergo several different processes before they leave the bed as gas and/or elutriated particles. Each individual biomass char particle will have a unique experience in the bed as it undergoes an individualized combination of these processes in varying degrees. The following paragraphs detail these processes as understood in the literature. Collectively, they describe the fate of the char in the fluidized bed.

Carbon-oxygen reaction

Oxygen is present in the lower portion of the bed of an air blown gasifier. The carbon in the char may react with oxygen by the heterogeneous exothermic carbon-oxygen reaction (Equation 1) often termed glowing combustion. For this gas-solid reaction to occur a series of events must take place. O_2 must be transported from the surrounding gas to the surface of the char particle. If active carbon sites are not readily available on the surface the O_2 will diffuse into the pores of the char particle until encountering an active C site in the interior of the particle. The O_2 molecule reacts with the C on the surface and CO is released into the pore. The CO diffuses out of the pore to the surface and from the surface into the bulk gas flow. The slowest step in this series controls the rate of the overall process and is referred to as the rate limiting step. The identity of the rate limiting step can change as mass transfer rates and/or chemical reaction rates are altered.

The carbon-oxygen reaction (Equation 1) is extremely fast at typical biomass gasification temperatures, especially when compared to the carbon gasification reactions. At 800°C the carbon-oxygen reaction has been shown to be at least five orders of magnitude faster then gasification by steam (Equation 3) or carbon dioxide (Equation 2) and eight orders of magnitude faster than carbon gasification by hydrogen (Equation 4) [36, 69]. When chemical kinetics are fast, as is the case with the carbon-oxygen reaction, mass transport from the bulk fluid and/or pore diffusion into the particle are often unable to keep up and one of these becomes the rate limiting step [17, 65, 66]. In the aggressively mixed environment of the fluidized bed, mass transfer rates to the surface of the particle are high and consequently pore diffusion is often identified as the limiting step when biomass char reacts

with oxygen [17, 35, 65-67, 75]. When pore diffusion limits the reaction most of the conversion takes place at or near the surface of the particle.

Although Equation 1 describes the overall chemical reaction, the details of how the carbon-oxygen reaction takes place at the surface of a biomass char particle covered with ash are not well understood. What is clear is that certain compounds dispersed in the char can act to catalyze the oxidation reaction. Alkali metal oxides are present in biomass in measurable quantities (0.02 – 2.5 wt% df [1]). Because it is often the most abundant and most catalytically active of the alkali oxides present in biomass, potassium oxide has been shown to play the dominate role in facilitating carbon conversion at typical gasification temperatures (500°C – 1000°C) [69]. McKee [69, 76] suggest the following catalyzed reaction sequence for the oxidation of carbon in the presence of K_2O:

Equation 16 $K_2O + ½\ O_2 \Leftrightarrow K_2O_2$

$K_2O_2 + C_s \Leftrightarrow K_2O + CO$

with the overall reaction:

$C_s + ½\ O_2 \Leftrightarrow CO$

The presence of a catalyst in the char tends to speed up reactions and allows them to make significant progress at lower temperatures. It is clear that the catalytic affect of some of the components of the biomass ash are part of why biomass char is very reactive as described earlier.

Gasification

The carbon in the char particles in the reactor can also be consumed by the endothermic, gas-solid, steam gasification (Equation 3) and/or carbon dioxide gasification (Equation 2) reactions. As mentioned previously, CO_2 gasification rates are 4 - 100 times slower than H_2O gasification and both are approximately five orders of magnitude slower than the carbon-oxygen reaction [36, 69]. With lower chemical reaction rates and with the char located in the high mass transfer environment of the fluidized bed, it is not surprising that

researchers have observed that chemical kinetics limit char gasification rates at temperatures below 900°C [11, 37, 77].

To gasify char by H_2O and CO_2 a source of water and carbon dioxide are required. Water is released from the biomass into the reactor during drying but is also formed when organic hydrogen and oxygen are combined during devolatilization and by the oxidation of H_2. Likewise, CO_2 is produced during volatile release but is also present as a product of carbon oxidation.

Potassium as well as other alkali metals have also been shown to be extremely effective catalysts for the gasification reactions just as they were for the carbon-oxygen reaction [55, 60, 70, 71, 78]. Gasification rates of coal and graphite were increased dramatically by the addition of potassium carbonate (K_2CO_3) [71]. Likewise, removing alkali from biomass char with an acid wash resulted in significant reductions in gasification rates [68, 70]. For gasification by steam the proposed mechanism involves potassium carbonate and is given by [71]:

Equation 17 $K_2CO_3 + 2C_s \Leftrightarrow 2K + 3CO$

$2K + 2H_2O \Leftrightarrow 2KOH + H_2$

$2KOH + CO \Leftrightarrow K_2CO_3 + H_2$

with the overall reaction:

$C_s + H_2O \Leftrightarrow CO + H_2$

and similarly for gasification by carbon dioxide [71]:

Equation 18 $K_2CO_3 + 2C_s \Leftrightarrow 2K + 3CO$

$2K + CO_2 \Leftrightarrow K_2O + CO$

$K_2O + CO_2 \Leftrightarrow K_2CO_3$

with the overall reaction:

$$C_s + CO_2 \Leftrightarrow 2CO$$

The presence of alkali in biomass can dramatically increase char gasification rates but the degree of carbon conversion also depends on the residence time of the char in the reactor. Large carbon conversion efficiencies are realized when reaction rates are high and residence times are long.

Ideally all of the char carbon would be converted to gas by gasification or carbon-oxygen reaction. However, before they have a chance to be completely converted, char particles can be reduced to elutriable size by a number of means: attrition, primary fragmentation, secondary fragmentation, and percolative fragmentation. Each of these is detailed in the sections that follow.

Attrition

Attrition is the physical erosion of the outside surface of particles due to the grinding action of the bed material and generally results in fine, elutriable particles. The physical reduction of particles by attrition is important for many fluidized bed processes. Given the friable nature of biomass char one would expect that attrition would play a significant role in reducing char particles down to elutriable size. However, from studies on coal combustion [79, 80] and biomass combustion [58] there is evidence that the contribution of purely mechanical attrition to the generation of char fines is relatively minor. Potentially, other means of reduction or conversion may occur so rapidly or to such a great extent, that reduction by pure attrition becomes relatively insignificant [54, 58, 81].

Primary fragmentation

The rapid heating, drying, and volatile release experienced by the solid biomass feedstock as it enters the bed can cause large thermal and pressure induced structural stress within the particles. These stresses can fragment the particle into pieces that are generally of the same order of magnitude in size as the parent particle. Fracturing due to drying or devolatilization is referred to as primary fragmentation. Primary fragmentation is illustrated in Figure 11.

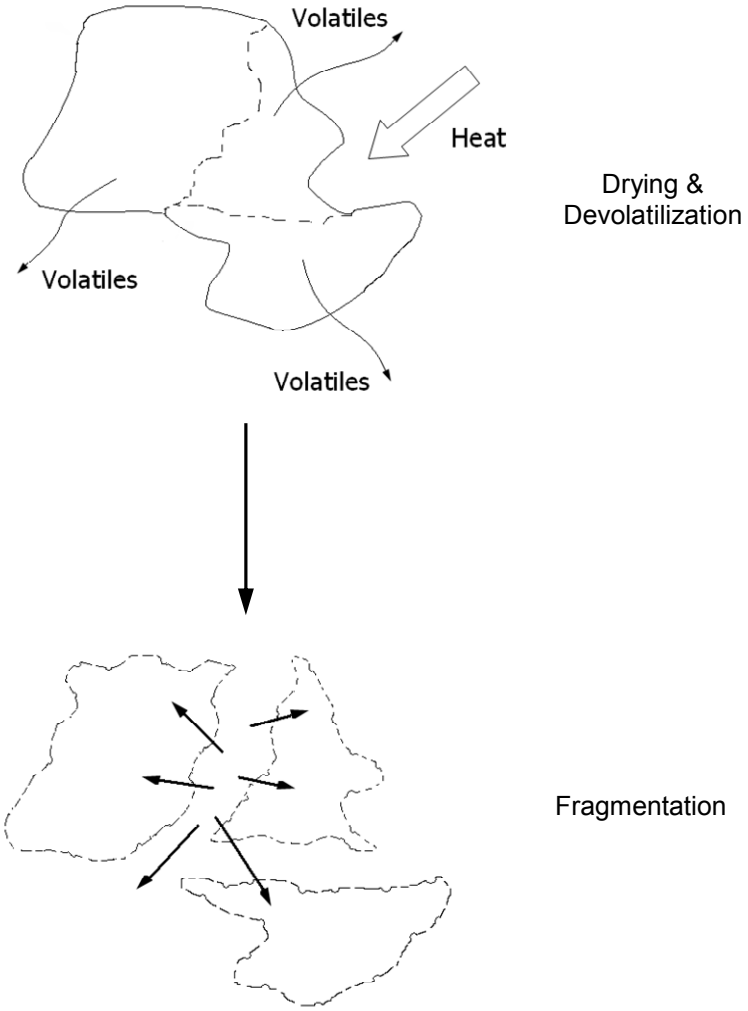

Figure 11. Primary fragmentation of char

Because this fragmentation is caused by gas pressure induced by devolatilization one might expect that the rate or degree of primary fragmentation is significantly related to the mass fraction of volatile matter released by the solid fuel. However, recent fragmentation research [81] shows no such correlation in comparisons between coal and biomass. The propensity of a solid fuel particle to fragment during devolatilization is more likely related to the combination of the particle's volatile content and its inability to locally relieve internal pressure without fracturing. The majority of biomass derived from vascular plant material is anisotropic, comprised of an extensive network of cells aligned along the axis of growth. During devolatilization the cell walls along the axial direction tend to rupture readily, relieving pressure before there is extensive damage in the radial direction. So, for example, even though a biomass particle may have three times the volatile content of a coal particle, the ability of the biomass to axially release the volatiles without fracturing could lead to a primary fragmentation rate that is comparable to the coal particle [81]. A comparison [57] between different types of biomass, however, does show some correlation between increased volatile content and the increased likelihood of fragmenting during pyrolysis. But even in this study [57] it appears that structural differences between the different biomass particles have a greater influence on primary fragmentation rates than does volatile content.

Because of the increased difficulty of the volatile release, it is expected that for the same type of biomass, larger fuel particles will fragment more than smaller ones. In the case of pine wood chips this conclusion is supported by data of Scala *et al*. [57] and in the case of beech wood spheres by the work of Jand and Foscolo [50]. A doubling of the diameter of the wood chips resulted in nearly a two fold increase in the propensity of the fuel particles to undergo primary fragmentation [57]. Similarly, it is also anticipated that increased particle heat transfer and/or devolatilization temperature could lead to increased primary fragmentation caused by increased pressures associated with the larger volumes of volatile gas produced under these conditions.

Secondary fragmentation

As an irregularly shaped char particle undergoes conversion, it can separate into pieces, often two, as bridge material connecting different parts of the char particle is consumed or weakened. This phenomenon is termed secondary fragmentation and is illustrated in Figure 12. Because secondary fragmentation often results in two fragments, the pieces are generally of the same scale in size as the original char particle. Secondary fragmentation is

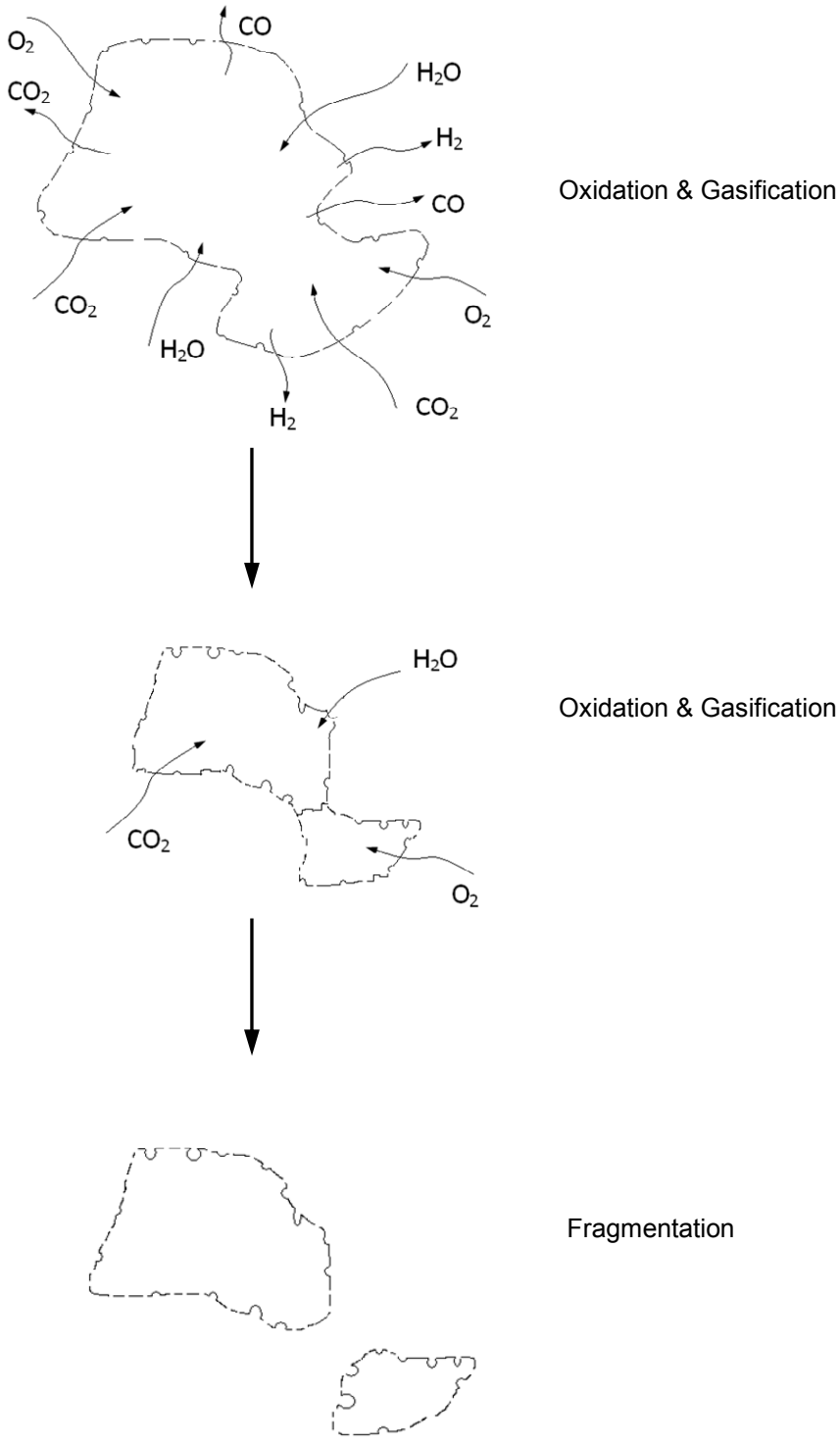

Figure 12. Secondary fragmentation of char

distinguished from attrition in that attrition generally results in fine, elutriable particles while secondary fragmentation particles are typically much larger. Scala and Chirone [81] attempted to assess the extent of this process for several solid fuels but their results are based only on the quantification of particles that were large enough to collect. Their tests were performed in an oxidative environment and as others [58] have indicated, the methodology employed does not allow quantification of the particles that may have been completely combusted after fragmentation or were too small to be collected. Although the extent of secondary fragmentation in biomass char is unknown, it is clear that the process plays a role in reducing the size of the char particles in at least some circumstances [58, 81].

Percolative fragmentation

In addition to being broken apart by primary fragmentation, secondary fragmentation, and attrition, and being reduced by oxidation and gasification, char can also undergo percolative fragmentation. Percolative fragmentation is a process by which gasification and/or oxidation enhance the porosity of a char particle or a portion of it, to the point that it is no longer structurally sound and breaks into a large number of small fragments as illustrated in Figure 13. Secondary fragmentation and percolative fragmentation are both caused by chemical conversion. However, percolation is distinguished from secondary fragmentation in that percolation involves the weakening of the entire structure of a char particle by conversion while secondary fragmentation involves consumption of bridge material between two portions of a char particle. All char particles are potentially susceptible to percolation while secondary fragmentation only affects duel lobed particles. Researchers suggest that percolative fragmentation is likely to occur when the porosity exceeds 70% [82]. Bar-Ziv *et al.* [56] refine this conclusion and suggest that the presence of a large number of meso pores and macro pores in addition to an overall porosity of 70% is required before percolative fragmentation will occur. They argue that micro pores do not tend to grow in size but simply change shape as carbon conversion progresses, leading to particle shrinkage rather than fragmentation [56]. Larger pores, by contrast, tend to expand during carbon conversion and ultimately threaten the structural integrity of a particle [56]. Biomass particles derived from plant material with a vascular cell structure tend to yield highly porous chars with a bias toward macro pores. Therefore it is not surprising that percolative fragmentation has been observed to play a dominate role in the comminution of biomass char in fluidized beds [54, 58]. Scala *et al.* [54, 58] reported peripheral percolation dominating the fragmentation of wood char during combustion. Peripheral percolative fragmentation occurs when conversion

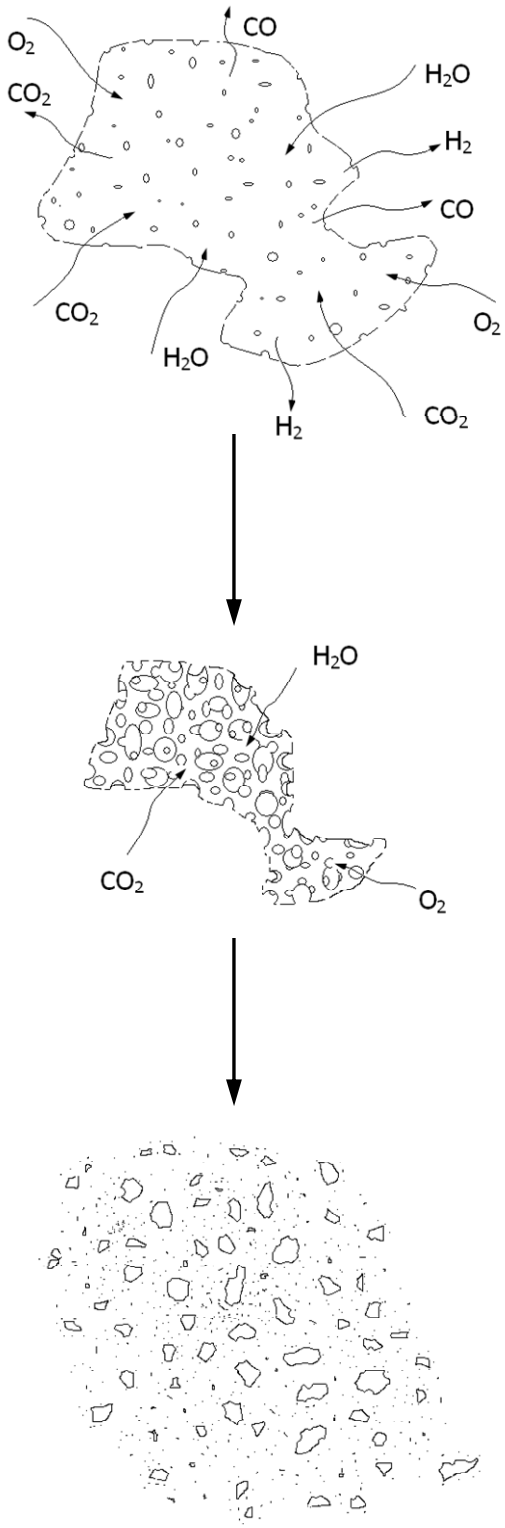

Figure 13. Percolative fragmentation of char

primarily occurs in the outer layers of the char particle, weakening this region and eventually causing the outer portion of the particle to fragment into a large number of fine particles.

Fragmentation of char in a fluidized bed due to percolation or peripheral percolation is sometimes referred to as chemically enhanced attrition. Use of this terminology acknowledges the fact that while the particles are brought to the point of fragmenting by chemical reaction, ultimately, it is the physical stresses imposed by adjacent particles colliding with its exterior that completes the process.

Segregation

In addition to attrition and fragmentation, a char particle may also experience a segregation process soon after its arrival in the bed [21, 28, 50, 51, 54, 83, 84]. Silica sand, with a density of approximately 2600 kg/m^3, is often used as a bed media during gasification. Typical biomass has a particle density less than half the value of sand. After the biomass is devolatilized, the resulting char will have a density that is substantially less than the original feedstock. As a result, biomass and its char are subject to buoyancy forces in the bed and may tend to float or segregate when introduced into the bed. Additionally, during devolatilization exogenous bubbles, or voids, have been observed forming around the biomass particle [51]. As these bubbles rise to the surface of the fluidized bed the biomass particle gets lifted by the motion of the wake solids [51, 83]. Consequently, even though the fuel may be fed into the bottom of the bed, the biomass particles may segregate to the top of the bed soon after introduction into the bed [50, 51, 84]. Experiments in which the bed was suddenly defluidized and chemical reactions quenched by cold diluent gas revealed that approximately 70% of the total mass of carbon contained in the bed was located in the top 30% of its volume [28]. One possibility is that segregation of the biomass char may reduce its attrition. While floating on the surface of the fluidized bed biomass char is not exposed to the harsh grinding activity typically experienced by particles deeper in the bed.

Agglomeration of char with bed media

To this point the discussion of char behavior in the bed has focused on the chemical and physical reduction of the char particle. Others have proposed particle enlargement by agglomeration. Scala *et al.* [58, 65] studying the combustion of biomass forward evidence for the formation of small char/bed media agglomerates within the fluidized bed. The authors maintain that the presence of agglomerates are required to explain the large loadings

of carbon observed in their bed and the high carbon conversions achieved in their experiments [58, 65]. Biomass contains alkali metals which can react with silicon in the bed sand and form low melting point eutectics [57, 74, 85]. These eutectics can coat the surface of the sand particles and are "sticky" at typical gasification temperatures. The authors claim that the char and sand particles form small agglomerates. As sand particles stick to char particles and each other, the effective size and density of the "char" particle is increased. Consequently, the agglomerate is less likely to elutriate. This essentially increases the residence time of the char in the bed, allowing conversion to progress.

Ejection and elutriation from the bed

A fluidized bed gasifier is typically operated at superficial velocities well above minimum fluidization ($U/U_{mf} > 5$). The superficial gas velocity is the volume flow rate of gas per cross sectional area of the gasifier) At these conditions the bed displays violent bubbling or boiling behavior and a splash zone of dilute solids is established in the freeboard above the dense phase of the bed. Bed media and char are ejected up into the splash zone when rising voids, often called bubbles, burst as they reach the surface of the bed [86].

Depending on their terminal velocity, the bed materials (the char and the bed media) can be divided into two fractions: fine and course particles. The terminal velocity of a particle is the maximum velocity the particle will attain in freefall under the force of gravity. At this velocity the force due to gravity is balanced by the drag force on the falling particle. All else being equal, particles with larger densities or lower drag coefficients have higher terminal velocities. In a gasifier, particles that have terminal velocities less than the superficial gas velocity are expected to be entrained in the upward gas flow and elutriated from the reactor. "Fine particles" by definition have terminal velocities that are less than the superficial gas velocity in the freeboard of the reactor. A "course particle", by contrast, is defined as having a terminal velocity that is greater than the superficial velocity of the exiting producer gas. Left to themselves, course particles in the freeboard are expected to eventually fall back down into the bed [86].

Fine as well as course particles are ejected from the bed into the freeboard as bubbles burst at the surface. Depending on their initial ejection velocity, terminal velocity, and interaction with other particles, individually particles will be projected to different heights into the freeboard. If the freeboard is sufficiently tall, by definition, the coarse particles will

return to the bed. The transport disengagement height for coarse particles (TDH(C)) is defined as the highest point up into the freeboard reached by any course particle. Therefore the concentration of coarse particles above the TDH(C) is zero [86].

The fate of the fine particles after ejection from the bed is not well understood. Fine particles are elutriable at gas velocities equal to or less than the superficial velocity. However, not all of the fine particles that are ejected from the bed elutriate from the reactor. The velocity profile of the gas in the freeboard is not uniform. There are regions, particularly near the walls, where the gas velocity is much less than the superficial velocity. If fine particles enter and remain in this region they could fall back into the bed, depending on their particular terminal velocity relative to the local gas velocity. Also, as the number of particles in the freeboard increases, it becomes increasingly likely that particles will collide with each other. If a fine particle collides and sticks to another particle the agglomerate may no longer be elutriable. In any event, regardless of the means, it is clear that some of the ejected fine particles are returned to the bed. As we move up the freeboard from the bed the concentration of coarse and fine particles decreases. As the particle concentrations decrease fewer fine particles are removed from the gas stream by the disengagement mechanisms just described. Consequently, if the freeboard is of sufficient length, eventually the concentration of fine particles in the gas flow becomes essentially constant with height. The transport disengagement height for fine particles (TDH(F)) is defined as the height above the bed at which the concentration of the fine particles is within 1% of its final value. Most (99% by definition) of the fine particles that make it above the TDH(F), elutriate. The fraction of the biomass carbon that leaves the reactor unconverted with these elutriated particles is the degree to which the total carbon conversion falls short of 100%. Therefore the freeboard section of the reactor is often designed with a larger diameter than the bed section to decrease the superficial gas velocity and encourage disengagement of particles from the gas flow. This not only encourages increased carbon conversion but also helps prevent loss of bed media out of the reactor [86].

2.3.3. Freeboard reactions

The gases that leave the bed must pass through the freeboard section of the gasifier before they exit the reactor. A char particle may repeatedly appear in the freeboard as it is

ejected and falls back into the bed until finally it is of elutriable size and leaves the reactor. During their time in the freeboard the char and the gases can undergo further chemical reaction.

The volatiles escaping the bed as a plume, separate bubbles, or as emulsion gas may undergo homogeneous gas-phase reactions as they pass through the freeboard. Because the oxidation reactions are so fast at gasification temperatures, the O_2 that enters with the fluidizing air is completely consumed in the lower regions of the bed. Therefore the two primary gas-phase reactions that can occur in the freeboard are thought to be the water-gas shift reaction (Equation 12) and the methanation reaction (Equation 13) [1]. Any tar still present in the producer gas leaving the bed may continue to be reduced by thermal cracking or steam reforming as it passes through the freeboard.

Without O_2 present in the freeboard gas stream the carbon in the char is reduced primarily by steam (Equation 3) and carbon dioxide (Equation 2) gasification. The significance of the contribution of freeboard char conversion to the total carbon conversion for the gasifier is not immediately clear based on published data. Miccio *et al.* [19] claim that a large portion (5 – 30% depending on the operating conditions) of the fixed carbon is converted after the char has left the bed. However, others have measured high carbon conversions for gasification of biomass in reactors operated with a "cold" (500°C - 650°C) freeboard, which effectively eliminates the endothermic carbon gasification reactions in this region [16, 26].

Miccio and coworkers [19] analyzing particulate samples from three different elevations in the freeboard above a fluidized bed note a significant decrease in the carbon content of the sampled particulate as the height above the bed increased. The authors conclude that a substantial amount of fixed carbon is converted in the freeboard as the char particles make their way out of the reactor. However, this conclusion may be unfounded given the nature of their experimental method. Their data set was collected from the freeboard section above a fluidized bed operating in the slugging regime. In this mode of operation a majority of the bed is periodically lifted by the fluidizing air as a unit, or slug. At some point above the distributor plate the integrity of the slug is lost and the bed collapses back down to the distributor plate. This type of pulsing bed behavior is characterized as having poor solids mixing, an increase in segregation behavior, and an increased tendency to spout [4, 86]. Slugging and spouting beds can eject large amounts of bed materials into the splash zone.

With this combination of operating conditions it is likely that particulate samples from the lower portions of the freeboard were draw from the splash zone of the reactor and would contain char particles that have not finished devolatilizing and/or char destined to fall back into the bed. Either scenario leads to an inflated estimate of the fixed carbon present in elutriable char at this low elevation in the freeboard. The authors recognize that the high percentage of bed media recovered in the samples collected closest to the bed confirm splash zone sampling. However, because of its low density it is expected that the splash zone of the char would reach higher freeboard elevations than would the bed media and therefore it is possible that particulate samples drawn at higher elevations above the bed are also biased by splash behavior even though they contain a limited amount of bed media. If samples of char are taken at elevations below the TDH(F) then they would not necessarily reflect the degree of conversion taking place in the freeboard but might simply reflective that char that has experienced more conversion would tend to be smaller and therefore would tend to be get lifted higher up into the freeboard.

Given the high rates of carbon conversion achieved by others in relatively cool freeboards and the uncertainty associated with the conclusions of Miccio *et al.* [19], it seems unlikely that a great deal of carbon conversion takes place in the freeboard over a bubbling fluidized bed as char elutriates from the reactor. However, it is possible that coarse char may experience conversion in the freeboard as it is repeatedly ejected from the bed. Coarse char is not elutriable by definition and returns to the bed.

2.3.4. Char collection

Eventually char is reduced to fines and is carried out of the reactor and is often passed through a cyclone separator. The particulate removed by the cyclone is collected and the journey from fuel hopper to cyclone catch is complete. In general, of the carbon that enters a gasifier with the biomass approximately 5 – 30% of it leaves the reactor unconverted. This directly corresponds to reported carbon conversion efficiencies of 70 – 95% [7, 14-18, 23, 24].

2.4. Potential Barriers to Complete Carbon Conversion

Carbon conversion is low during biomass gasification in a fluidized bed because average gasification rates are too low compared to the average residence time of the char in the reactor. Factors which can suppress char gasification rates are described in the next section while factors which can reduce char residence time are discussed in the subsequent section.

2.4.1. Potential limits to gasification rates

Although the reactivity of fresh biomass char has been shown to be at least 1000x that of coal char [67], there is evidence that at least under some circumstances high average rates of gasification are not maintained as the biomass char nears complete conversion. Several inhibitors to gasification rates are identified in the literature and are detailed in the following discussion.

2.4.1.1. Recalcitrant char

As described in Section 2.3.2.4 char derived from biomass yields high average reactivities but with very large standard deviations. Wornat *et al.* [75] report switchgrass and southern pine char particle reactivities that span the range between extremely reactive to almost inert. The presences of a significant fraction of carbon with low reactivity in biomass char could explain low values of carbon conversion even when average char reactivities are high. In this scenario reactive carbon in the char is quickly converted while the relatively recalcitrant fraction remains in intact. Eventually the char particles are reduced physically and/or chemically to elutriable size and exit the gasifier rich in recalcitrant carbon.

Biomass is composed of cellulose, hemi-cellulose, and lignin. The relative amounts of each vary between different types of biomass and potentially between individual particles derived from the same biomass. Research gives evidence that lignin tends to yield a large char fraction compared to the other two components [33, 38, 41, 47, 49, 87] Lignin is a phenylpropane-based polymer [1] which potentially transforms to aromatic ring structures similar to graphite during pyrolysis [88]. Bourke *et al.* [88] measured an average aromaticity of 70±10% in biomass chars pyrolyzed at 950°C. This, combined with other test results, led

the authors to conclude that char is composed of microcrystalline graphitic structures roughly the size of the micro pores [88]. Although these aromatic structures likely contain many active carbon sites when initially formed, it is conceivable that conversion depletes these sites leaving recalcitrant graphitic structures.

Due to lignin's propensity to form a large char fraction composed of aromatic structures one would expect lower carbon conversion values with increasing lignin content. At least one research group has given evidence of this connection. Hanaoka *et al.* [38] steam/air gasified lignin separate from cellulose and measured a carbon conversion 52.8% for lignin and 97.0% for cellulose.

2.4.1.2. Deactivation

While low carbon conversion may be explained all or in part by the presence of innate recalcitrant carbon structures in biomass there is also evidence that biomass char reactivity may decrease due to deactivation of active carbon sites as conversion nears completion [56, 66, 67, 69, 74, 75]. Several means of deactivation have been proposed in the literature and are briefly described below.

Thermal annealing, thermal deactivation, or graphitization is a high temperature transformation of the char structure resulting in a highly ordered and unreactive arrangement of the carbon atoms. Researchers have found that the potential for thermal annealing to occur in a char depends on the source of the char and on its preparation. Guerrero *et al.* [62] observed thermal deactivation due to structural ordering and micro pore coalescence at 900°C in eucalyptus char prepared by slow heating. They [62] also report results for eucalyptus char produced with rapid heating. In contrast to the slowly heated char, the rapidly heated char showed little evidence of graphitization [62]. Wornat *et al.* [74] claim that the large amount of oxygen present in biomass char leads to a highly cross-linked carbon structure that resists ordering. They [74] observed significant thermal annealing in coal chars which contain very little oxygen but limited annealing in pine and switchgrass chars. Similarly, Hurt [89] observed highly ordered carbon structures in samples of char derived from high rank coals but not in soft coals or biomass chars. He claims that carbon solids can be classified as either graphitizing or nongraphitizing [89]. According to Hurt, graphitizing carbons, such as the high rank coals, pass through a fluid stage during pyrolysis while others

do not [89]. He maintains that it is during this fluid state that the carbon structure becomes ordered and consequently less reactive [89]. Therefore, given the high heat transfer rates associated with fluidized bed gasification and in light of these published results, it seems unlikely that thermal annealing plays a prominent role in reducing biomass char reactivities.

Although the role of thermal annealing in decreasing biomass char reactivity during fluidized bed gasification seems minimal, other potential means of deactivation have been proposed. Several researchers have found that silicon (Si) within the biomass can combine with catalytically active alkali earth metal to form inactive silicates [68, 74, 75]. This deactivation becomes more likely as the mass fraction of ash in the char becomes higher as conversion proceeds. Phosphorus, present in all vegetative biomass in varying degrees, can also deactivate alkali by binding them as phosphates [69]. This process too becomes more prevalent as the ash becomes concentrated due to increased carbon conversion. As described in Section 2.3.2.4 alkali earth metals such as K can act as catalysts for the carbon/oxygen reaction and for gasification. The alkali appears to move across the surface of the carbon structure as tiny droplets as they facilitate the reactions. The mobility of these droplets is tied to their effectiveness as catalysts [69]. Here again, as conversion progresses catalyst droplet coalescence becomes increasing likely, resulting in a decrease in droplet mobility and a corresponding decrease in char reactivity [69]. Additionally, Henrich *et al.* [66] note decreases in the char surface area per unit mass at advanced stages of conversion of municipal waste char. Reductions in the specific surface area result in decreases in the number of active carbon sites which corresponds to decreases in the reactivity of the char. Several different deactivation mechanisms are described above but in all cases the likelihood of deactivation is increased as carbon conversion progresses, making conversion of the last bit of fixed carbon an ever increasing challenge as complete conversion is approached.

While some deactivation of the char by one or more of these mechanisms seems inevitable, their influence is not expected to be significant during typical gasification. All of the listed mechanisms become evident only at advanced stages of conversion in very controlled laboratory experiments. The low carbon conversion efficiencies realized during typical bubbling fluidized bed biomass gasification suggests that the char elutriates form the reactor well before deactivation is detectable. If the current barrier(s) to complete carbon conversion are removed it is conceivable that deactivation could become limiting.

2.4.1.3. Competing reactions

In addition to being influenced by the innate properties of biomass char, carbon conversion can also be limited by chemical reactions taking place in the vicinity of the particles. The carbon/oxygen reaction (Equation 1) and steam gasification (Equation 3) are the two primary paths for carbon conversion after devolatilization is complete. In both cases a limited supply of reactant can reduce conversion of solid carbon to gas.

By definition biomass gasification utilizes less oxygen then is required to completely combust the biomass. Oxygen can oxidize the carbon in the char but it can also react with tars and volatile gases released during pyrolysis. At gasification temperatures the carbon/oxygen reaction is very fast, consuming the O_2 soon after it enters the bed. Ideally, all of the incoming oxygen would react with char carbon releasing the required thermal energy to drive the gasification process while increasing carbon conversion. However, it is likely that tar, char, and volatile gas are all oxidized to some extent depending on the reactivity of each and the relative fraction of each entrained within the bed [17, 21, 90]. Tar and volatile gas in the bed act, in this circumstance, as barriers to high carbon conversion by consuming oxygen that could have converted solid carbon to gas.

Moisture is brought into the gasifier with biomass but also forms during pyrolysis and combustion. Steam gasification can be hindered by low concentrations of water in the reactor, particularly when relatively dry biomass is being fed. For this reason steam is often added to enhance gasification. Interestingly, the addition of steam is not always accompanied by increases in carbon conversion [17]. The water-gas shift reaction (Equation 12) is a competing reaction that may act as a barrier to steam gasification of char carbon as suggested by some researchers [17, 30, 87]. In this scenario added steam preferentially participates in the water-gas shift reaction rather than in steam gasification of solid carbon. Water combines with CO, elevating H_2 and CO_2 concentrations but leaving the solid carbon concentration unaffected. However, others document measurable improvements in the carbon conversion with the addition of steam [7, 18, 26, 32-34]. Based on the reported data it is not clear why added steam increases carbon conversion in some instants and not in others. Perhaps the diverse response to steam may be attributed to unique attributes of the particular char involved in each set of experiments.

Steam can also react with tar to reform it. Several researchers [7, 21, 22, 26, 32] report both lower char and tar loadings in the product gas when steam is added to the gasification process. At least one research team [90] claims that tar is more reactive than char. Regardless, it is clear that steam reacts with char and tar when both are present. Therefore tar can compete with char for available water, potentially acting as a barrier to complete carbon conversion.

2.4.1.4. Mass transport

Char conversion requires transport of reactants from the surrounding gas to the surface of the char particle and then likely into the pores of the particle. With the reactants present at active carbon sites chemical reaction can take place and is followed by transport of the products out of and then away from the char particle. By being the slowest portion of this sequence, one of these steps will limit conversion rates. Therefore, when mass transport is slow compared to the reactions, it can serve as a barrier to complete carbon conversion.

The reaction rates for gasification are much slower than for the carbon/oxygen reaction. When these lower gasification rates take place in the vigorously mixed, high transport environment of the fluidized bed, it is not surprising that gasification below 900°C is generally found to be limited by chemical kinetics rather than mass transfer [11, 28, 35, 37, 60, 66, 77, 89]. By contrast, the carbon/oxygen reaction occurs so rapidly at gasification temperatures that mass transport phenomena are identified as being the limiting step in the sequence [58, 65-67, 75]. However, even though mass transport is the rate limiting step for the carbon/oxygen reaction, O_2 is completely consumed during gasification. Therefore with the carbon/oxygen reaction going to completion and with the gasification reactions being limited by chemical kinetics, mass transport phenomena do not appear to pose a significant barrier to carbon conversion during fluidized bed biomass gasification.

2.4.1.5. Pluming and segregation

Pluming and char segregation (Section 2.3.2.4) can potentially reduce char conversion rates. If moisture and volatiles released from the biomass form a plume to the surface of the bed, potentially only a small fraction of the available steam may be entrained and gasification

of char may be limited. Because oxygen is rapidly consumed in the lower portions of the bed, segregated char floating on the surface of the fluidized bed will not have an opportunity to participate in the carbon/oxygen reaction. Additionally, segregated char in the splash zone or near the surface of the bed may experience significantly lower mass transfer rates than char vigorously mixed within the bed, potentially limiting gasification rates. However, there are no experimental studies to support or refute these hypotheses.

2.4.2. Potential limits to char residence time in the reactor

One of the most direct barriers to complete conversion of solid carbon to gaseous carbon is char elutriation. During the life of every char particle a point is reached where the combination of its size, density, and drag are such that the particle's terminal velocity is less than or equal to the superficial gas velocity in the reactor. When this point is reached it is likely that the char's remaining residence time in the gasifier is short, although interactions with other entrained particles and/or the wall of the reactor can delay the particle's escape as described in Section 2.3.2.4. Reaching elutriable size not only limits residence time but also the extent of addition reaction.

2.4.2.1. Biomass fines

Unless screened, biomass usually enters the gasifier with a wide size distribution. Below some critical size biomass particles yield chars that are immediately elutriable after devolatilization. While this elutriable fresh char may not leave the reactor immediately it is likely to have an average residence time that is shorter than char derived from larger biomass particles. When the elutriable-upon-injection fraction of the biomass feed is significant it can noticeably reduce average carbon residence times in the reactor, creating a barrier to complete carbon conversion.

2.4.2.2. Comminution

Carbon conversion is maximized for a given set of operating parameters when char particles are reduced to elutriable size by chemical reaction alone. Attrition, fragmentation,

and percolative fragmentation can reduce the average time that char particles spend in the reactor, limiting their conversion. When active, these comminution phenomena, acting individually or in concert, are barriers to increased carbon conversion.

2.4.3. Summary

Carbon conversion in fluidized bed biomass gasification is rarely complete. Conversion is limited because average chemical reaction rates are too slow compared to the average residence time of the char in the reactor. While limits to char reaction rates and residence times can be described separately, they are intertwined. The relative speed of a reaction is defined in relationship to the average residence time of the char. Further, the chemical reaction rate is inversely related to the particle's residence time. Increased reaction rates correspond to a decrease in residence times with the potential net effect of little or no change in the carbon conversion efficiency. Because of the many factors that can affect carbon conversion and the degree to which they are interconnected it is not always clear how variations in the operating parameters result in the observed efficiencies. The goal of the current research is to bring a measure of clarity to this situation through the development and application of a carbon conversion analysis methodology.

3. EXPERIMENTAL EQUIPMENT AND METHODS

Gasification of biomass in a bubbling fluidized bed is a complex thermal/chemical process. Carbon conversion efficiencies are not always published for biomass gasification research. When given, the response of carbon conversion to changes in the operating parameters is often simply presented with little or not explanation for the behavior. As such the data does little to expose the underlying mechanism controlling carbon conversion. Therefore to facilitate a deeper understanding of the intricacies of carbon conversion during biomass gasification, a carbon conversion analysis methodology is developed for this study. The method requires measurement of several parameters using batch and steady state experiments but helps reveal the factors that limit carbon conversion by allowing chemically converted char carbon to be distinguished from char carbon that leaves the reactor due to elutriation.

Batch experiments and steady state experiments are performed in the laboratory scale (10 kW thermal) gasifier illustrated in Figure 14 to shed light on the factors which limit carbon conversion in biomass gasification. The batch experiments use the gasifier to pyrolyze small quantities of biomass to determine the fixed carbon yield at typical gasification conditions. Steady state gasification experiments analyze the flow of carbon through the reactor as biomass is continuously fed over several hours. The results of both types of experiments are combined through a methodology designed to help illuminate the carbon conversion process during biomass gasification.

3.1. Primary Experimental Systems

The primary experimental equipment is described below in the context of four main subsystems: the gasifier system, the isokinetic sample system, the continuous emission monitor (CEM) sample system, and the data acquisition and control system.

3.1.1. Gasifier system

The gasifier system consists of a fuel feed system, the reactor shell, the fluidized bed, the steam injection system, and the cyclone particulate separation and exhaust system.

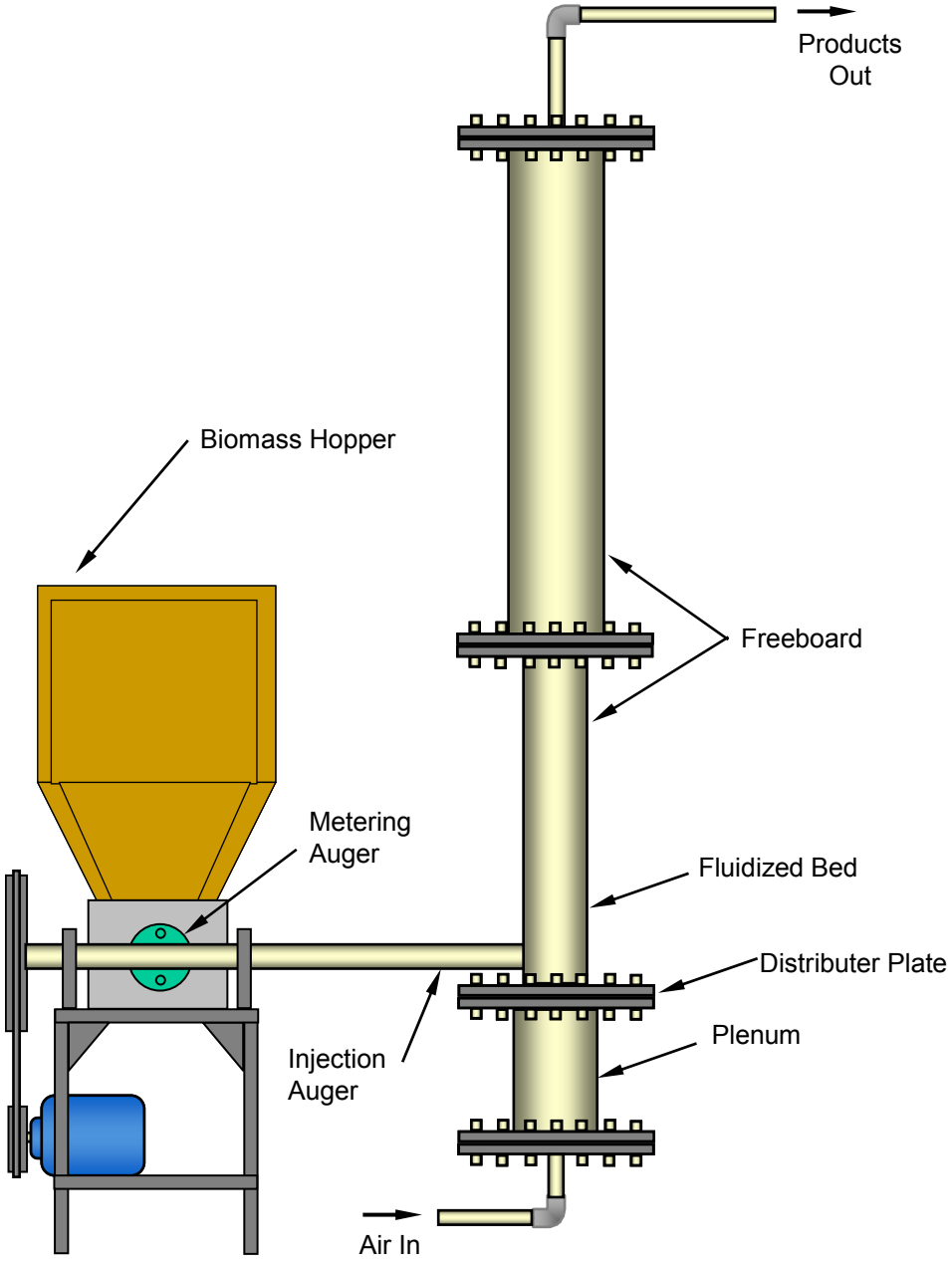

Figure 14. Diagram of the fluidized bed gasifier

3.1.1.1. Fuel feed system

The fuel feed system is shown in Figure 14 and is comprised of a fuel hopper and two augers. The hopper of the Acrison Model 105Z-E volumetric feed system provides biomass to a metering auger which is controlled by a variable speed drive system, manually set for the desired biomass feed rate. The metering auger empties perpendicularly into the high speed injection auger. The injection auger delivers the biomass into the bed of the gasifier 5.08 cm (2") above the distributor plate. A water jacket surrounding the injection auger near the gasifier cools the auger housing to help prevent the biomass from breaking down before it enters the sand bed. A portion (~ 10%) of the fluidizing gas is diverted before entering the plenum and is directed into the injection auger. The gas, which flows through the injection auger and into the bed, provides additional cooling of the auger system.

3.1.1.2. Reactor

The gasifier reactor is described as four sub-assemblies: plenum, distributor plate, lower reactor, and upper reactor. These four sections of the gasifier are flanged allowing assembly and disassembly of the unit.

The plenum is located at the bottom of the gasifier as shown in Figure 14. The gasifier sand bed can be fluidized with a wide variety of gases including: air, N_2, and CO_2. The fluidization gas enters the plenum through a steel pipe. A Watlow Star Wound Cable Heater (3000 W) located in the plenum can be used to heat the fluidizing gas before it passes through the distributor plate and into the bed.

The distributor plate is located above the plenum and is constructed of 1.27 cm (1/2") thick Inconnel plate to withstand high temperatures. The plate is used to separate the bed from the plenum and to evenly distribute the fluidizing gas to the bed. To this end, 14, 3.57 mm (9/64") diameter holes are drilled through the plate in a geometric pattern to ensure good fluidization.

The lower section of the reaction chamber is constructed of 9.53 cm (3.75") ID Inconnel 625 tube 81.3cm (32") in length. This section of the reactor contains the bed and lower freeboard. The temperature in the bottom section of the reaction chamber is controlled by two sets of electrical guard heaters (not shown in the figure). The heaters are semi-

cylindrical ceramic fiber heaters manufactured by Watlow for operation up to 1100°C (2000°F) and are placed around the outside of the reactor. The first set of heaters is 30.5 cm (12") tall, provides 2500 Watts, and is primarily used to control the temperature of the fluidized bed. The second set of heaters is 45.7 cm (18") tall, is rated for 3500 Watts, and maintains temperature in the first freeboard section of the gasifier.

The upper portion of the reactor is constructed of 15.2 cm (6") ID Inconnel 625 tube 122 cm (48") in length. This top section of the freeboard is designed with a larger diameter to lower the superficial gas velocity and encouraging disengagement of particulate from the gas flow. The temperature of this upper section is controlled by two sets of identical guard heaters (not shown). Each set of heaters is composed of two Watlow 4200 Watt semi-cylindrical ceramic fiber heaters 45.7 cm (18") tall.

3.1.1.3. Fluidized bed

The bed is a mixture of silica sand and ground quarry limestone. The total mass of bed media is maintained at approximately 2000 grams and is initially formulated with 70% sand and 30% limestone. Limestone used in the bed is either calcined in a laboratory furnace or in the gasifier by heating it to 700°C - 900°C for a minimum of 30 minutes. Calcining converts calcium carbonate ($CaCO_3$) to calcium oxide (CaO) and CO_2. The softer limestone attrites faster than the sand during operation and is elutriated from the reactor over time, and therefore requires periodic replenishing. During gasification experiments calcined limestone is added to the bed at an approximate rate of 20 g/hr. As described in Section 2.3.2.1 the calcined limestone combines with alkali from the biomass and prevents bed agglomeration by raising the melting temperature of the eutectics [39, 40]. As an additional precaution against the build up of alkali in the bed the sand and limestone are periodically removed and replaced with fresh material.

The size distribution of the bed sand is given in Table 4 and shown in Figure 15. This size distribution yields a mass weighted average diameter of 0.321 mm. The hydrodynamic weighted average diameter is an estimate of the size of a monodispersed population of particles that would yield the same surface area to volume ratio as the given population. The calculation assumes spherical particles and is defined as [4]:

Equation 19 $$\bar{d}_p = \frac{1}{\sum\left(\frac{x_i}{d_{pi}}\right)}$$

where

x_i = mass fraction for sieve interval i
d_{pi} = average particle diameter for sieve interval i

The hydrodynamic diameter of the sand used this study is equal to 0.308 mm.

The static bed has a diameter of 9.53 cm (3.75”) and is approximately 20.3 cm (8”) tall giving it an aspect ratio of 2.1. The minimum fluidization velocity (U_{mf}) of the bed was measured to be 2.06 cm/s at 700°C.

Table 4. Size distribution of bed sand

Sieve Size	Mass Fraction (%)
500-600	0.23
425-500	3.39
355-425	28.04
300-355	26.46
250-300	27.64
212-250	12.67
180-212	1.22
150-180	0.32
0-150	0.04

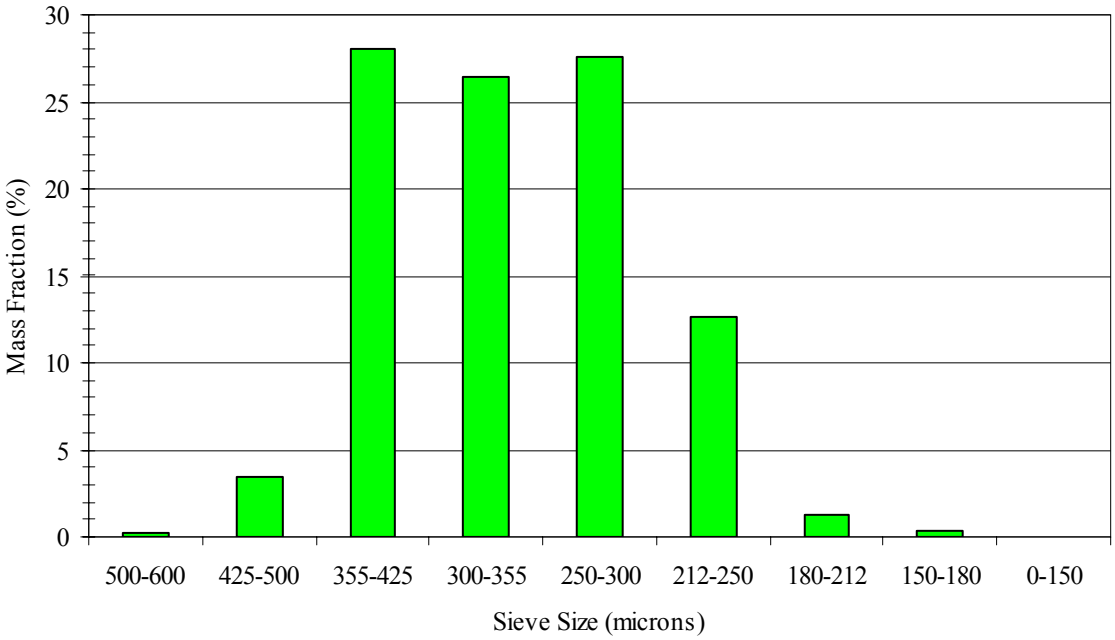

Figure 15. Size distribution of bed sand

3.1.1.4. Steam injection system

Some of the experiments add wet steam to the fluidized bed. The wet steam is provided by pumping water through a heated pipe before injecting it into the gasifier. The details of the system are described below.

Water is withdrawn from a bucket using a peristaltic pump (Masterflex L/S variable speed economy drive pump with an Easy-Load II head) and piped into a six foot section of 9.53 mm (3/8") stainless steel tube. The bucket of water is placed on a scale (Acculab Vicon VIS-5101 10 kg) and the average mass flow rate of wet steam to the reactor is measured by noting the mass change of water in the bucket over a particular time period. The 9.53 mm (3/8") stainless steel tube is wrapped with electrical resistance heat tape (Amptek Flexible Electric Heating Tape) which converts some of the water to steam as it makes its way to the gasifier. The wet steam is added to the bed of the gasifier through a thermocouple port 10.2 cm (4") above the distributor plate and radially across from the fuel injection port.

3.1.1.5. Cyclone particulate separator and exhaust system

The product gas leaving the gasifier is directed to the downdraft combustor as shown in Figure 16, using 1.27 cm (1/2") black steel pipe. On its way the gas stream is passed through a cyclone particulate separator as indicated in the figure. The cyclone uses centripetal force to remove large (> ~10 μm) particulate. A natural gas flame is maintained and excess air is provided at the top of the downdraft combustor to burn the products of gasification before they are vented from the building. To prevent condensation of tar the temperature of the cyclone and the piping between the gasifier and the combustor is maintained above 450°C by wrapping with electrical resistance heating tape (Amptek Flexible Electric Heating Tape) and a layer of high temperature glass insulation.

3.1.2. Isokinetic sample system

An isokinetic sample of the gasifier product stream is removed after the gas has passed through the cyclone separator as shown in the schematic of Figure 17. The isokinetic sample probe is constructed of 3.18 mm (1/8") (0.787 mm wall) stainless steel tube and occupies less than 10% of the cross-sectional area of the total flow stream, minimizing flow disruptions. The inlet of the probe extends upstream into the producer gas outlet pipe at least two pipe diameters and is located at least eight pipe diameters downstream of any flow disturbances which is consistent with EPA Method 1A [91]. The sample flow rate through the probe is adjusted during each experiment so that the velocity of the gas entering the probe is equal to the velocity of the bulk gas flowing in the pipe. By matching the bulk gas velocity the probe collects a representative sample of the gas stream including its particulate loading.

Shortly after the gas sample is extracted from the gasifier outlet pipe the 3.18 mm (1/8") diameter sample probe transitions to 9.53 mm (3/8") stainless steel tube to reduce pressure drop in the pipe. The sample stream passes through a quartz fiber thimble filter (Advantec MFS) to remove additional particulate before heading to an impinger train. The gas sample system from the isokinetic probe to the impinger train is maintained above 450°C to minimize tar condensation in the piping. The piping is wrapped with electrical heat tape and insulation, while the thimble filter and its housing are located in an insulated enclosure maintained at 450°C with three 500 W Watlow finned heating elements.

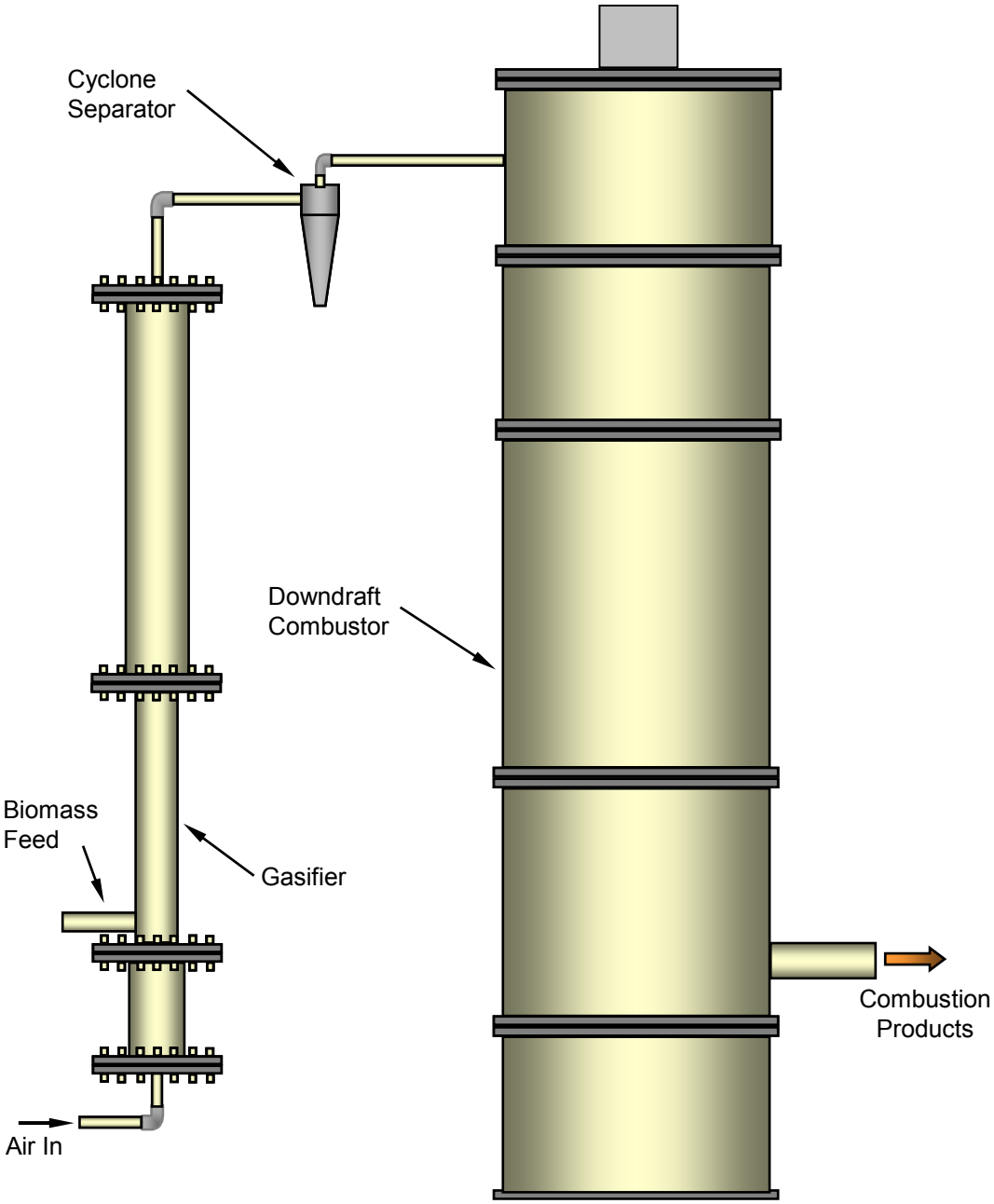

Figure 16. Gasifier with downdraft combustor

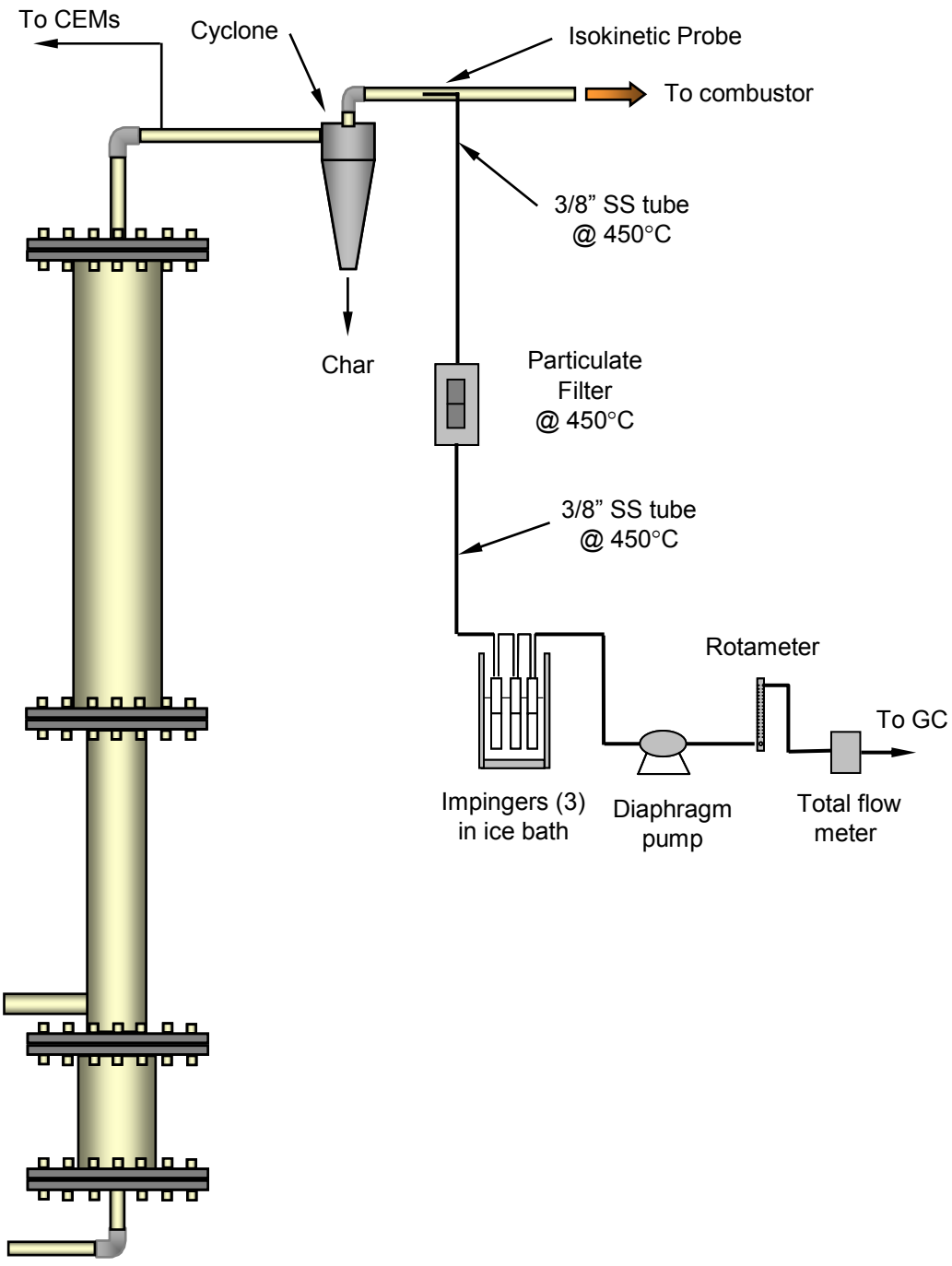

Figure 17. Schematic of gasifier with sample systems

As shown in the figure the sample stream passes through three stainless steel impingers after leaving the thimble filter. Custom fabricated from stainless steel pipe and pipe caps, the three impingers are plumbed in series and placed in an ice bath. Tar and water vapor in the producer gas condense into the impingers and glass wool serves as a barrier filter at the outlet of each impinger to help ensure a dry, tar and particulate free sample gas stream at the exit of the train.

A vacuum pump (Gast 120V, 2.1 amp) pulls the conditioned gas sample through the thimble filter and impinger train before sending it through a rotameter and on to a dry test meter (Schlumberger Gullus 2000). The rotameter is used to adjust the sample flow rate to achieve isokinetic sampling while the dry test meter is used to record the total volume of gas sampled.

Before being vented from the building the sample gas stream is passed by a micro gas chromatograph (micro-GC or just GC) sampling port. The micro-GC was manufactured by Varian (Model CP-4900) and is equipped with a 10 m molsieve 5A column and a 10 m pora plot Q column. Both columns are equipped with thermal conductivity detectors. The GC samples the gas approximately every four minutes measuring and recording the concentration of N_2, O_2, H_2, CO, CO_2, C_2H_2, C_2H_4, and C_2H_6. The calibration of the GC was verified before each experiment using certified calibration gases ensuring measurement accuracies of ±0.3 vol/vol %. The calibration of the GC was always within tolerance and did not require re-calibration during the course of the experiments performed for this study.

3.1.3. Continuous emission monitors (CEMs) sample system

The CEMs are used to measure the O_2, CO, and CO_2 concentration of a product gas stream. The CEMs are plumbed to the outlet of the gasifier as shown in Figure 17. A slip stream of product gas to be analyzed by the CEMs is drawn in through a 9.53 mm (3/8”) stainless steel sample port and delivered to the CEMs via a 6.53 mm (1/4") stainless steal tube. Because the CEM sample line is not heated any tar present in the sample stream will condense out onto the inner walls of the sample piping. However, CEM analysis of

gasification products in this study was limited to small batch samples of biomass so tar condensation in the CEM sample lines was minimal.

The gas sample stream is conditioned before being sent to the CEMs. A Balston particulate filter removes char and ash while a Balston acid mist filter is incorporated to remove acidic compounds from the sample stream.

Properly conditioned the gas sample is ready to be analyzed. A California Analytical Instruments Fuel Cell Oxygen Analyzer (Model 100F) measures the O_2 concentration of the gas. CO and CO_2 concentrations are measured with a California Analytical Instruments ZRH Infrared Gas Analyzer. The CEMs were calibrated using certified calibration gas each day they were used. Calibration ensured a minimum accuracy for the gas concentrations of ±0.1 vol/vol %.

3.1.4. Data acquisition and control

National Instruments Labview software loaded onto an IBM compatible computer provides a graphic user interface, monitors and records various operating parameters, and allows for control of some set points. The Labview software utilizes a 12 bit D/A and A/D card for data and control signals.

Temperature is measured at several locations within the gasifier and down draft combustor. Type K thermocouples with an electronic ice point are utilized for this purpose. These temperatures as well as measured concentrations from the CEMs are displayed and recorded though Labview. Samples are generally recorded at 10 second intervals during continuous feed experiments and at 1 second intervals during batch experiments.

Three pressure transducers (a Modus Instruments, model T20-05005, and two Lucas Schaevitz, model P3061-20WD) are used to monitor fluidization in the bed. One transducer measures the pressure of the bed 10.2 cm (4”) above the distributer plate relative to atmospheric pressure. The other two transducers monitor pressure differentials within the reactor. One transducer assess pressure differences between taps located 10.2 cm (4”) and 15.2 cm (6”) above the distributer plate while the other monitors taps located at 10.2 cm (4”)

and 35.6 cm (14") above the plate. In the present study this information is used qualitatively to verify that biomass is being fed into the gasifier and to ensure that the bed has not agglomerated. The biomass releases its volatile gas soon after entering the bed causing large pressure fluctuations. These are detected by the pressure transducers and displayed on the screen. Under normal fluidization the fluidizing gas essentially supports the weight of the bed. Pressure measurements at different heights above the distributor plate will yield different values corresponding to the different portions of the bed being supported above the pressure tap. Agglomeration of the bed is suggested when the pressure drop between different heights in the bed tends toward zero. As the bed agglomerates, fluidization is lost and the fluidizing gas begins to channel between the agglomerates, experiencing very little pressure drop as it makes its way to the top of the bed. The gas flow is no longer supporting all of the bed resulting in a decrease in differential pressure measurement.

The Labview software controls the electric plenum heater and the electric guard heaters which encase the gasifier. Set points for the heaters are adjusted through the graphic interface and thermocouples on the inside surface of the heaters provide feedback for the PID controllers. The fluidizing gas volumetric flow rate is adjusted through the graphic interface but a self contained mass flow controller (Alicat Laminar Mass Flow Controller rated for 0 – 150 slpm with an accuracy of ±1.5 slpm) maintains the flow at the set point.

3.2. Carbon Conversion Analysis Methodology

To facilitate uncovering the mechanisms which control carbon conversion during gasification of biomass in a bubbling fluidized bed, an analytic methodology was developed. The method is based on a mass balance of the pyrolytic fixed carbon as it enters and leaves the reactor. The term pyrolytic fixed carbon refers to the portion of the entering carbon that remains in the char after devolatilization of the biomass in the fluidized bed is complete. This is to distinguish it from fixed carbon as determined by an ASTM proximate analysis. The amount of carbon remaining after devolatilization depends on the particle temperature and heating rate [29, 30, 41-48], which are likely different during fluidized bed gasification of biomass compared to the ASTM proximate analysis. The distinction between pyrolytic and ASTM fixed carbon is explained further in a subsequent discussion. Data gathered from steady state experiments and batch experiments are combined with the pyrolytic fixed carbon

mass balance expression into a methodology. The methodology enables the fraction of the entering pyrolytic fixed carbon that is chemically converted to be distinguished from that leaving the reactor due to elutriation. Monitoring chemical and elutriation rates as operating parameters are varied reveals the mechanism which limits carbon conversion during fluidized bed gasification of biomass.

3.2.1. Model development

During gasification pyrolytic fixed carbon enters the reactor with the biomass and either leaves by being chemically converted to gas or by being elutriated as char. After initiation of gasification pyrolytic fixed carbon, in the form of char, increases in the reactor until a steady state concentration is achieved. A model based on a mass balance of the pyrolytic fixed carbon entering and leaving the gasifier is developed. The transient model incorporates experimental data and can be used to predict the carbon loading in the reactor at any instant in time. The model is integrated into a carbon conversion methodology which enables quantification of the rate that pyrolytic fixed carbon leaves the reactor by chemical processes as compared to char elutriation. Scala *et al*. [58] developed a similar technique but in the context of biomass combustion. In the following discussion the transient model is developed, evaluated, and incorporated into the carbon conversion analysis methodology.

Figure 18 shows a control volume around the gasifier. Pyrolytic fixed carbon enters the bed with the biomass at feed rate F. Pyrolytic carbon can leave the reactor by one of two means: by being converted to a carbonaceous gas or by being elutriated with char. The mass of pyrolytic carbon in the reactor (W_C) may vary with time and depends on the pyrolytic fixed carbon feed rate (F) relative to the elutriation rate (R_e) and the chemical reaction rate (R_r). Performing a mass balance on the pyrolytic fixed carbon for the control volume of Figure 18, the differential change in the mass of carbon (dW_C) in the reactor during differential time (dt) is given by:

Equation 20 $$dW_C = F\,dt - R_e\,dt - R_r\,dt$$

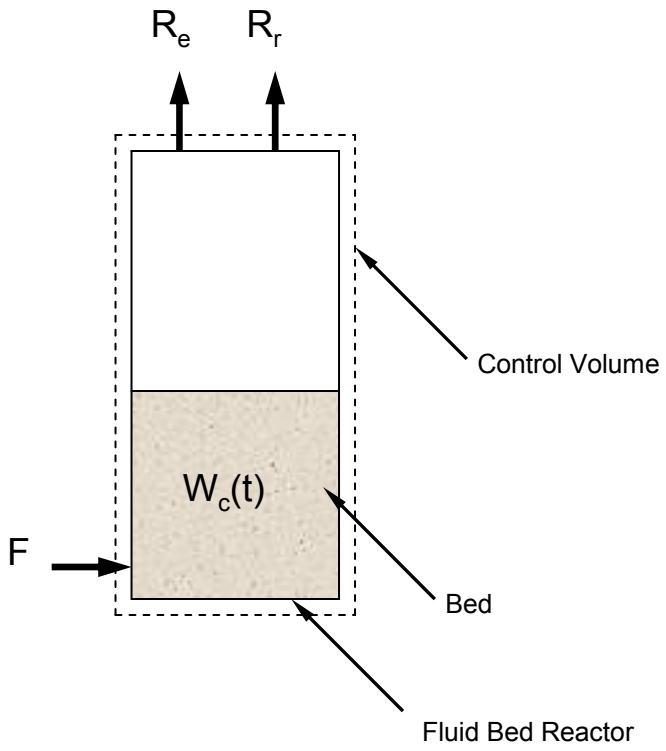

W_c = mass of carbon in the reactor (g)
F = pyrolytic fixed carbon feed rate (g/s)
R_e = pyrolytic fixed carbon elutriation rate (g/s)
R_r = pyrolytic fixed carbon chemical reaction rate (g/s)

Figure 18. Control volume used for the pyrolytic fixed carbon mass balance

which yields the differential equation:

Equation 21 $$\frac{dW_C}{dt} = F - R_e - R_r$$

Recognizing that the elutriation [79, 86] and chemical reaction rates are proportional to the mass of carbon in the reactor:

Equation 22 $$R_e = k_e W_C$$

and

Equation 23 $$R_r = k_r W_C$$

where k_e is the carbon elutriation rate constant and k_r is the gas-solid chemical reaction rate constant both with units of s^{-1}. The total carbon removal rate (R_t) is the sum of the removal rates by reaction and elutriation:

Equation 24 $$R_t = R_e + R_r = k_e W_C + k_r W_C = (k_e + k_r) W_C$$

Combining the carbon elutriation rate constant with the chemical reaction rate constant gives the total carbon removal rate constant:

Equation 25 $$k_t = k_r + k_e$$

Substitution of Equation 24 and Equation 25 allow simplification of Equation 21 to:

Equation 26 $$\frac{dW_C}{dt} = F - k_t W_C$$

Separation of variables yields:

Equation 27 $$\frac{dW_C}{F - k_t W_C} = dt$$

Given the initial condition, $W_C(t = 0) = 0$, Equation 27 is integrated as:

Equation 28 $$\int_0^{W_C} \frac{dW_C}{F - k_t W_C} = \int_0^t dt$$

If F and k_t are constant in time, the left-hand side of Equation 28 is of the form:

Equation 29 $$\int \frac{dx}{a + bx} = \frac{1}{b} \ln(a + bx)$$

Therefore integrating Equation 28:

Equation 30 $$\frac{1}{-k_t} \ln(F - k_t W_C)\Big|_0^{W_C} = t$$

which becomes:

Equation 31 $$\frac{1}{-k_t} \left[\ln(F - k_t W_C) - \ln(F)\right] = t$$

and can be rearranged as:

Equation 32 $$W_C(t) = \frac{F}{k_t} \left[1 - \exp(-k_t t)\right]$$

Given F and k_t, Equation 32 is a model that can be used to predict the mass of carbon in the reactor at any time, t. At large times ($t = t_{ss}$) a steady state carbon loading in the reactor is approached and the model reduces to:

Equation 33 $$W_C(t_{ss}) = \frac{F}{k_t}$$

rearranging:

Equation 34 $$k_t = \frac{F}{W_C(t_{ss})}$$

Equation 34 allows calculation of k_t if F and $W_C(t_{ss})$ are known. $W_C(t_{ss})$ is measured experimentally at the conclusion of a steady state gasification test as described in a subsequent section. F is the pyrolytic fixed carbon feed rate which in general depends on the temperature of the bed, the rate at which the biomass is heated in the bed, the dry biomass

feed rate, and the type of biomass being fed. In principle F can be determined using data gathered at times near the initiation of gasification. This is shown by application of a Maclaurin series expansion:

Equation 35 $$e^{ax} = 1 + ax + \frac{(ax)^2}{2!} + \frac{(ax)^3}{3!} + \dots$$

to Equation 32 to yield:

Equation 36 $$W_C(t) = \frac{F}{k_t}\left\{1 - \left[1 - k_t t + \frac{(-k_t t)^2}{2!} + \frac{(-k_t t)^3}{3!} + \cdots\right]\right\}$$

For early times ($t << 1/k_t$) the series is reasonably approximated by the first two terms giving:

Equation 37 $$W_C(t) = \frac{F}{k_t}\{1 - [1 - k_t t]\} = F t$$

Therefore the pyrolytic fixed carbon feed rate can be determined by accurate measurement of $W_C(t)$ soon after gasification is initiated:

Equation 38 $$F = \frac{W_C(t)}{t} \qquad \left(t << 1/k_t\right)$$

However, the early stages of gasification are characterized by significant temperature fluctuations as excess oxygen entrained in the bed oxidizes the initial portions of biomass entering the reactor. The pyrolytic fixed carbon feed rate depends on the temperature of the bed and therefore can not be accurately assessed during initial gasification characterized by non-isothermal behavior. An alternate method to determine F multiplies the dry biomass feed rate by the pyrolytic fixed carbon fraction as measured by batch pyrolysis experiments and is described in more detail in a subsequent section.

3.2.2. Model evaluation – population balance

The transient model for the carbon loading in the reactor given in Equation 32 assumes that the rate of carbon removal from the gasifier is proportional to the mass of carbon in the reactor. For this assumption to be valid the size distribution of the char particles in the reactor, and the average physical properties of the char, including density, porosity, and

reactivity, must all be relatively constant in time. By definition all of these properties are constant during steady state gasification and therefore the assumption that the carbon removal rate is proportional to the mass of carbon in the reactor is justified for large times. However, during transient behavior some of the listed properties may change with time. This may cause the carbon removal rate from the gasifier to no longer be strictly proportional to the mass of the carbon in the reactor, decreasing the accuracy of the model during transient behavior.

As soon as biomass is introduced into the bed the temperature increases as excess O_2 entrained in the bed rapidly combusts the entering biomass. While the properties of the entering biomass may be assumed to remain unchanged in time, the discussion in Section 2.3.2.4 makes clear that the devolatilization process and the properties of the resulting char depend on the temperature of the bed. However, the temperature transients due to initiation of gasification are short lived (5 – 10 min.) relative to the time it takes to reach the steady state carbon loading in the bed (2 – 6 hours). Therefore variations in char properties, such as the fixed carbon fraction, density, and chemical reactivity, are expected to be relatively minor during the transient development of the carbon load in the reactor. However, while variations in char properties due to temperature transients tend to decay soon after the introduction of biomass, it is unclear how the size distribution of the char in the bed evolves during startup. Gas-solid chemical reactions that are limited by mass transfer are enhanced when the surface area-to-volume ratio of the solid particles is increased. For spherical particles the surface area-to-volume ratio increases as the diameter of the particles decreases. Therefore, significant shifts in the average diameter of the population of char particles in the reactor during transient gasification would tend to decouple the carbon removal rate from the mass of carbon in the reactor. In this case the carbon removal rate from the reactor would no longer be strictly proportional to the mass of carbon in the reactor, reducing the validity of the proposed model during transient operation.

A sense of the degree to which the surface area per unit mass of the population of char particles in the reactor shifts during the initiation of gasification was determined by applying a transient model based on a population balance, which tracks the size distribution of the char particles in the reactor. It allows calculation of the instantaneous mass distribution function, $\lambda(D,t)$, of the particles as the population changes in time. The average particle diameter for the population is calculated at a given time by integrating the mass distribution function with respect to the particle diameter, D. A general description of the population balance model

can be found in reference [2]. The basic form of the population balance used for this study follows that of Junk and Brown [92]:

Equation 39
$$\frac{\partial}{\partial t}\lambda(D,t) = F(D,t) + \frac{\partial}{\partial D}\left[\frac{k}{D}\lambda(D,t)\right] - \frac{3k}{D^2}\lambda(D,t)$$

where

$\lambda(D,t)$ = instantaneous mass distribution of char (g/mm)
$F(D,t)$ = instantaneous feed rate of char per unit size (g/s/mm)
k = reaction rate coefficient (mm^2/s)
D = char particle diameter (mm)

This formulation assumes that the chemical reaction rates are limited by diffusion. Gas-solid reactions that are limited by diffusion rates occur primarily on the surface of the particle and therefore the char is assumed to shrink uniformly in diameter while maintaining a constant density. As presented, Equation 39 does not explicitly consider attrition, fragmentation, or elutriation of char. However, as a surface effect, attrition and the corresponding elutriation of the resulting fines, can be treated as an enhancement to the reaction rate coefficient, k.

The left-hand side of Equation 39 is the time rate of change of the instantaneous mass distribution function, which trends to zero as steady state operation is approached. A steady state feed rate is assumed for this study reducing the instantaneous char feed rate, F(D,t), to a constant. The second term on the right-hand side of Equation 39 represents the movement of particles from larger sizes to smaller sizes as they shrink due to chemical reaction and attrition. The last term represents the rate that mass is removed from the gasifier as gaseous products of chemical reactions or by elutriation of attrited fines.

To calculate the evolution of the mass distribution function in time a finite difference formulation of Equation 39 is developed. The mass distribution function is discretized in size by considering n particle diameter intervals, each ΔD wide. Therefore each size interval, i, contains a quantity of mass, m_i, given by:

Equation 40
$$m_i = \lambda(D_i,t)(\Delta D)$$

where D_i is the average diameter of the particles in size interval i. As mentioned, the total feed rate of char particles and its size distribution are assumed to be constant in time for this study. The distribution of the feed is discretized:

Equation 41 $F_i = F(D_i,t)(\Delta D)$

where F_i is the steady mass feed rate of char entering the reactor within size interval i. Applying the above definitions and allowing time to proceed stepwise, Equation 39 is recast to give the change in the mass of char in size interval i per time step Δt:

Equation 42 $$\frac{\Delta m_i}{\Delta t} = F_i + \left(\frac{m_{i+1}}{\Delta D} \frac{k}{D_{i+1}} - \frac{m_i}{\Delta D} \frac{k}{D_i} \right) - \frac{3 m_i k}{D_i^{\,2}}$$

The second term on the right-hand side deserves further explanation. The first portion of this term accounts for the rate that mass enters size interval i from the next largest size interval, i+1, as those particles shrink due to chemical reaction and attrition. The second part of the term accounts for the mass of particles shrinking out of size interval i and into the next smallest interval.

A finite difference equation based on Equation 42 is written for each size interval i and is entered into a spreadsheet:

Equation 43 $$m_i(t + \Delta t) = m_i(t) + \Delta t \left[F_i + \left(\frac{m_{i+1}(t)\, k}{\Delta D\, D_{i+1}} - \frac{m_i(t)\, k}{\Delta D\, D_i} \right) - \frac{3 m_i(t)\, k}{D_i^{\,2}} \right]$$

Given the feed rate, its size distribution, and the reaction coefficient, k, time is advanced and the quantity of char in the reactor increases until a steady state char loading is approached. At a given time the total mass of char in the reactor is calculated by:

Equation 44 $$W_{char}(t) = \sum_{i=1}^{n} m_i$$

The mass weighted average diameter of char particles in the reactor at a given instant in time is calculated:

Equation 45 $$D_{ave}(t) = \sum_{i=1}^{n} \frac{m_i(t)}{W_{char}(t)} D_i$$

A formula for the specific surface area, the surface area per unit mass, of the char particles in the reactor is derived by assuming that the char particles are spheres. The volume of an individual spherical char particle is given by:

Equation 46 $$V_{particle} = \frac{\pi D_{particle}^3}{6}$$

The mass of the char particle is:

Equation 47 $$m_{particle} = \rho V_{particle} = \frac{\rho \pi D_{particle}^3}{6}$$

where ρ is the density of the char. The surface area of the particle is given by:

Equation 48 $$A_{s,particle} = \pi D_{particle}^2$$

The number of particles in a given size interval i of the finite differenced population balance is found by dividing the char mass in the interval, m_i, by the mass of the average sized particle in the interval as calculated using Equation 47 with $D_{particle} = D_i$ giving:

Equation 49 $$(\text{no. of particles})_i = \frac{m_i}{\left(\rho\pi/6\right)D_i^3}$$

The total surface area of the particles in interval i is the product of the number of particles in interval i (Equation 49) and their average surface area (Equation 48):

Equation 50 $$A_{s,i} = \left(\frac{m_i}{\left(\rho\pi/6\right)D_i^3}\right)\left(\pi D_i^2\right) = \frac{6m_i}{\rho D_i}$$

Combining Equation 50 and Equation 44, the instantaneous specific surface area of the char in the reactor, a_s, is calculated as the total surface area of the char divided by its total mass:

Equation 51 $$a_s(t) = \frac{\sum_{i=1}^{n} A_{s,i}}{\sum_{i=1}^{n} m_i} = \sum_{i=1}^{n} \frac{6}{\rho D_i}\left(\frac{m_i}{W_{char}(t)}\right)$$

To test the sensitivity of the finite difference calculations to the total number of size intervals, n, three cases are presented. The three versions differ by the total number of size intervals, n, used to discretize the mass distribution function. In each case the model was given the same input information ($\Delta t = 0.01$ min, $k = 0.1$ mm^2/min, $F = 0.5$ kg/min char with diameter of 0.95 mm and 0.5 kg/min char with diameter of 0.45 mm) and was allowed to run until the total mass of char in the reactor and the average char diameter reached steady state, at which point $t = t_{ss}$. The steady state mass of char in the bed and the average char diameter for each of the three cases is given in Table 5. As shown in the table, increasing the total number of size intervals from 10 to 50 impacted the steady state mass of char in the reactor and the average particle diameter. However, a further increase from 50 to 100 intervals resulted in only minor refinement.

Table 5. Population balance: sensitivity to n ($\Delta t = 0.01$ min, $k = 0.1$ mm^2/min, $F = 0.5$ kg/min char ($D_i = 0.95$ mm) and 0.5 kg/min char ($D_i = 0.45$ mm))

Case	n	$m(t_{ss})$ (kg)	% Change from Previous Case (%)	D_{ave} (t_{ss}) (mm)	% Change from Previous Case (%)
Case I	10	1.14	-	0.741	-
Case II	50	1.11	2.46	0.721	2.71
Case III	100	1.11	0.13	0.723	0.29

The sensitivity of the finite difference calculations to the time step size was also assessed. A time step of $\Delta t = 0.01$ min was used to calculate the values given in Table 5. Using n = 100 and a time step $\Delta t = 0.005$ min gave the same asymptotic values for the mass and average diameter of the char particles in the gasifier. However, with $\Delta t = 0.02$ min the calculations for the smallest diameter intervals became unstable.

Therefore, based on the sensitivity studies a finite difference model utilizing 100 size intervals and a time step size of 0.01 min or smaller was used to perform the subsequent population balance analysis.

The impetus for introducing the population balance is to shed light on the extent that the surface area per unit mass (specific surface area) of the char in the reactor changes during

initiation of gasification. However, the degree to which the specific surface area of the char in the reactor changes during start-up is dependent on the size distribution of the char fed into the gasifier. The size distribution of the char feed, that is of the char left after devolatilization of the biomass is complete, is not known but is estimated as follows. The size distribution, as determined by screening, of the fine ground seed corn used in this study is given in Figure 19. As described in Section 2.3.2.4 biomass char tends to shrink during devolatilization. Therefore, taking the size distribution of the corn (Figure 19) and assuming that primary fragmentation does not occur and that ground seed corn char shrinks 30% during devolatilization, results in the size distribution of char shown in Figure 20. The char enters the population balance model with this size distribution through the variable F_i. Each size fraction of the incoming char is fed into the size interval i in the population balance which has a size closest to that of the char fraction. The other input parameters for the population balance model are given in Table 6. The specific surface area of the char in the reactor, a_s, is calculated for these conditions using Equation 51 and is plotted as a function of time in Figure 21. The figure shows a sudden decrease in surface area early in time and more gradual behavior as the simulation approaches steady state. For this case the specific surface area drops from an initial value of 45 mm^2/g down to a steady value of 27 mm^2/g - a 40% decrease. Although the population balance predicts a significant decrease in surface area, much of the decrease happens soon after gasification begins and therefore it is not obvious to what extent this change in surface area compromises the validity of the pyrolytic fixed carbon mass balance model developed in Section 3.2.1. To assess the impact this decrease in specific surface area has on the accuracy of the mass balance model, the results of the population balance simulation are used to formulate a mass balance model and the results of the two simulations are compared.

Table 6. Population balance input parameters

Input Paramter	Symbol	Value
time step size	Δt	0.00500 min
reaction rate coeficient	k	0.100 mm^2/min
maximum char diameter	D_{max}	2.20 mm
size interval width	ΔD	2.20 mm/100
char density	ρ_{char}	300 kg/m^3
total char feed rate	F	1.00 kg/min

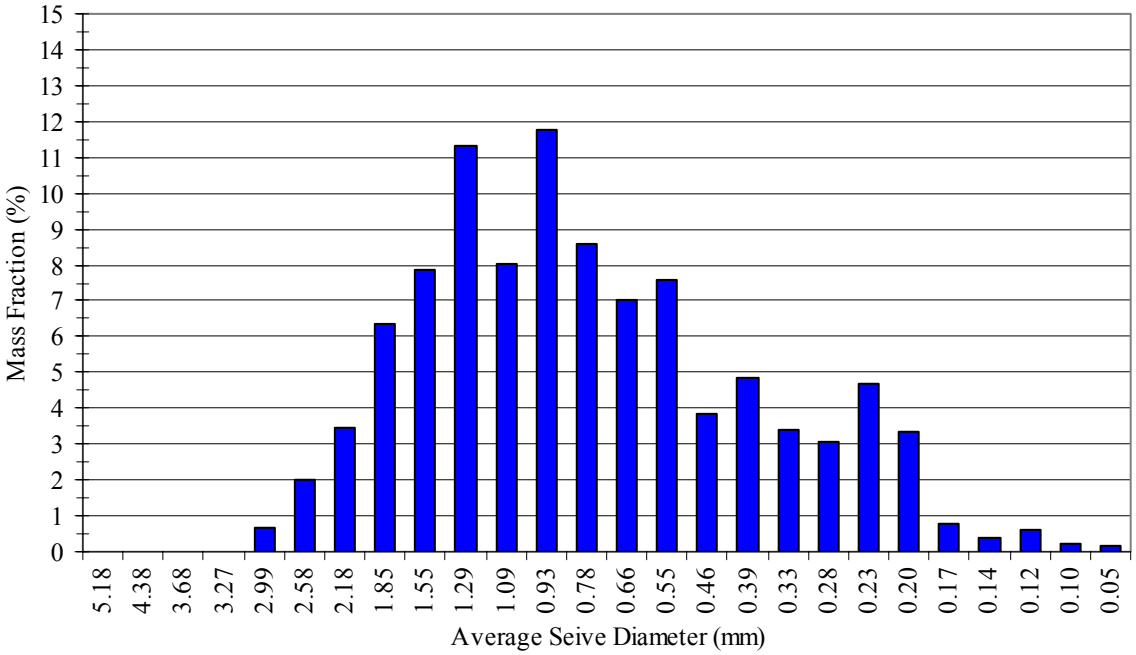

Figure 19. Size distribution of fine ground seed corn as determined by screening

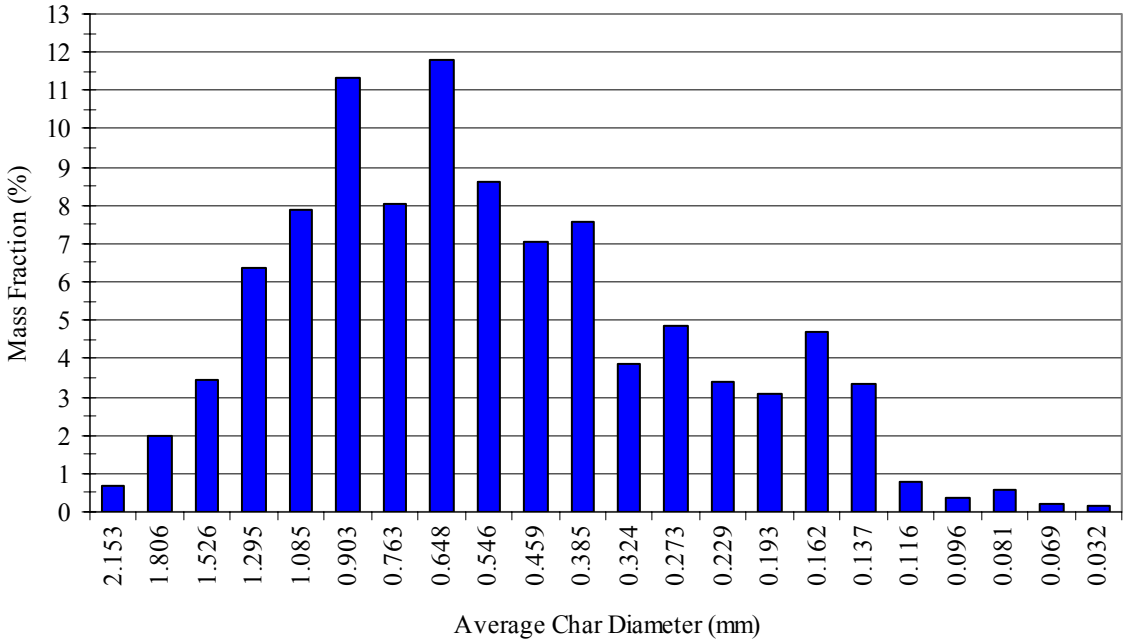

Figure 20. Estimated size distribution of char produced from fine ground seed corn

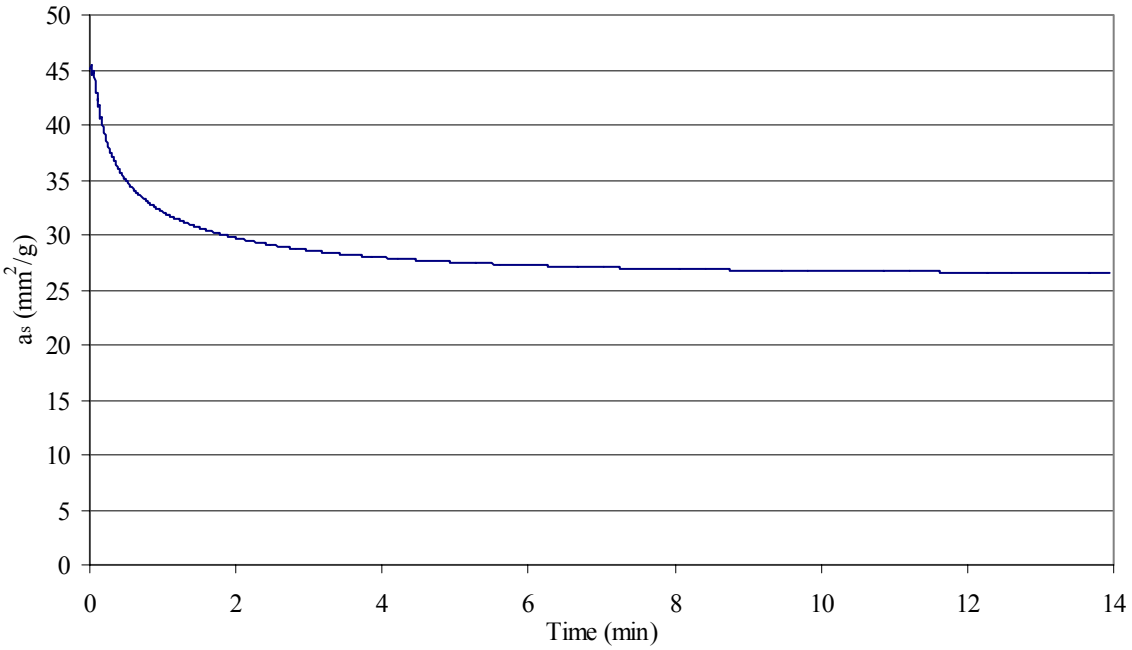

Figure 21. Population balance: specific surface area as a function of time

Application of the mass balance model is outlined in Section 3.2.1. Although the mass balance model was developed to assess the flow of fixed carbon in the reactor it is equally applicable to tracking the flow of char as char is essentially composed of carbon. The instantaneous mass of char in the bed, $W_{char}(t)$ as estimated with the population balance model (Equation 44), is plotted as a function of time in Figure 22. The figure shows the mass of char in the gasifier increasing from an initial value of zero to a steady state loading ($W_{char}(t_{ss})$) of 1.26 kg. The feed rate of char, F, for these simulations is set at 1.00 kg/min which is used in conjunction with $W_{char}(t_{ss})$ in Equation 34 to calculate k_t to be equal to 0.794 min^{-1}.

The mass balance model's expression for the instantaneous mass of char in the reactor is written by substituting the k_t and F values from the population simulation, into Equation 32:

$$W_{char}(t) = 1.26\left[1 - \exp(-0.794t)\right]$$

where t is in minutes and W_{char} is in kg. The mass balance model's prediction of W_{char} as a function of time is also plotted in Figure 22. As shown in the figure the mass balance model over predicts the mass of char in the reactor at times by as much as approximately 25% when compared to the population balance simulation. While the match between the predictions of

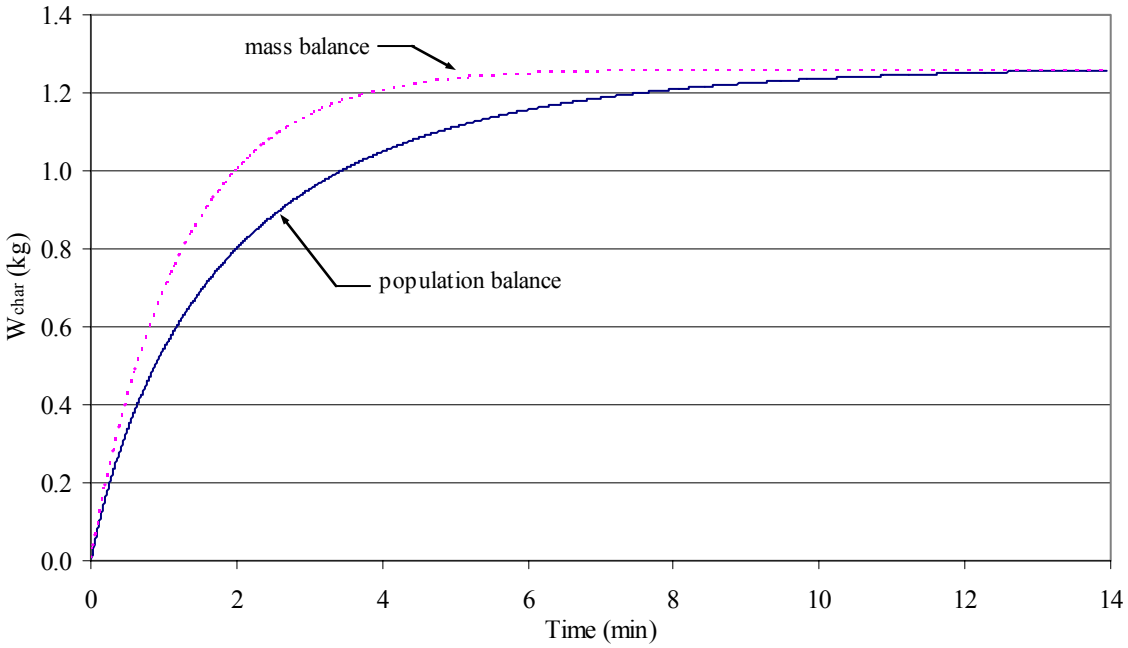

Figure 22. Mass of char in the reactor as predicted by the population balance model and the mass balance model

the two models is not perfect, the two simulations agree to within 10% for most times despite the 40% variation in the specific surface area.

3.2.3. Model evaluation – experimental

The transient mass balance model is further evaluated by comparing predicted reactor carbon loadings to experimentally measured values. To apply the mass balance model the steady state mass of carbon in the reactor, $W_C(t_{ss})$, for a particular set of operating conditions is required. The mass of the carbon in the reactor is measured by combusting the carbon in the reactor at the conclusion of a steady state experiment. The carbon content of the reactor is assessed by summing the carbon that leaves the reactor as a gas or as char during this combustion or burnout phase. A detailed description of the measurement of $W_C(t_{ss})$ using this technique is given in Section 3.2.4. Table 7 shows measurements of $W_C(t_{ss})$ made for two experiments that gasified ground seed corn (11.0 wt % moisture) at 715°C with an ER equal to 0.27. Both measurements were made by burning out the bed after more than eleven hours of gasification and when averaged give $W_C(t_{ss})$ equal to 390 g of carbon. To complete

the formulation of the mass balance model the pyrolytic fixed carbon feed rate, F, is also required. In principle F can be determined using Equation 38 and measurement of the carbon loading in the reactor near the initiation of gasification. At early times F is the slope of the carbon loading transient as illustrated in Figure 23. However, in practice, temperature fluctuations in the bed, caused by the combustion of biomass when it is first introduced into the bed, prevent accurate measurement of F by this method. Therefore F is alternatively found as the product of the pyrolytic fixed carbon fraction and the dry biomass feed rate:

Equation 52 $$F = f \times \dot{m}_{b,dry}$$

The pyrolytic fixed carbon fraction, f, refers to the portion of the entering carbon that remains in the char after devolatilization of the biomass in the fluidized bed is complete and is revealed through batch pyrolysis experiments described in a subsequent section. For ground seed corn devolatilized at 715°C pyrolysis experiments show f to be 0.137 g of pyrolytic fixed carbon per g of dry ground seed corn. The dry biomass feed rate for the data of Table 7 is 0.662 g/s, resulting in F equal to 0.0906 g of pyrolytic fixed carbon/s. With F and $W_C(t_{ss})$ determined k_t is calculated using Equation 34 to be 232×10^{-6} s. The values of F and k_t are substituted into Equation 32 yielding the transient model for the fixed carbon load in the reactor in grams:

Equation 53 $$W_C(t) = 390\left[1 - \exp(-0.000232\, t)\right]$$

This expression predicts the pyrolytic fixed carbon load in the reactor as a function of time when gasifying at the stated conditions. The model and the data used to generate it are shown in Figure 23.

Table 7. Steady state reactor carbon loads for gasification of ground seed corn at 715°C with an ER of 0.27

Time Gasifying (hr)	$W_C(t_{ss})$ (g)
11.5	400
11.6	380

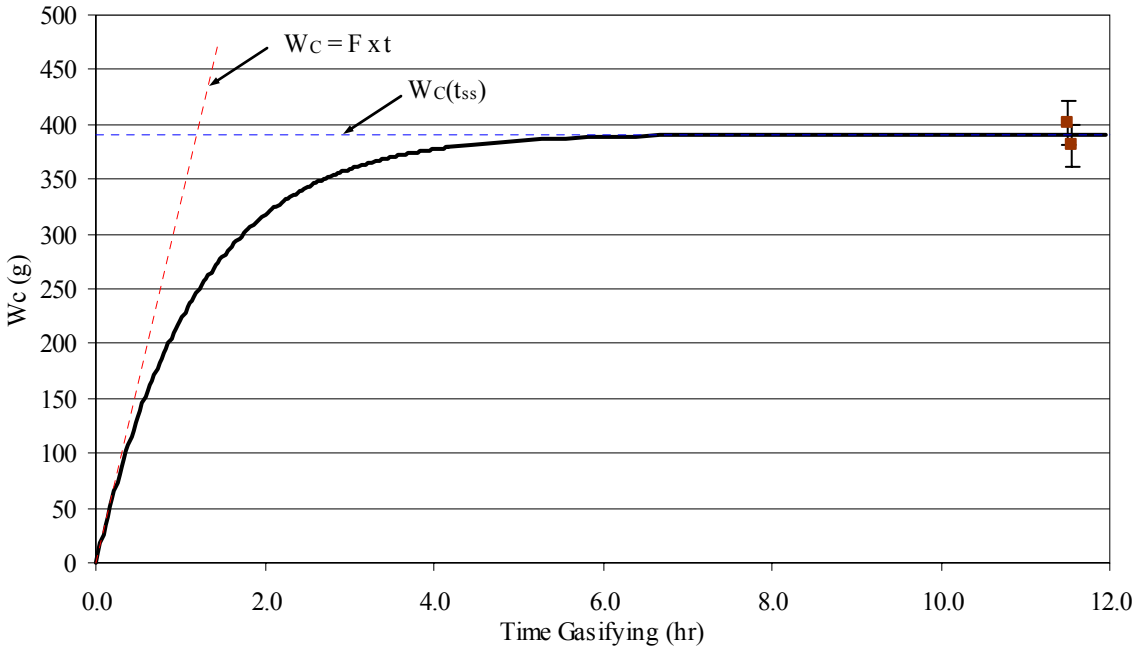

Figure 23. Reactor carbon load transient model and the experimental data used to generate it for gasification of ground seed corn at 715°C with ER = 0.27

Evaluation of the model is accomplished by making additional measurements of the mass of carbon in the reactor after various lengths of time gasifying ground seed corn at the same conditions used to generate the model. Figure 24 compares experimentally determined carbon loads in the reactor to the transient loading profile predicted by the mass balance model. The figure shows excellent agreement between the measured loads and those predicted by the model. The relatively large error bars early in time reflect unsteady behavior during start-up of gasification. The temperature of the bed jumps 50°C to 100°C when biomass is first introduced into the reactor. Temporal fluctuations in the bed temperature persist for approximately the first 15 minutes of gasification. The rate that fixed carbon is fed into the gasifier depends on pyrolytic fixed carbon fraction of the biomass which, in turn, depends on the devolatilization temperature [29, 30, 41-48]. At lower bed temperatures larger fractions of the incoming biomass remain in the bed as pyrolytic fixed carbon. As bed temperatures increase, more of the carbon in the entering biomass is converted to gas during pyrolysis, leaving behind smaller quantities of fixed carbon. For short gasification experiments the variation in the pyrolytic fixed carbon feed rate due to temperature transients can significantly affect the instantaneous amount of carbon accumulated in the reactor. However, as the time spent gasifying becomes long compared to

the initial temperature transients, the time averaged pyrolysis temperature approaches the isothermal gasification temperature used to generate the model. This gives rise to decreased uncertainties later in time as shown in Figure 24.

The model is compared to additional experimental data in Figure 25. The data of Figure 24 is also included in Figure 25 for comparison of ER values. The new data is for the gasification of ground seed corn (11 wt % moisture) at 719°C and an ER = 0.31. Once again very good agreement is demonstrated between the pyrolytic fixed carbon mass balance model and the experimentally measured reactor carbon loadings. Also note the dramatic impact that the ER value has on the carbon loading. These ER effects are considered in detail in Section 4.2.2.

The pyrolytic fixed carbon mass balance model has been compared to a population balance model and to experimental data. It has been shown to be in general agreement with the population balance model and capable of replicating experimental data accurately. In addition it should be noted that although the mass balance model is derived and evaluated as a transient model it is utilized in the present study to analyze gasification during steady state operation. During steady state operation the mass balance models inability to account for transient development of the size distribution of the char in the reactor does not impact its accuracy. By definition the size distribution of the char particles in the reactor should not fluctuate significantly with time at steady state and therefore any model inaccuracies associated with these variations should disappear. At steady state the accuracy of the model becomes dependent only on the accuracy of the experimental measurements made under steady state operation and not on the model's ability or inability to predict transient behavior. Although the pyrolytic fixed carbon mass balance model is able to predict the build-up of carbon in the reactor with time, its real power is realized during steady state gasification when, coupled with steady state elutriation data, it is used to discern the relative importance of the mechanisms by which carbon leaves the gasifier.

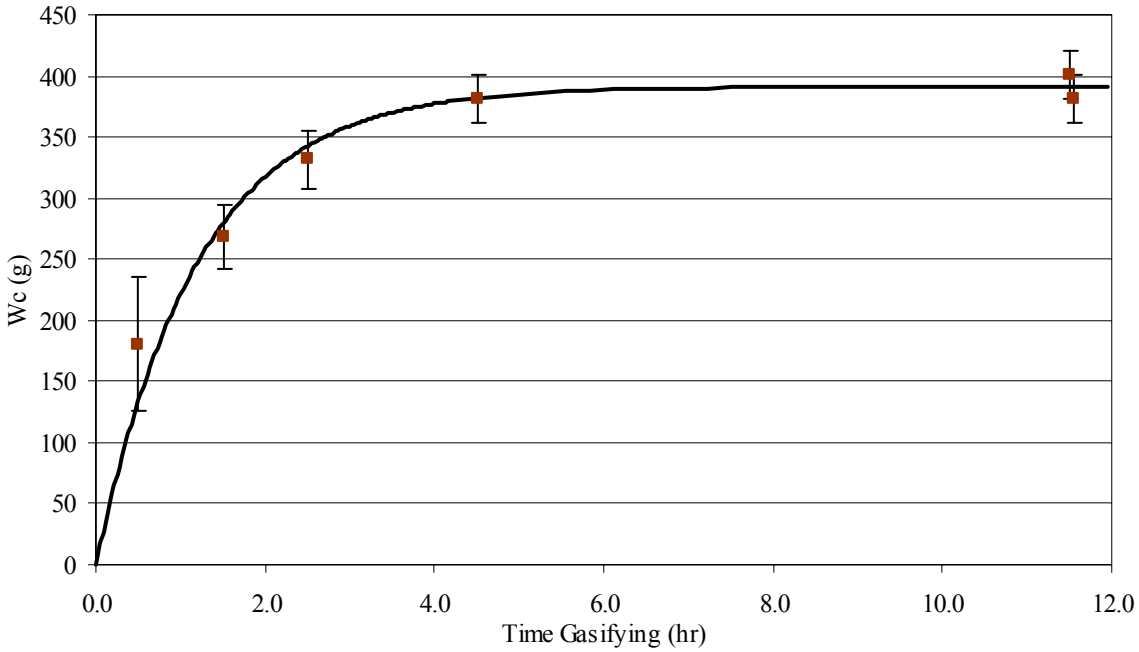

Figure 24. Comparison between experimentally determined carbon loads in the reactor and model predictions for gasification of ground seed corn at 715°C with ER = 0.27

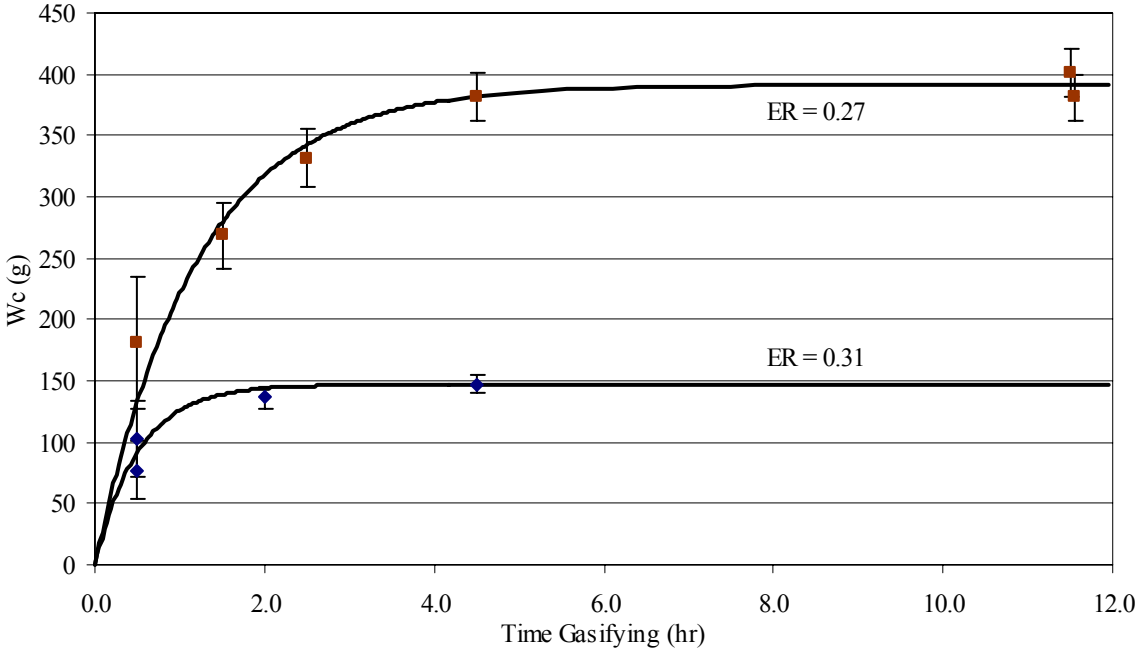

Figure 25. Comparison between experimental carbon loads in the reactor and model predictions for gasification of ground seed corn at 715°C and two ER values

3.2.4. Carbon loading in the reactor

The carbon loading, $W_C(t)$, is the total mass of carbon present within the reactor at a given instant in time and is required to perform the pyrolytic fixed carbon mass balance. It includes the carbon in the char as well as in the volatiles. During early times after initiation of gasification, carbon loadings will be small with a majority of the carbon present due to volatiles. However, as gasification continues the quantity of char builds in the reactor while the carbon contribution of the volatiles remains essentially constant. Given sufficient time at consistent gasification conditions the mass of carbon in the reactor approaches a steady state value. With a relatively consistent volatile contribution across the gasification experiments of this study, the magnitude of the steady state carbon loading in the reactor is directly tied to the average residence time of the char particles in the reactor. Large char residence times correspond to large carbon loadings in the reactor and vise versa. The residence time for a particular char particle may depend on several factors including its size, reactivity, and susceptibility to comminution. A methodology to measure the total mass of carbon present in the fluidized bed gasifier at a given instant in time is developed in the following discussion.

The amount of carbon accumulated in the reactor during a test is determined by combusting it at the end of the test while monitoring the gaseous carbon and the solid carbon content of the gas stream leaving the gasifier. Therefore the first step in assessing the carbon loading is to transition from gasification mode to combustion mode by discontinuing the biomass feed. If the bed is fluidized with air or O_2, combustion of the bed contents begins immediately. Burnout, as it is often called, can take from minutes to hours depending on several factors including the amount of carbon in the reactor, the reactivity of the carbon, and the amount of air supplied to the bed. During burnout carbon can leave the reactor by being converted to a gas or by being elutriated with char. The carbon content of the product stream leaving the reactor is quantified with the cyclone particulate separator and the isokinetic sample train shown in Figure 17.

After the product stream leaves the gasifier it flows through a cyclone separator which removes most of the large (>10 μm) particulate matter. At the beginning of burnout a clean, pre-weighed cyclone catch can is installed on the cyclone to collect the removed particulate. The concentration of particulate matter in the producer gas downstream of the cyclone is determined by drawing an isokinetic sample of the gas as described in Section 3.1.2. The

isokinetic sample flow rate is adjusted with the rotameter to obtain parity between the gas velocity at the probe tip and that in the gasifier outlet stream.

The velocity of the gas in the gasifier outlet piping can be calculated given the volumetric flow rate of the fluidizing air at standard temperature and pressure (STP), the N_2 concentration in the exiting gas, and the cross sectional area of the outlet piping. The calculation is based on the fact that on a dry basis the nitrogen concentration of the fluidizing air will be diluted in proportion to the additional volume of gas released during gasification and is given by:

Equation 54 $$V_{pg} = \frac{n_{N_2,a}}{n_{N_2,pg}} \frac{Q_a}{A_{pipe}}$$

where

V_{pg} = average producer gas velocity in the outlet pipe

$n_{N_2,a}$ = volume fraction of N_2 in dry air = 0.7808

$n_{N_2,pg}$ = volume fraction of N_2 in the dry producer gas at STP

Q_a = volumetric flow rate of fluidizing air at STP

A_{pipe} = inner cross sectional area of the outlet pipe

The N_2 concentration in the producer gas is measured with the micro-GC. The required volumetric flow rate in the isokinetic sample system, Q_{probe}, is calculated so that the flow velocity in the isokinetic probe matches the velocity in the gasifier outlet pipe:

Equation 55 $$Q_{probe} = V_{pg} \times A_{probe}$$

where

A_{probe} = cross sectional area at probe tip

The particulate matter in the isokinetic sample stream is substantially removed in the quartz thimble filter described in Section 3.1.2. The thimble filter is held at 450°C during sample collection to prevent tar from condensing in the filter. Therefore, new thimble filters are prepared by baking them at 450°C for a minimum of 15 minutes to drive off moisture and

volatiles. The baked thimble filter is weighed on a AE ADAM AAA/L Series high precision scale while still warm to establish it's clean, dry condition.

After burnout is complete the cyclone catch and thimble filter are weighed to determine the mass of particulate captured by each. The cyclone catch can is sealed immediately after it is removed from the cyclone to minimize variations in the mass of the collected material due to movement of moisture and/or volatile organics to or from the char. When possible the thimble filter is recovered from the heated enclosure and weighed while still warm. At times when fresh recovery is not feasible, the filter is reheated to 100°C for a minimum of 30 minutes to drive off any absorbed moisture and then removed and weighed warm.

The particulate removed from the gas stream by the cyclone and thimble filter contains carbon and ash. The carbon content of the cyclone and filter catch is determined by ashing. One to three samples of well mixed char and ash from the cyclone catch are weighed in crucibles. The cyclone catch samples and the recovered thimble filter are ashed by placing them in a bench top furnace held at 700°C - 800°C for a minimum of four hours. The char samples and thimble filter are removed from the furnace and weighed while still warm. The fraction of mass lost during ashing is attributed to oxidation of the carbon present in the sample.

The total quantity of carbon leaving the reactor by elutriation is the sum of the mass of carbon in the coarse particulate matter captured in the cyclone ($m_{C,PMC}$) and the mass of carbon in the fine particulate matter ($M_{C,PMF}$) which passes through the cyclone. The mass of carbon filtered by the cyclone is determined by multiplying the total mass of material collected with the cyclone by the carbon fraction of its catch as determined by ashing samples of the collected material. The concentration of carbon downstream of the cyclone is estimated using the thimble filter catch of the isokinetic slip stream as follows:

Equation 56
$$m_{C,PMF} = \frac{m_{C,thimble} Q_a}{Q_{probe}}$$

where

$m_{C,thimble}$ = mass of carbon collected in the thimble filter

The mass of the carbon in the thimble filter is determined by ashing as described above. The average volume flow rate of the sample is calculated by dividing the total volume of the

isokinetic sample measured using the dry test meter (see Section 3.1.2), by the sampling time. The sampling time is the time required to complete burnout.

During burnout the gaseous carbon content of the gas stream leaving the bed is estimated by analyzing the isokinetic sample flow using the micro-GC. The isokinetic sample system is shown in Figure 17. The GC is the last station in the sample train and is used to determine the concentrations of N_2, O_2, H_2, CO, CO_2, CH_4, C_2H_2, C_2H_4, C_2H_6, and C_3H_8 in the particulate, tar, and moisture free sample flow. Figure 26 shows concentration vs. time profiles for CO, CO_2, CH_4, and C_2H_4 as measured by the GC beginning near the end of gasification and on through bed burnout (see experimental data sheet 20060608 in Appendix A for gasification parameters). The contributions of C_2H_2 and C_3H_8 to the total carbon loading in the reactor proved to be insignificant and these and other hydrocarbons larger than C_2H_6 released during burnout were not included in calculating the carbon loading. The concentration of C_2H_6 is small (0.3 vol %) and therefore is not displayed in Figure 26 but the contribution of C_2H_6 is included as part of the calculations to determine the instantaneous mass of carbon in the gasifier.

Owing to the length of the sample train there is a time lag between gas sampling and gas analysis. As shown in Figure 26 the concentrations of CO, CO_2, CH_4, and C_2H_4 are at or near their maximum values at the point of transition from gasification to burnout. Therefore to accurately assess the amount of carbon in the gasifier when burnout is started, it is important that the inherent time lag in the GC sample train be accurately accounted for in the calculations. The lag time for a particular sample flow rate was determined by a series of step tests. In the absence of fuel, a step change in the composition of the gas being supplied to the gasifier was initiated and after a certain length of time a GC analysis of the sample flow was performed. The length of the time between the step change and the GC sample was decreased for each test until the GC no longer detected the step change. The lag time in the sample system at a particular sample flow rate is the shortest length of time between the step change and GC sample for which the GC is still able to detect the change in the gas concentration. Table 8 presents a summary of the results of these step tests for three sample flow rates. For sample flow rates of 1 – 3 slpm the lag times ranged from a maximum of nearly three minutes down to one and half minutes. As expected higher sample flow rates lead to shorter sample system response times. The linearity of the data in Table 8 is evident, justifying linear interpolation between the listed values.

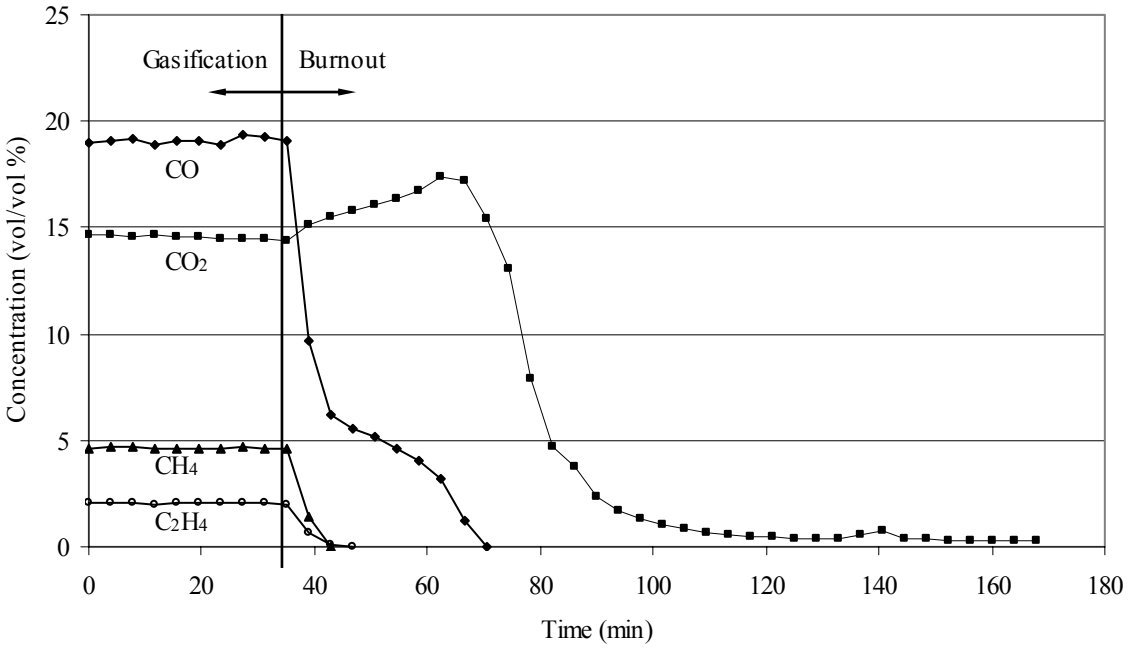

Figure 26. Transient gas concentrations during the bed burnout of test number 20060608 (see Appendix A)

Table 8. GC sample system lag times for various sample flow rates

Sample Flow Rate (slpm)	GC Time Lag (s)
1	166
2	127
3	90

The mass of carbon that leaves the bed as a gas during burnout is determined by integrating the transient carbonaceous gas concentration profiles in time. The integration starts at the beginning of burnout and ends when the carbon content of the burnout products becomes insignificant. The GC analysis of the burnout products is discrete, sampling approximately every four minutes. Therefore integration of the concentration profiles is estimated using a finite difference approximation. The mass of gaseous carbon leaving the reactor with gas species i over the time period Δt is given by:

Equation 57 $$\Delta m_{C,i} = \frac{n_{N_2,a}}{n_{N_2,p}} Q_a \, \Delta t \, \frac{n_{i,ave} M_{C,i}}{\bar{v}_{IG}}$$

where

i = CO, CO_2, CH_4, C_2H_4, and C_2H_6

$n_{N_2,p}$ = average N_2 concentration in the products over Δt

$n_{i,ave}$ = average volume fraction of carbonaceous gas species i over Δt

$M_{C,i}$ = molecular weight of carbon in carbonaceous gas species i

Δt = discrete time step

$\bar{v}_{IG}$ = molar specific volume for an ideal gas at STP = 22.4 L/mol

The first term in this expression uses the ratio of the nitrogen concentration of the air entering the gasifier to the nitrogen concentration in the gas leaving the gasifier, and the volumetric flow rate of air entering the unit, and the time period to estimate the volume of product gas that left the gasifier during Δt. The second portion of Equation 57 calculates the mass of carbon per unit volume.

To find the total mass of gaseous carbon leaving the reactor, Equation 57 is summed over all the discrete time intervals, Δt, starting from the beginning of burnout (t = 0) until its conclusion ($t = t_f$) and for each carbonaceous gas species i (CO, CO_2, CH_4, C_2H_4, and C_2H_6):

Equation 58 $$m_{C,gas} = \sum_{i} \sum_{t=0}^{t=t_f} \Delta m_{C,i}$$

Therefore the total mass of carbon in the reactor, W_C, at a given instant during gasification, is given by the sum of the carbon that leaves the reactor as either elutriated solid or as a gas during a burnout, which was initiated at that instant:

Equation 59 $$W_C = m_{C,PMC} + m_{C,PMF} + m_{C,gas}$$

3.2.5. Biomass feed rate

During steady feed rate experiments biomass is injected into the gasifier using the hopper/auger system. The average biomass feed rate during these tests is determined by performing a "hopper balance". In preparation for a steady feed rate experiment the hopper is filled with a known quantity of biomass by weighing it with a CCI HS-30 load cell. After each test, or two tests if the same feed rate is used for both, the contents of the hopper are carefully removed and weighed with the load cell to determine the total mass of biomass remaining in the hopper. The difference between the mass of material loaded into the hopper initially and that remaining in the hopper after the completion of the test gives the total quantity gasified. This procedure is referred to as "balancing the hopper". The length of time that fuel is fed into the gasifier is also recorded, allowing calculation of the average biomass feed rate.

3.2.6. Pyrolytic fixed carbon fraction

The term pyrolytic fixed carbon fraction, f, refers to the portion of the entering carbon that remains in the char after devolatilization of the biomass in the fluidized bed is complete. This is to distinguish it from fixed carbon as determined by an ASTM proximate analysis. The amount of carbon remaining after devolatilization depends on the particle temperature and heating rate [29, 30, 41-48], which are likely different during fluidized bed gasification of biomass compared to the ASTM proximate analysis. Although temperature and heating rate wield the most influence on the fixed carbon fraction, the length of time that devolatilization is allowed to proceed may also have an impact, as secondary pyrolysis can continue over several minutes.

Proximate analysis uses a method based on ASTM D3172 [93]. The specifics of the method are listed in Table 9. As noted in the table, the volatile matter content of the biomass is determined by pyrolyzing the sample in a covered crucible at 950°C for 7 minutes and noting the resulting mass loss. Combustible material remaining in the sample after pyrolysis is removed during ashing. The mass lost during ashing is attributed to fixed carbon. While the proximate analysis methodology provides a standardized means of comparing different types of biomass it does not accurately model the conditions experienced by biomass in the bubbling fluidized bed gasifier used for this study in at least three significant ways. First, the

pyrolysis temperature of 950°C used for the ASTM test is higher than the gasification temperatures (700°C - 800°C). Secondly, the heating rates of the biomass sample in a covered crucible are expected to be much lower than those experienced in the dynamic environment of the fluidized bed. Finally, devolatilization is allowed to proceed for 7 minutes during the ASTM test while the average char residence time in the bed can exceed 20 minutes. Given the differences between the ASTM methodology and actual gasification, measurement of the pyrolytic fixed carbon fraction under gasification conditions is warranted.

Table 9. Proximate analysis test method based on ASTM D3172 [93]

Component	Temperature	Time	Conditions
moisture	105°C	1 hour	24 LPM desiccated air
volatile matter	950°C	7 minutes	covered crucible - reducing
ash	20 - 250°C (ramp)	20 minutes	12 LPM air exchange
	250 - 500°C (ramp)	20 minutes	12 LPM air exchange
	500 - 600°C (ramp)	20 minutes	12 LPM air exchange
	600°C	3 hours	12 LPM air exchange
fixed carbon (by difference)	-	-	-

Biomass can be batch fed into the gasifier utilizing a system of two valves, which empty into the injection auger as shown in Figure 27. With the bottom valve closed, the top valve is opened and a batch sample of biomass is added. The top valve is then closed and the lower valve is opened to admit the biomass batch into the injection auger system, which rapidly feeds it into the bed. Batch pyrolysis experiments were designed to measure the variation of the pyrolytic fixed carbon fraction, f, with temperature under gasification conditions. Proper design of the batch pyrolysis methodology that adequately replicates the devolatilization environment while maximizing the accuracy of the results required careful consideration of the details of biomass pyrolysis.

3.2.6.1. Biomass pyrolysis

Biomass pyrolysis comprises two stages: primary and secondary [47, 49, 50]. Primary pyrolysis is characterized by rapid release of volatile gas during the first few seconds after

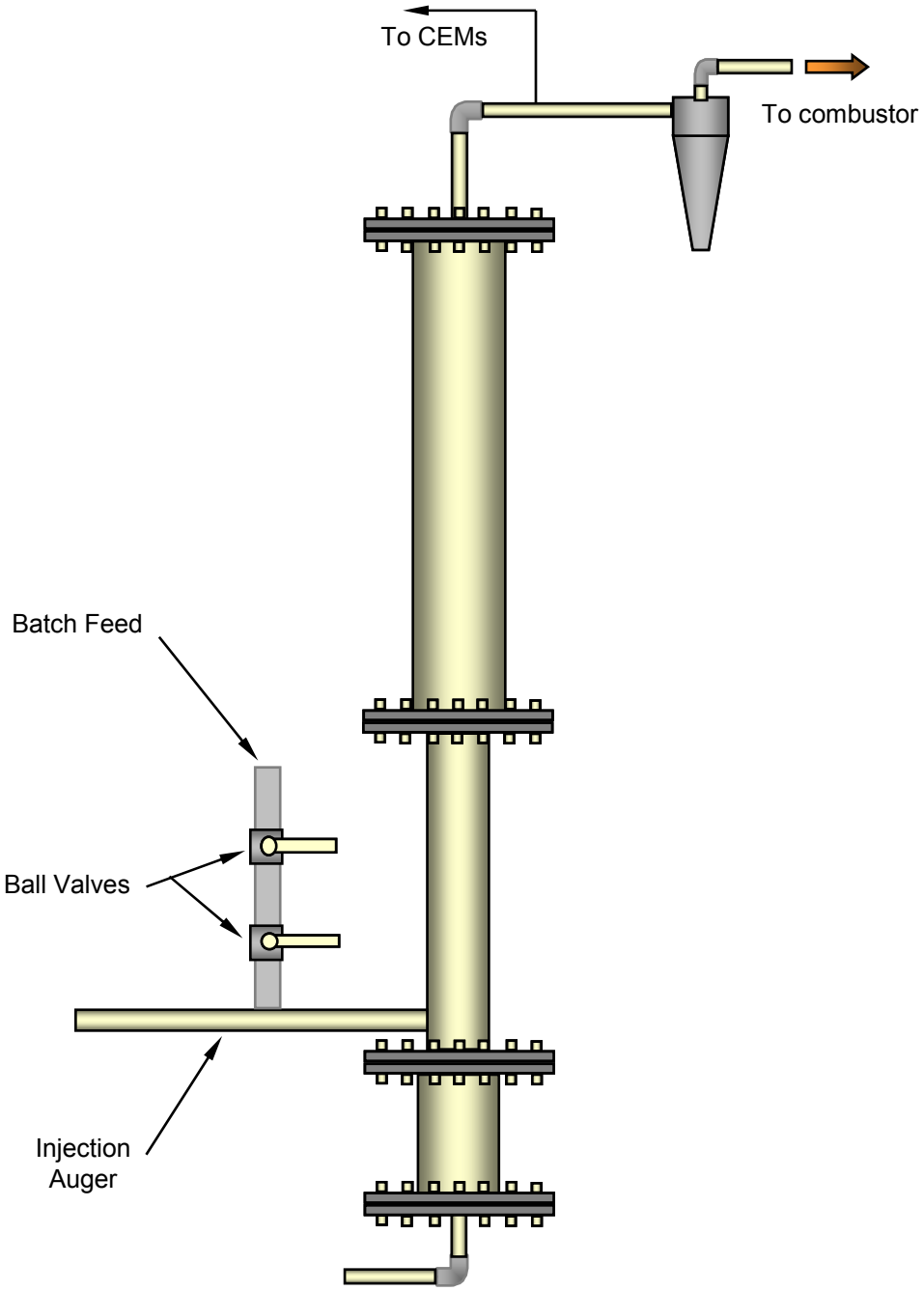

Figure 27. Gasifier with batch feed system installed

the biomass has entered the bed. By contrast, secondary pyrolysis proceeds at much lower rates, occurring over the course of several minutes [47, 49, 50]. Over 90% of the volatile gas is released during primary pyrolysis [49]. Although not fully understood, secondary pyrolysis may be driven by free oxygen in the biomass char reacting with the char carbon to form CO_2. The rate and extent of primary and secondary pyrolysis depends, among other things, on the heat transfer rate as well as on the pyrolysis temperature [47, 49].

Figure 28 is a plot of primary and secondary devolatilization for 5 grams of ground seed corn injected into a bed fluidized with N_2 and maintained at 800°C with the electric heaters surrounding the gasifier. Continuous emission monitors (CEMs), described in Section 3.1.3, were used to record the CO_2 concentration vs. time profile during pyrolysis. Although the CEM sampling system is not fast enough to accurately assess the peak concentration during primary pyrolysis, it is able to distinguish between primary and secondary pyrolysis as shown in the figure. The CO_2 concentration peaks very soon after biomass injection, decreases rapidly as primary devolatilization concludes, and then tails off more slowly during the secondary release. The radically different time scales for primary and secondary pyrolysis suggests that the process can be approximated by a two term exponential decay model of the form:

Equation 60 $$n_{CO_2} = A_p \exp\left(-t/\tau_p\right) + A_s \exp\left(-t/\tau_s\right)$$

The parameters τ_p and τ_s are the decay time constants for primary and secondary pyrolysis, respectively. The parameter A_p is the pre-exponential constant for the decay of the primary pyrolysis products while A_s serves that role for secondary pyrolysis. The constants in this expression were determined by comparison of the model to experimental data for early times (primary pyrolysis) and for later times (secondary pyrolysis). In both cases the decay expression was linearized by taking the natural log and was then fit to experimental data to assess the constants. For the data of Figure 28 A_p is equal to 0.2, τ_p is 0.2 min, A_s is found to be 0.009, and the time constant for secondary pyrolysis, τ_s, is 7 min. With these parameters the resulting CO_2 decay expression for the data of becomes:

Equation 61 $$n_{CO_2} = 0.2\exp\left(-t/0.2\,\text{min}\right) + 0.009\exp\left(-t/7\,\text{min}\right)$$

Figure 29 plots the decay expression and the data used to generate it. For clarity, the experimental data in this figure is plotted as a solid line while symbols are used to display the decay model. The figure shows that the two term decay model is a good approximation of the transient CO_2 concentration profile during pyrolysis of ground seed corn. Knowledge of the relative magnitude and time duration of primary pyrolysis compared to secondary pyrolysis was used to design the batch pyrolysis experiment methodology described in the next section.

Primary and secondary pyrolysis are driven by thermal energy. As evidenced by their decay parameters, secondary pyrolysis occurs slowly compared to primary pyrolysis, releasing a small quantity of volatile matter over an extended period of time. Therefore, secondary pyrolysis requires lower rates of energy addition to proceed than does primary pyrolysis. Although the time constant for the decay of secondary pyrolysis products is much greater than for primary pyrolysis, it is still less than the average residence time of the char in the reactor during the steady state gasification experiments of this study which ranged between 21 – 77 minutes. (The average char residence time for the steady state experiments can be found in Appendix A.) With the average char particle residing in the reactor a minimum of three times longer than τ_s and over 100 times longer than τ_p, nearly all of the biomass particles in the reactor during steady state gasification will have finished primary devolatilization and the vast majority will have experienced extensive secondary pyrolysis. Therefore, the carbon present in a steady state reactor is predominately fixed carbon. This conclusion has significant ramifications for the design of the batch experiments subsequently described.

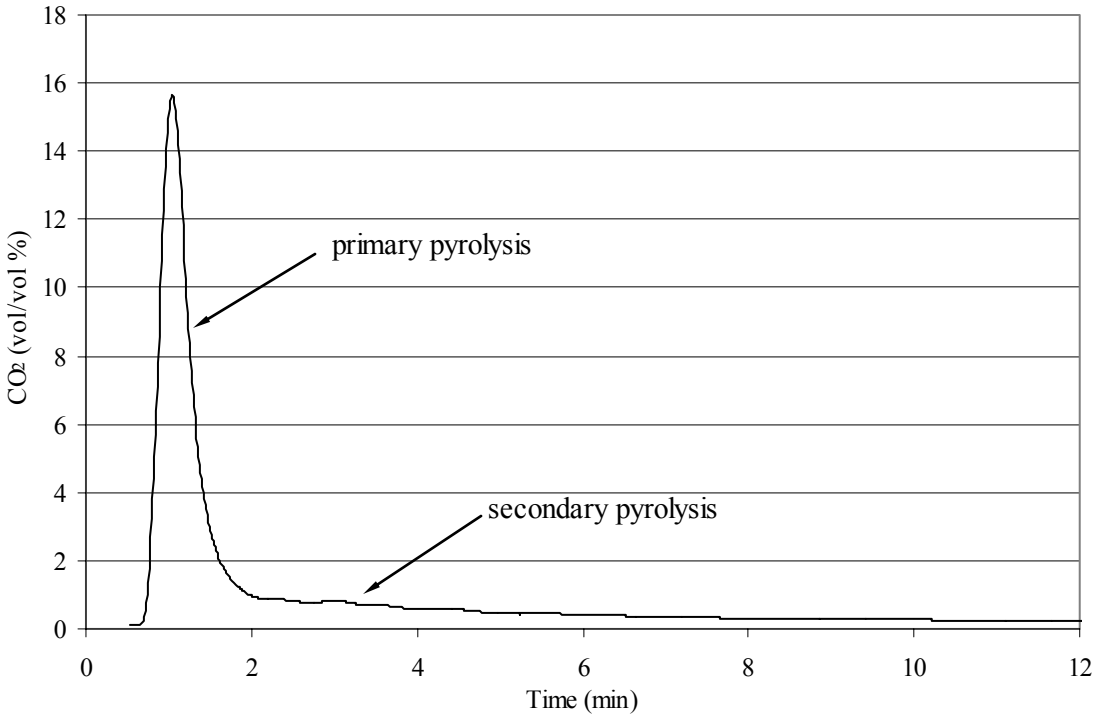

Figure 28. CO_2 as a function of time for pyrolysis of 5 g of ground seed corn in a fluidized bed maintained at 800°C

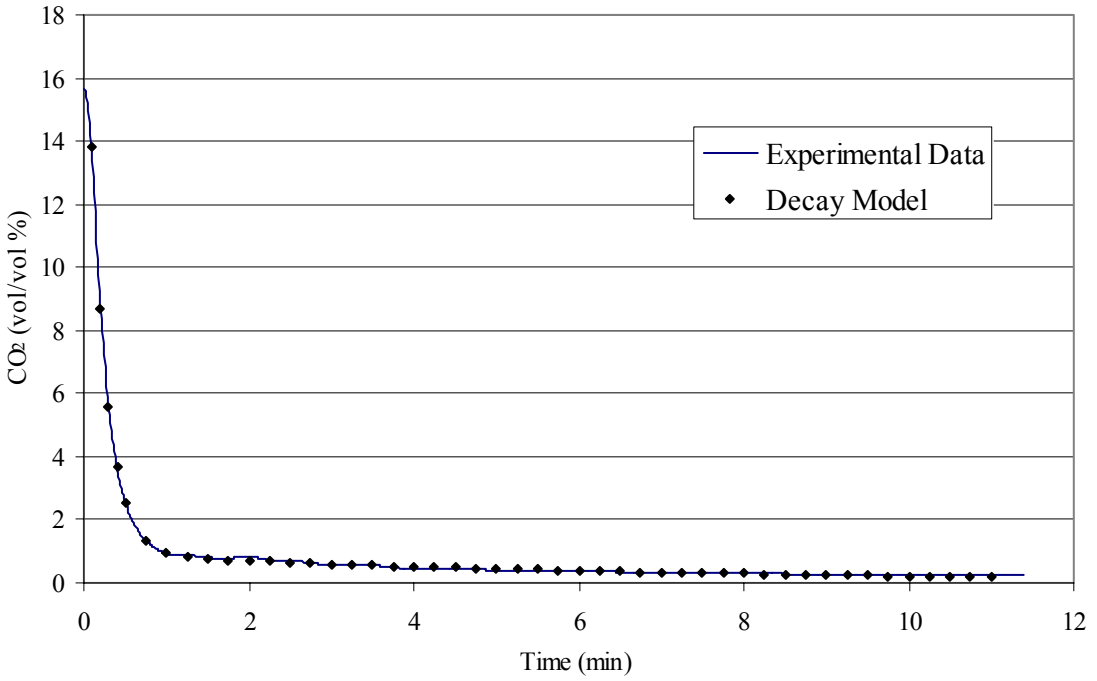

Figure 29. Pyrolysis decay model and experimental data from which it was derived (the data is shown as a solid line while the model is represented with symbols)

3.2.6.2. Batch pyrolysis experimental methodology

Multiple batch trials in the gasifier revealed an optimum biomass batch sample size of approximately 5 - 15 g on a dry basis. Smaller samples than this did not yield sufficient quantities of fixed carbon to measure accurately, while larger samples altered the temperature of the bed significantly during pyrolysis. Batch trials showed no significant difference between as received biomass (10 – 15% moisture) and bone-dry samples.

The batch pyrolysis experimental methodology was designed based on the insights gained from the investigation of primary and secondary pyrolysis. In practice a 10 g batch sample is injected into a hot bed held at the desired temperature with the electric guard heaters and fluidized with 40 slpm of N_2 to drive the primary pyrolysis reactions. This initial portion of the batch experiment is intended to simulate the devolatilization environment experienced by the biomass particles during steady state gasification. Because primary devolatilization happens very quickly this first stage of the batch experiment is limited in its duration. Two minutes after sample injection the N_2 flow rate is reduced from 40 slpm to 10 slpm to minimize elutriation during the second portion of the experiment. The bed is held at temperature for this second phase of the experiment while the biomass sample continues to undergo secondary pyrolysis. At 10 slpm the bed remains fluidized, ensuring some mixing. Secondary pyrolysis is a relatively slow process requiring modest heating rates; therefore this less aggressive fluidization should not hinder its advance. Secondary pyrolysis is allowed to proceed for 28 minutes. The test is concluded by switching the fluidizing medium from N_2 to air, initiating bed burnout. The small quantities of CO and CO_2 released during combustion of the pyrolytic fixed carbon remaining in the reactor are recorded using the CEMs (Section 3.1.3). These CO and CO_2 profiles are then integrated over time using a method similar to that described in Section 3.2.4 to determine the total mass of carbon in the reactor at the end of pyrolysis.

A fluidizing gas flow of 40 slpm used in the initial part of the batch test is lower than the typical 50 slpm used for most of the gasification experiments in this study but it was chosen as a compromise. Larger N_2 flows tend to enhance elutriation rates making accurate assessment of the pyrolytic fixed carbon fraction more difficult. However, if superficial velocities through the bed are too low the large heat transfer rates characteristic of a highly fluidized bed may be compromised to the point of altering primary pyrolysis. A gas flow of 40 slpm results in a superficial gas velocity through the bed of 9.36 cm/s which is four to

five times higher than the minimum fluidization velocity of the bed (U_{mf} = 2.06 cm/s) measured at 700°C, ensuring very good bed mixing and heat transfer. In addition, the rate of volatile gas release immediately after injection of the batch sample into the bed is at least a factor of two larger than that experienced during the steady state gasification experiments. The larger volatile release is due to the fact that injection of a 10 g batch sample over a time interval of a few seconds corresponds to a much larger biomass feed rate than experienced during typical steady state operation. The larger volatile release early in the batch experiment leads to larger superficial gas velocities through the bed, which could increase heat transfer rates, compensating for the lower fluidization gas flow rate.

Despite the reduction of the fluidization flow rate after the completion of primary pyrolysis, inevitably some carbon was elutriated out of the reactor as char particles. To estimate elutriated carbon during batch experiments the cyclone catch and isokinetic thimble filter were recovered after two or three similar batch experiments. Collection of char over more than one batch experiment ensured that measurable quantities of material were gathered. The carbon content of the cyclone catch and isokinetic thimble filter were assessed using the ashing method described in Section 2.2.3. The estimated loss of carbon from the reactor by elutriation during the batch experiments was always less than 10% of the total pyrolytic fixed carbon measured.

At the conclusion of a batch experiment the pyrolytic fixed carbon fraction, f, of the biomass sample was determined by summing the carbon burned out of the reactor ($m_{C,gas}$) with the elutriated carbon ($m_{C,e}$) and dividing by the mass of dry biomass injected ($m_{b,dry}$):

Equation 62 $$f = \frac{m_{C,gas} + m_{C,e}}{m_{b,dry}}$$

3.2.7. Carbon conversion analysis methodology

A carbon conversion analysis technique was developed based on the application of the mass balance model to the flow of pyrolytic fixed carbon during steady state gasification. The method requires knowledge of the pyrolytic fixed carbon feed rate (F), the carbon loading in the reactor at steady state ($W_C(t_{ss})$), and the carbon elutriation rate ($R_e(t_{ss})$) during

steady state operation at the gasification conditions of interest. These parameters are determined through experimental measurement. With this data the mass balance model is used to discern the fraction of pyrolytic fixed carbon leaving the reactor as converted gas compared to that leaving by elutriation. The relative size of these two fractions can then be compared at different gasification conditions, shedding light on the intricacies of carbon conversion.

During steady state gasification the quantity of carbon in the reactor is constant. The mass flow of pyrolytic fixed carbon entering with the biomass is balanced by the mass flow of pyrolytic fixed carbon leaving the reactor due to chemical reaction and elutriation. Establishing steady state gasification may require several minutes or several hours depending on the operating conditions. While steady temperatures in the reactor are typically achieved after just a few minutes, true steady state gasification requires establishment of the asymptotic fixed carbon load in the reactor, which can be a relatively slow process. Figure 25 illustrates the variability of this process for two different ER values. At an ER equal to 0.27 the large steady state carbon loading is reached after approximately eight hours of gasification. By contrast the much smaller steady state loading for an ER equal to 0.31 is achieved in less than three hours. Determination of the existence of steady state operation during a gasification experiment is based on experience and is later verified using data from the experiment and the pyrolytic fixed carbon mass balance model as follows. Rearrangement of Equation 32 gives an expression for the time as a function of the instantaneous carbon load, $W_C(t)$:

Equation 63 $$t = -\frac{1}{k_t} \ln\left[1 - \frac{W_C(t)\, k_t}{F}\right]$$

Substituting Equation 33 yields:

Equation 64 $$t = -\frac{1}{k_t} \ln\left[1 - \frac{W_C(t)}{W_C(t_{ss})}\right]$$

Therefore the calculated time to reach 99% of the steady state asymptotic carbon loading is found by setting $W_C(t)/W_C(t_{ss})$ to 0.99 which gives:

Equation 65 $$t = -\frac{1}{k_t} \ln[0.01]$$

The value of k_t is determined using experimental measurements and Equation 34. After each experiment this estimated time to reach steady state is compared to the length of time spent gasifying to verify that data was gathered after the reactor had accumulated a full loading of carbon. The time to reach 99% carbon loading is calculated for each steady state experiment and is listed on the data summary sheets found in Appendix A.

The steady state carbon elutriation rate, $R_e(t_{ss})$, is determined from the cyclone catch and thimble filter catch. After steady state gasification is established char is captured by the cyclone and collected in a clean, pre-weighed catch can over a measured length of time, Δt. Concurrently, an isokinetic sample of the producer gas downstream of the cyclone is drawn through a clean, pre-weighed thimble filter. After the sampling period the cyclone catch and thimble filter are recovered, weighed, and ashed to determine their carbon content as described in Section 3.2.4. The thimble filter data is used to estimate the mass of carbon in the fine particulate matter ($m_{C,PMF}$) remaining in the producer gas after it has passed through the cyclone. The cyclone catch is used to estimate the mass of carbon in the coarse particulate matter leaving the gasifier ($m_{C,PMC}$). The steady state carbon elutriation rate, $R_e(t_{ss})$, is calculated:

Equation 66 $$R_e(t_{ss}) = \frac{m_{C,PMC} + m_{C,PMF}}{\Delta t}$$

After the steady state elutriation data is collected the experiment is concluded by burning out the bed (Section 3.2.4) to determine the steady state mass of carbon in the reactor, $W_C(t_{ss})$.

The pyrolytic fixed carbon feed rate, F, is determined by Equation 52 with knowledge of the pyrolytic fixed carbon fraction, f, and the dry biomass feed rate, $\dot{m}_{b,dry}$. The pyrolytic fixed carbon fraction is measured using batch pyrolysis experiments (Section 3.2.6). At the conclusion of a steady state experiment the dry biomass feed rate is determined with knowledge of the moisture content of the fuel and by performing a hopper balance (Section 3.2.5).

Knowledge of $W_C(t_{ss})$ and $R_e(t_{ss})$ allow calculation of the elutriation rate constant, k_e, for an experiment by rearrangement of Equation 22:

Equation 67 $$k_e = \frac{R_e(t_{ss})}{W_C(t_{ss})}$$

The value of k_t is found using Equation 34. The chemical reaction rate constant, k_r, is then found by rearrangement of Equation 25. Knowledge of k_e and k_r shed light on how the pyrolytic fixed carbon in the gasifier is either gasified or elutriated as a function of operating conditions. Comparing these rate constants for gasification at various operating conditions facilitates understanding the impact that those operating parameters have on the intricacies of carbon conversion.

The pyrolytic fixed carbon conversion, η_{fc}, is defined as the percent of the pyrolytic fixed carbon entering the reactor with the biomass that is converted to a gas and is given by:

Equation 68 $$\eta_{fc} = 1 - \frac{R_e(t_{ss})}{F}$$

While η_{fc} is a measure of the degree of conversion to gas of just the fixed carbon entering the gasifier, the total carbon conversion, η_{tc}, is the degree to which of all the carbon entering the reactor, fixed and volatile, is converted to a gas. It is defined using the rate of carbon elutriation, $R_e(t_{ss})$, and the mass flow rate of total carbon entering the reactor with the biomass, $\dot{m}_{C,b}$:

Equation 69 $$\eta_{tc} = 1 - \frac{R_e(t_{ss})}{\dot{m}_{C,b}}$$

or in terms of η_{fc} as:

Equation 70 $$\eta_{tc} = \frac{(1 - \eta_{fc} F)}{\dot{m}_{C,b}}$$

The carbon conversion calculated in this manner is fundamentally identical to the definition given previously in Equation 5, which considers solid carbon leaving the reactor to be the only unconverted carbon.

3.3. Uncertainty Analysis

The uncertainty in experimentally measured parameters was conservatively estimated based on the limitations of the equipment and methodology employed and has been affirmed

by repeated measurements made under similar operating conditions. The experimentally measured quantities were used to calculate other parameters such as k_e, k_r, η_{fc}, and η_{tc}. The uncertainty in the calculated values was estimated using error propagation as outlined in Reference [94]. The interested reader is directed to Appendix B for a detailed description of the uncertainty analysis utilized including an example of its application to a particular experiment. The experiments in this study are each unique and therefore confidence intervals were calculated for each using a spreadsheet. The results of the uncertainty analysis for the individual tests are given in the experimental data summary sheets of Appendix A.

4. RESULTS AND DISCUSSION

The goal of these experiments is to understand carbon conversion during fluidized bed gasification of biomass. To this end the carbon conversion analysis method developed in the last chapter is applied to measurements made during gasification of ground seed corn. The characteristics of the ground seed corn used for the experiments are presented first, followed by a discussion of the experimental results.

4.1. Properties of Ground Seed Corn

Discarded seed corn was employed as a model biomass fuel for several reasons. Corn grain is relatively dense compared to many other types of biomass which facilitates its handling. The increased density translates into smaller volumes of material to store and transport and leads to a decreased tendency to form dust. Another benefit of using seed corn as a feedstock is that it feeds consistently. Many types of biomass form planer or cylindrical structures when ground but seed corn forms particles with a high degree of sphericity. Unlike the spherical particles of ground seed corn, the high geometric aspect ratios of other types of ground biomass encourage bridging behavior in the feed system making the establishment of steady state feed rates more difficult. Additionally, the low ash content of corn helps reduce the accumulation of alkali in the fluidized bed, prolonging the bed's useful life.

4.1.1. Thermochemical properties

A proximate, ultimate, and an ash analysis of a sample of the ground seed corn used in this study was performed by Hazen Research Inc., Golden, Colorado. Table 10 and Table 11 give the results of the proximate analysis and ultimate analysis, respectively. The results of a chemical analysis of the ash are given in Table 12.

Table 10. Proximate analysis of ground seed corn

Biomass Component	Ground Seed Corn (% wt, dry)
Volatile	86.44
Fixed Carbon	11.77
Ash	1.79

Table 11. Ultimate analysis of ground seed corn

Biomass Component	Ground Seed Corn (% wt, dry)
C	48.91
H	5.95
O	41.46
N	1.73
S	0.16
Ash	1.79

Table 12. Analysis of the ash content of ground seed corn

Ash Component	Mass Fraction (%)
SiO_2	9.25
Al_2O_3	2.03
TiO_2	0.04
Fe_2O_3	0.89
CaO	2.67
MgO	12.30
Na_2O	0.18
K_2O	29.00
P_2O_5	38.07
SO_3	0.58
Cl	0.01
CO_2	0.22
Balance	4.76

Because the moisture content of ground seed corn can fluctuate with variations in the relative humidity, it was measured often during the course of this study. To check the moisture content a 50 – 100 g sample of corn was withdrawn from the storage container. To ensure a representative sample the corn in the storage bin was mixed before sampling. The sample was spread as a thin layer in an aluminum foil pan and weighed. The corn and the pan were placed in a drying oven maintained at 105°C for a minimum of 12 hours, and then weighed. Samples dried for more than 12 hours did not loose significant additional mass indicating that the sample was essentially bone dry after 12 hours in the oven. Using the original weight, the dry weight, and the weight of the empty foil pan, the moisture content of the ground corn was determined. As can be ascertained from the experimental summary sheets in Appendix A, the moisture content varied between 11.2 – 13.1%, averaging 12.0%.

4.1.2. Size distribution

The seed corn was delivered as whole kernel and was reduced in size using a portable agricultural feed grinder. The corn was ground in batches on an as-needed basis. The size distribution of the ground corn was controlled by the operating parameters of the grinding process. A majority of the experiments conducted for this study utilized fine ground corn but a coarse grind was also used. The bar graph in Figure 30 gives the size distribution for the fine ground corn while Figure 31 show the size distribution for the coarse. The size distributions in Figure 30 and Figure 31 were determined by passing two samples of each grade of corn through as series of standard ASTM sieves. The bar graphs displayed in the figures represent the averages of the two screenings for each grade. Based on the results of these screenings the mass weighted average diameters and the hydrodynamic weighted diameters (Equation 19) of the two grades are calculated and given in Table 13.

Table 13. Average diameters for fine and coarse ground seed corn

Corn Grade	Mass Weighted Diameter (mm)	Hydrodynamic Weighted Diameter (mm)
Fine	0.961	0.577
Coarse	1.902	1.003

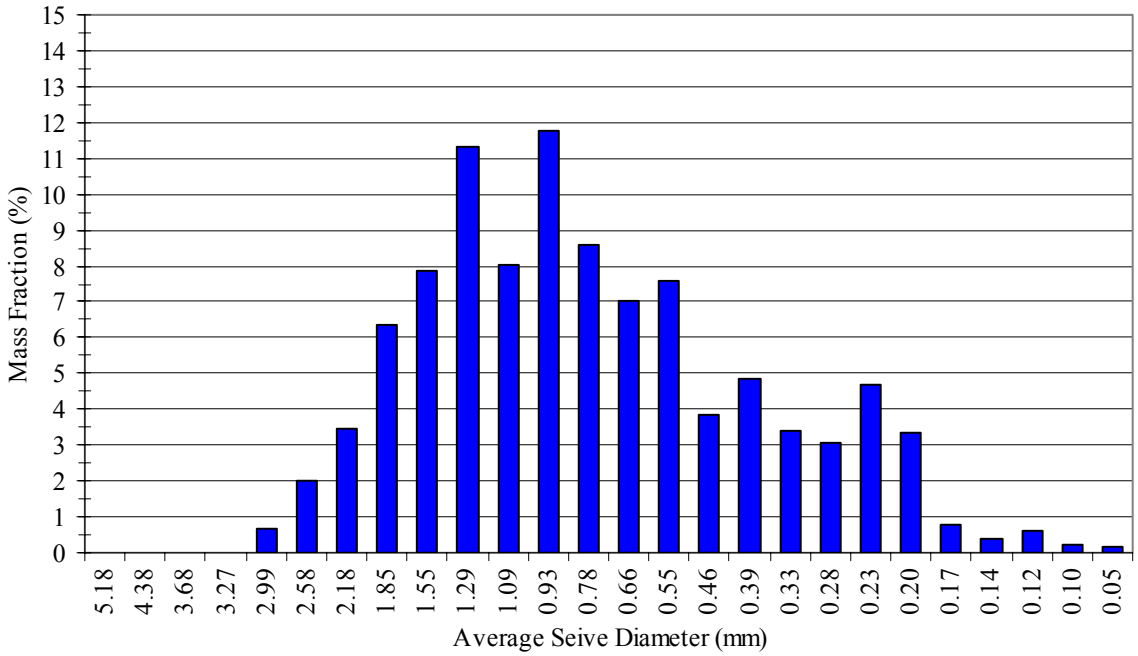

Figure 30. Size distribution of fine ground seed corn as determined by screening

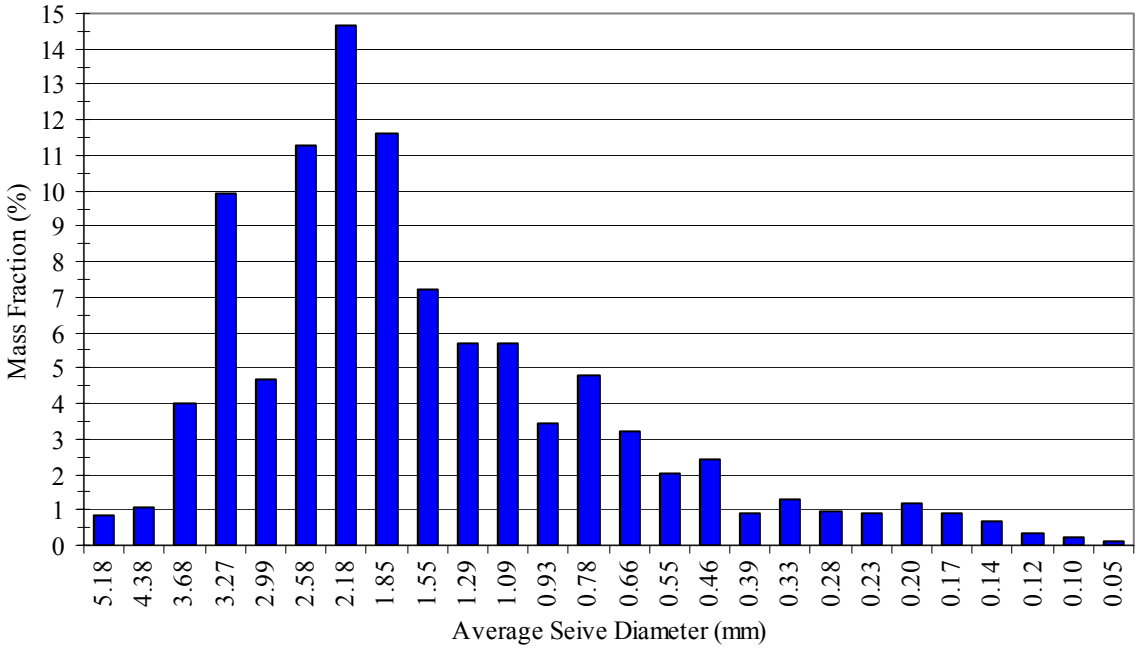

Figure 31. Size distribution of coarse ground seed corn as determined by screening

4.1.3. Pyrolytic fixed carbon fraction

The pyrolytic fixed carbon fraction, f, is the mass fraction of the biomass that remains as solid carbon after devolatilization in the fluidized bed is complete. Its value as a function of temperature is required to apply the carbon conversion analysis technique described in the previous chapter. It was measured using the batch experiment methodology described in Section 3.2.6. The results of several batch experiments utilizing fine ground seed corn are given in Figure 32. The open symbols represent the experimental data while the solid symbols are group averages, normalized in both pyrolytic fixed carbon fraction and temperature. While there is some scatter in the data, a decreasing trend in the pyrolytic fixed carbon fraction with increasing temperature is evident, which is consistent with published results [29, 30, 41-49]. The figure, in agreement with published data [29, 41-44, 46], also suggests that this decreasing trend is more pronounced at lower temperatures and tends to level off at higher temperatures. It should also be noted that the proximate analysis (Table 10) yielded a fixed carbon fraction of 11.77% which is within the range of pyrolytic fixed carbon fractions measured here.

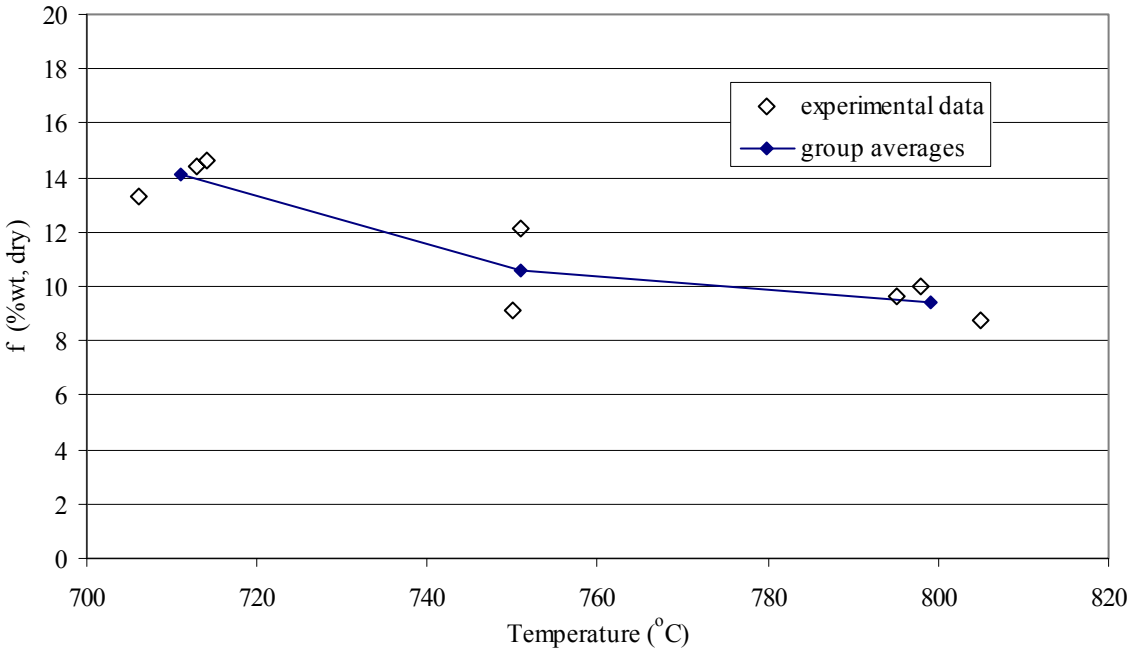

Figure 32. Pyrolytic fixed carbon fraction of fine ground seed corn as a function of temperature

4.2. Steady State Experimental Results

4.2.1. Base case experiments

The base case was tested in triplicate to determine whether results were repeatable. The base case temperature (750°C) and equivalence ratio (0.27) are near the middle of the ranges of these parameters studied in this report. A summary of the experimental parameters and calculations for the base case tests is given in Table 14.

Table 14. Summary of base case experiment data

Test	Temp (°C)	Feed (dry g/s)	ER	$W_C(t_{ss})$ (g)	$R_e(t_{ss})$ (x10^3 g/s)	k_r (x10^6 s^{-1})	k_e (x10^6 s^{-1})	η_{fc} (%)	η_{tc} (%)	Data Sheet Appendix A
#1	750	0.69±0.1	0.27±0.005	320±15	11±0.5	190±30	34±2	85±2	96.7±0.2	20060620
#2	750	0.69±0.1	0.27±0.005	320±15	11±0.5	190±30	36±2	84±2	96.6±0.2	20060621
#3	750	0.65±0.1	0.28±0.005	260±10	9.4±0.5	230±40	36±2	86±2	97.0±0.2	20060616

The test data of Table 14 show excellent repeatability within the uncertainty in the results across all parameters except for the dry fuel feed rate, the steady state carbon loading in the reactor, $W_C(t_{ss})$, and the steady state carbon elutriation rate, $R_e(t_{ss})$. The divergence of $W_C(t_{ss})$ in Test #3 compared to the other two tests was caused by the variation in the dry fuel feed rate for Test #3. The dry fuel feed rate was not always perfectly repeatable, leading to variations in the ER values between experiments. Test #1 and #2 in the table were performed with the same feed rate and therefore were performed at the same equivalence ratio. However, the feed rate for Test #3 was 6% lower which lead to a 6% increase in ER. This small increase in ER resulted in a 20% decrease in $W_C(t_{ss})$ and a 15% decrease in $R_e(t_{ss})$ as shown in the table. However, the difference in the values of $W_C(t_{ss})$ and $R_e(t_{ss})$ for Test #3 are not large enough to cause significant variation in the calculated parameters k_r, k_e, η_{fc}, and η_{tc}, which are most critical for the carbon conversion methodology . Therefore, these base case experiments illustrate the repeatability of the experimental methodology within the uncertainty in the results.

4.2.2. Effect of equivalence ratio

Increasing the equivalence ratio during gasification of biomass is a proven means of increasing carbon conversion [7, 14, 16-20]. Variations in ER are studied in this section to verify that trend and to seek additional insights gleaned from performing the carbon conversion analytical technique described in Section 3.2.7.

Carbon conversion analysis was applied to seven experiments utilizing fine ground seed corn and the results are summarized in Table 15. The gas-solid chemical reaction rate constant, k_r, and the elutriation rate constant, k_e, for the 750°C and 800°C gasification experiments are plotted as functions of the equivalence ratio in Figure 33. Linear regression lines have been added to the figures for clarity. Both graphs show k_r increasing linearly with increased ER. This increasing k_r is the result of increasing char oxidation as equivalence ratio increases.

Table 15. Fine ground seed corn gasification data used to analyze the effect of ER

Temp (°C)	ER	Steam (mol/mol fc)	U_{fb} (cm/s)	$W_C(t_{ss})$ (g)	k_r ($x10^6$ s^{-1})	k_e ($x10^6$ s^{-1})	η_{fc} (%)	η_{tc} (%)	Data Sheet Appendix A
750	0.27	0.9±0.15	31±1	320±15	190±30	34±2	85±2	96.7±0.2	20060620
750	0.27	0.9±0.15	31±1	320±15	190±30	36±2	84±2	96.6±0.2	20060621
750	0.28	0.9±0.15	30±1	260±10	230±40	36±2	86±2	97.0±0.2	20060616
750	0.34	0.9±0.15	28±1	140±5	370±60	48±3	89±2	97.5±0.1	20060607
800	0.24	1.0±0.15	38±1	200±10	290±50	68±4	81±3	96.4±0.2	20060629
800	0.27	1.0±0.15	35±1	140±5	400±70	56±4	88±2	97.6±0.1	20060622
800	0.37	1.0±0.15	30±1	71±5	590±90	61±4	91±1	98.2±0.1	20060602

For these experiments higher ER values are achieved by decreasing the biomass feed rate while maintaining the same air flow. This causes the superficial gas velocity in the reactor to decrease as the equivalence ratio is increased due to the decreased volume of volatiles released caused by the lower biomass feed rates. Most biomass contains small quantities of nitrogen so little N_2 gas is released during gasification. Therefore, the volume flow rate of gas leaving the reactor can be calculated by measuring the dilution of the N_2 that enters the reactor with the fluidization air. The volumetric flow of producer gas, Q_{pg}, leaving the freeboard is calculated by:

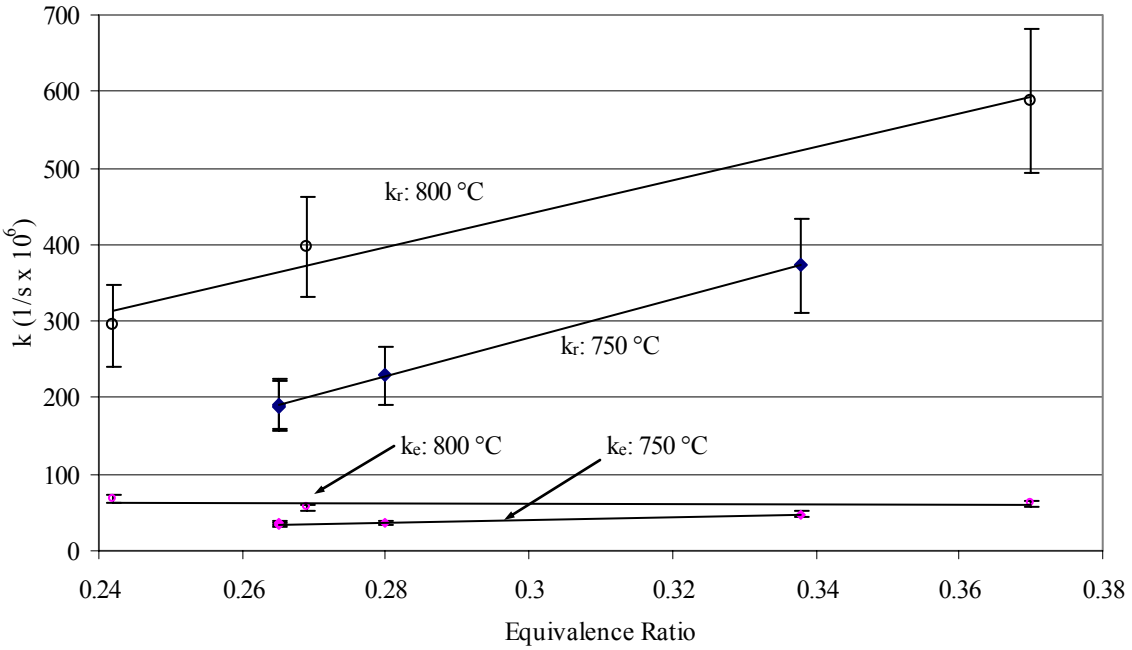

Figure 33. Chemical rate constant and elutriation rate constant as a function of ER for gasification of fine ground seed corn at 750°C and 800°C

Equation 71 $$Q_{pg} = Q_a \frac{n_{N_2,a}}{n_{N_2,pg}}$$

where

$n_{N_2,a}$ = volume fraction of N_2 in dry air = 0.7808

$n_{N_2,pg}$ = volume fraction of N_2 in the dry producer gas at STP

Q_a = volumetric flow rate of fluidizing air at STP

The N_2 concentration of the producer gas leaving the gasifier is measured for each of these experiments using a gas chromatograph and can be found in the experimental data summary sheets in Appendix A. Knowing the volumetric flow of producer gas and the cross sectional area of the freeboard, the superficial gas velocity is calculated as:

Equation 72 $$U_{fb} = \frac{Q_{pg}}{A_{fb}} \frac{T}{T_{STP}}$$

where

A_{fb} = cross sectional area of the freeboard
T = gasification temperature (K)
T_{STP} = standard absolute temperature (273 K)

Assuming ideal gas behavior and with the freeboard pressure near atmospheric the temperature ratio in this expression compensates for the decrease in gas density realized at higher temperatures. The superficial gas velocities in the freeboard are listed in Table 15. For the 750°C experiments a 10% drop in the average gas velocity is realized across the range of ER tested. Similarly, a decrease in the average gas velocity of 21% is shown when moving from minimum to maximum ER for the 800°C data. The elutriation rate constant has been shown to increase in proportion to the superficial gas velocity raised to a power ranging between 2 and 4 [86, 95]. Therefore, the decreasing superficial gas velocities realized with increased ER are expected to lead to lower elutriation rate constants. However, Figure 33 shows k_e slightly increasing with ER for the 750°C data while the 800°C data shows a constant trend. Constant or increasing elutriation rates in the face of decreasing superficial gas velocities suggest increased comminution of the char with increased ER. In this proposed scenario the additional O_2 present at higher ER values causes peripheral percolation similar to behavior observed during combustion experiments [58, 81]. Peripheral percolation is a form of percolation (Section 2.3.2.4) in which conversion primarily takes place in the outer extremities of the particle resulting in catastrophic failure of its outer layers. Peripheral percolation is often referred to as chemically enhanced or chemically assisted attrition because in a fluidized bed it is likely that mechanical stress ultimately causes the failure of the outer particle layers after they have been weakened by chemical conversion. Scala *et al*. [58] report the importance of peripheral percolation during the combustion of black locust char. Scala and Chirone [81] found the fines generation rate for some biomass chars to be proportional to the carbon combustion rate at the surface of the particle, suggesting to them the occurrence of peripheral percolation. Accelerated comminution of char particles due to enhanced oxidation of char is likely the reason that k_e values hold constant or increase with increasing ER.

Figure 33 also allows comparisons of the elutriation and kinetic rate constants as a function of gasification temperatures. Somewhat surprisingly the elutriation constant is higher for gasification at 800°C than at 750°C. However, increased k_e with temperature is explained by the increase in the average gas velocity in the freeboard as shown in Table 15. The increased superficial gas velocities are caused by the expansion of the gas due to the

higher temperatures and by the increased volatile release experienced at higher gasification temperatures [42, 47-49].

Steam (Equation 3) and CO_2 (Equation 2) gasification reactions are endothermic and are therefore expected to become more active as temperatures increase. The data of Figure 33 are consistent with this expectation showing k_r values approximately 150 x 10^{-6} s^{-1} higher for 800°C compared to 750°C regardless of ER. The influence of temperature on the gasification process is further explored in the next section.

Increased reaction rates coupled with constant elutriation rates should result in improved carbon conversion. The pyrolytic fixed carbon conversion, η_{fc} (Equation 68), and the total carbon conversion, η_{tc} (Equation 69), are plotted as functions of ER in Figure 34 for 750°C gasification and for 800°C in Figure 35. As expected increased fixed carbon and total carbon conversion are realized with increased equivalence ratio for both gasification temperatures. Note the larger increase in η_{fc} at low equivalence ratios compared to higher ER values shown in Figure 34 but particularly in Figure 35. This trend is reflective, in part, of the decreasing quantity of carbon present in the reactor as the ER is increased. Figure 36 plots $W_C(t_{ss})$ as a function of ER for 750°C and 800°C gasification and reveals the inverse trend in the carbon loading compared to η_{fc} trend in Figure 34 and Figure 35. As the char loading in the reactor decreases fewer active carbon sites are available to take advantage of the additional O_2 available at higher ER values and a diminishing benefit for improved carbon conversion is realized.

Figure 34 and Figure 35 also show total carbon conversion tracking pyrolytic fixed carbon conversion but with smaller percentage changes. This is expected as η_{tc} is the sum of the carbon conversion due to devolatilization and to fixed carbon reaction. The fraction of the carbon released during devolatilization is much larger than what remains as fixed carbon and is expected to remain constant as ER is increased.

The ER experiments performed with fine ground seed corn for this study show increasing carbon conversion with increased equivalence ratios consistent with published data [7, 14, 16-20]. Application of carbon conversion analysis revealed chemical reaction rates increasing linearly with increased ER over the ranges tested. The analysis also showed steady or slightly increasing elutriation rates with increased ER in spite of decreasing reactor

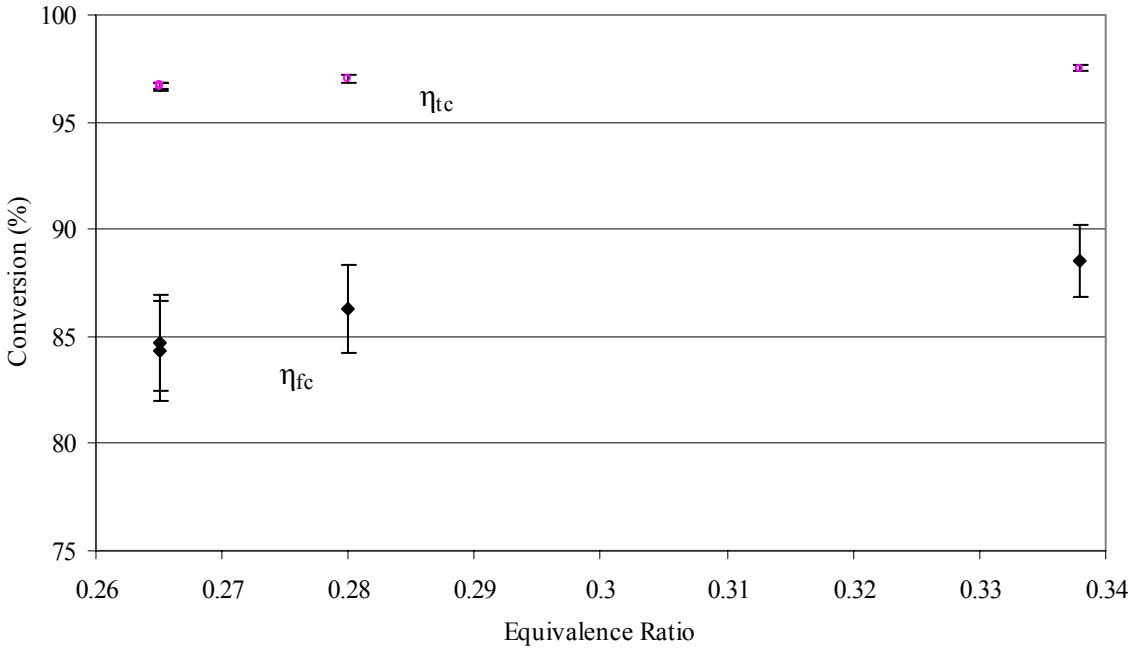

Figure 34. Total carbon and fixed carbon conversion as a function of ER for 750°C gasification of fine ground seed corn

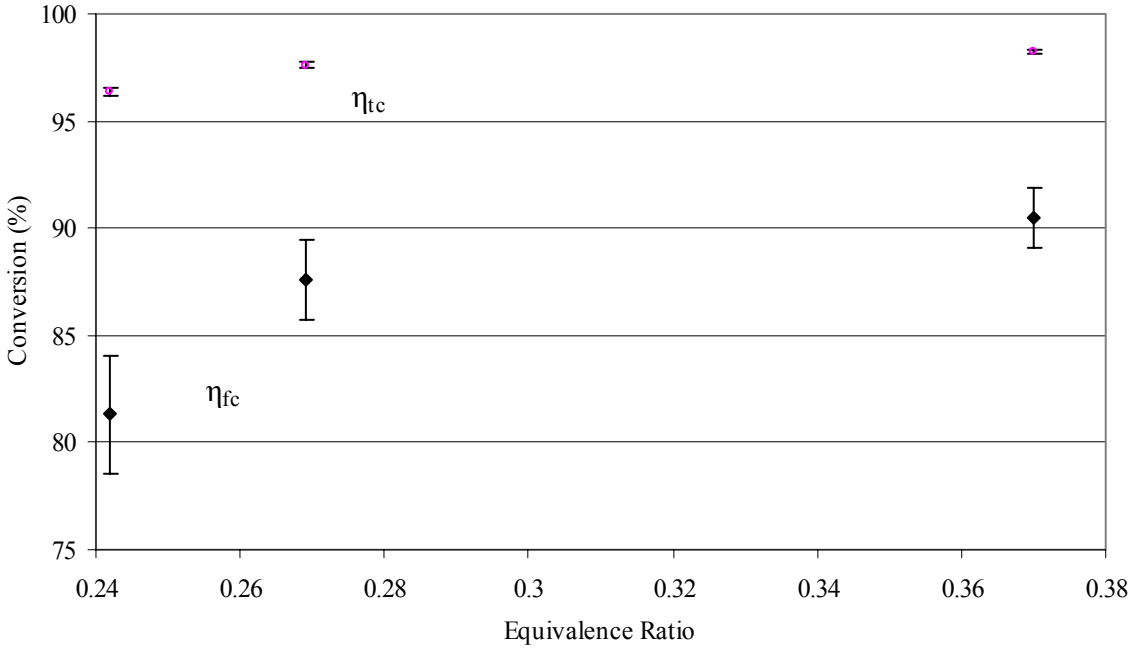

Figure 35. Total carbon and fixed carbon conversion as a function of ER for 800°C gasification of fine ground seed corn

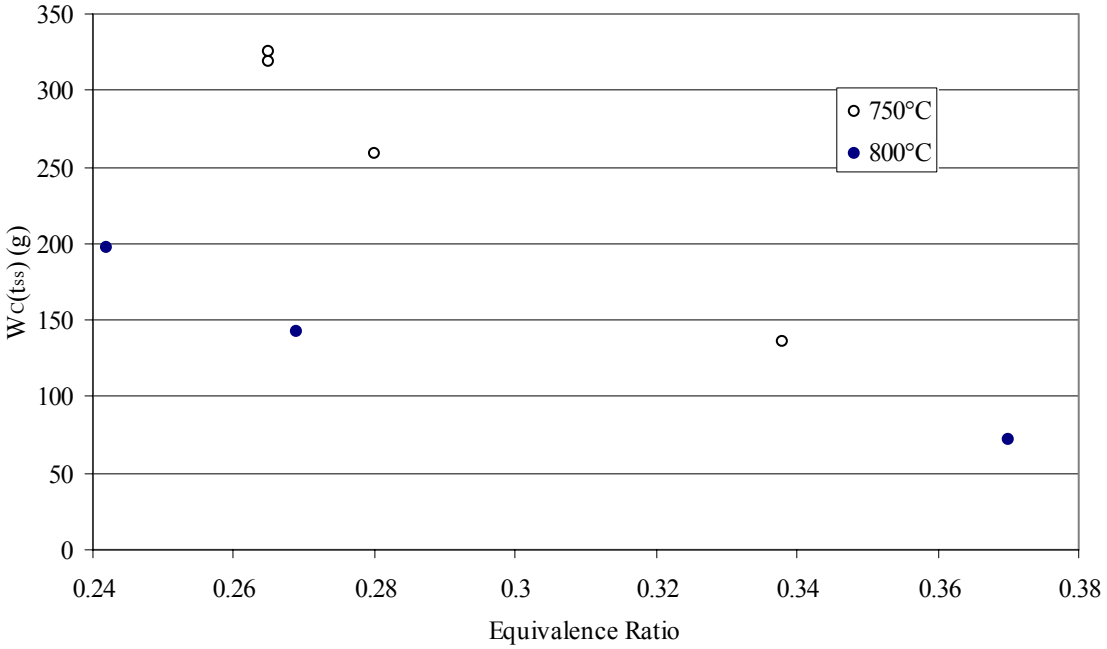

Figure 36. Steady state carbon loading as a function ER for 750°C and 800°C gasification of fine ground seed corn

gas velocities. This suggests that chemically enhanced attrition may be active during gasification of fine ground seed corn, limiting carbon conversions from going higher.

4.2.3. Effect of temperature

Steam and carbon dioxide gasification of solid carbon are endothermic reactions. Endothermic reactions are enhanced as temperatures rise leading many researchers to explore increased gasification temperature as a means of increasing gasification rates and carbon conversion [7, 13, 14, 16, 18, 19, 22-26]. However, researchers often see little or no improvement in carbon conversion with increased temperature [7, 13, 14, 16, 18, 19, 22-26]. With hopes of shedding light on this apparent contradiction carbon conversion analysis was applied to four experiments performed over a range of temperature. The experimental data and results are summarized in Table 16.

Table 16. Fine ground seed corn gasification data used to analyze the effect of temperature

Temp (°C)	ER	Steam (mol/mol fc)	U_{fb} (cm/s)	k_r ($x10^6$ s^{-1})	k_e ($x10^6$ s^{-1})	η_{fc} (%)	η_{tc} (%)	Data Sheet Appendix A
715	0.27	0.6±0.15	28±1	190±30	29±4	87±2	96.3±0.4	20060224
750	0.27	0.9±0.15	31±1	190±30	34±2	85±2	96.7±0.2	20060620
750	0.27	0.9±0.15	31±1	190±30	36±2	84±2	96.6±0.2	20060621
800	0.27	1.0±0.15	35±1	400±70	56±4	88±2	97.6±0.1	20060622

Figure 37 plots k_r and k_e for the data set. The figure shows a dramatic increase in the chemical reaction rate with increased temperature as k_r values nearly double over the temperature range investigated. Kinetically limited reactions rates tend to increase exponentially with temperature typically following the Arrhenius equation (Equation 8)[96]. Taking the natural log of both sides of Equation 8 linearizes the expression:

Equation 73 $$\ln k = \ln A + \left(-E/R\right)1/T$$

Plotting $\ln(k_r)$ vs. 1/T for the k_r data of Table 16 gives Figure 38. The uncertainty values in Figure 38 are found by taking the natural log of the upper and lower limits of each k_r data point given in the table. Linear regression of the data in Figure 38 yields the best fit line shown. Comparing the linear regression equation Figure 38 and Equation 73 reveals that the slope of the best fit line (-9.4) is equal to –(E/R). The activation energy, E, is referred to as the apparent activation energy when the experimental measurements may include mass transfer effects. With R equal to 8.3 J/mol K the apparent activation energy for these experiments is found to be 78 kJ/mol. It is widely thought that gasification rates are limited by chemical kinetics when operating in a fluidized bed below 900°C [11, 28, 35, 37, 60, 66, 77, 89]. Reported activation energies for steam gasification of biomass char range from 140 to 300 kJ/mol [27, 28, 35, 70]. At approximately half the value of the reported activation energies, the apparent activation energy measured here suggests that the reactions in these experiments are limited by pore diffusion [11, 96] which does not agree with the results of other researchers [11, 28, 35, 37, 60, 66, 77, 89]. However, because the concentrations of reactants and products are not controlled across these experiments, it is not possible to draw definitive conclusions from these results regarding the limiting step in the reaction sequence.

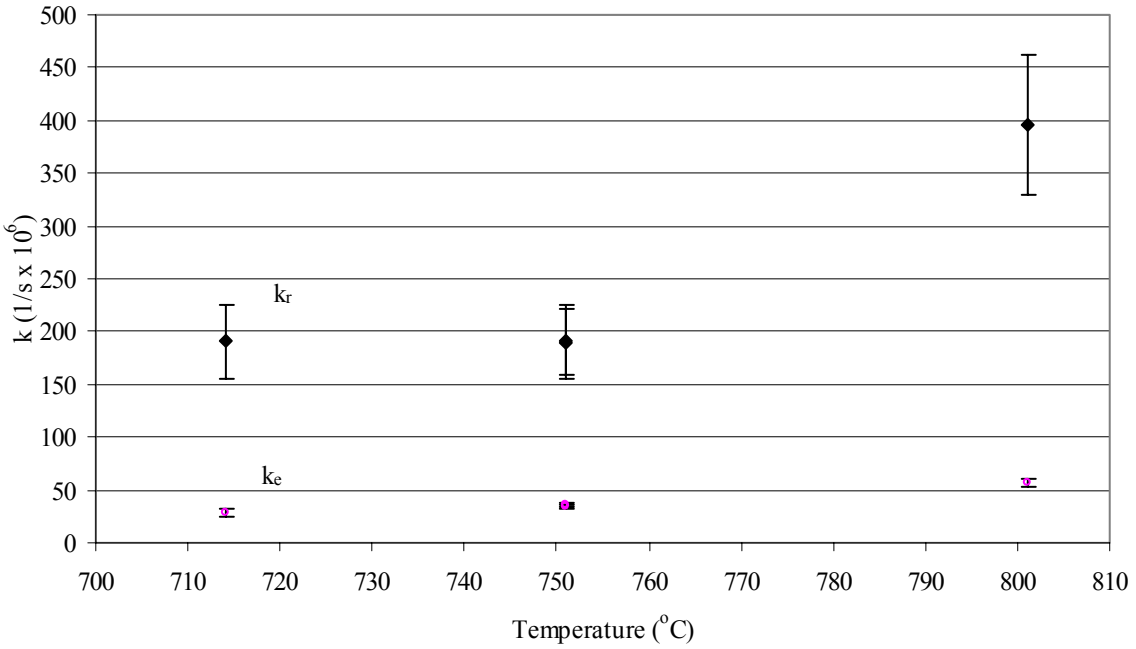

Figure 37. Chemical rate constant and elutriation rate constant as a function of temperature for the gasification of fine ground seed corn at an average ER of 0.27

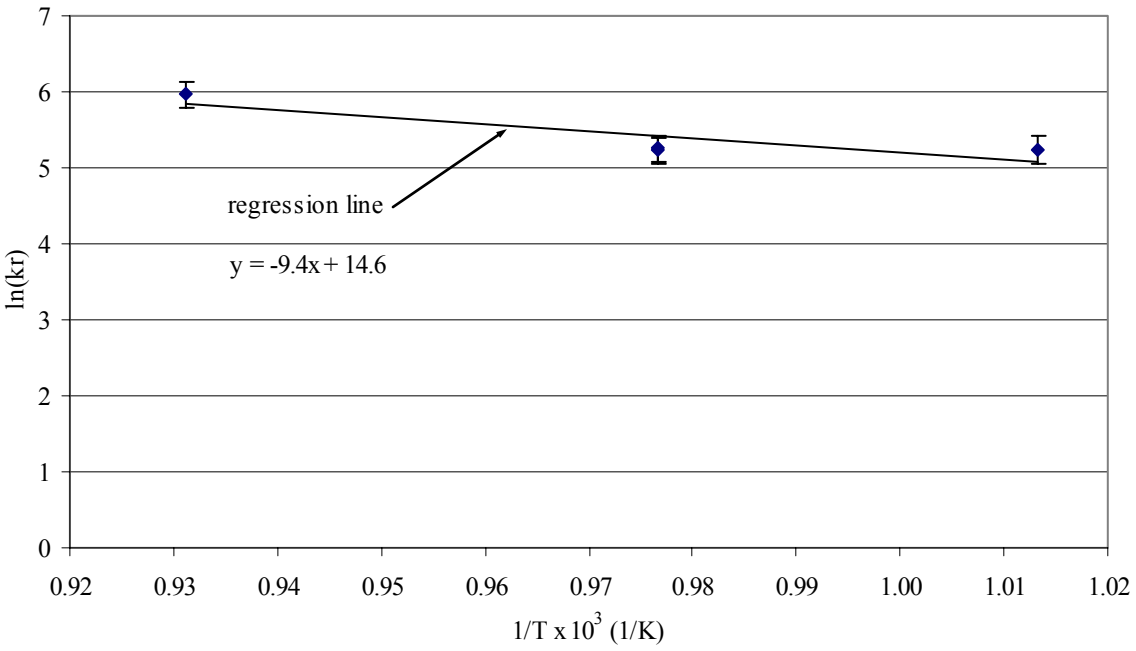

Figure 38. The natural log of k_r as a function of 1/T for gasification of fine ground seed corn at an average ER of 0.27

Figure 37 shows a large increase in the chemical activity as the temperature is increased to 800°C but note that the elutriation rate constant also increases during this interval. Whether this increase in elutriation is caused by an increase in chemically enhanced attrition due to the added chemical activity, increased fragmentation due to the higher temperature, increased elutriation due to increased producer gas velocities realized at higher temperatures, or some combination of these, is not discernable from this data. However, regardless of the mechanism the net result is detrimental to carbon conversion. Figure 39 plots carbon conversion as a function of gasification temperature for the experiments of Table 16. Within the uncertainties the figure shows little or no change in η_{fc} across the entire temperature range and only a modest increase in η_{tc} due in part to the additional volatile release experienced at the higher temperatures [42, 47-49]. Therefore, despite the fact the chemical conversion per unit mass of fixed carbon doubles over the range of temperature tested, a near doubling of the elutriation rate prevents a significant increase in the carbon conversion. This observation may shed light on the weak influence of temperature on the carbon conversion reported but not explained by many researchers [7, 13, 18, 19, 22, 23, 25, 26]. The lack of improved carbon conversion with increased temperature observed by others is consistent with the beneficial increase in gasification rate being offset by increased commutation as witnessed here. Under this scenario carbon conversion is not limited by either mass transport or chemical kinetics but by competition from comminution of the char, which increases with temperature.

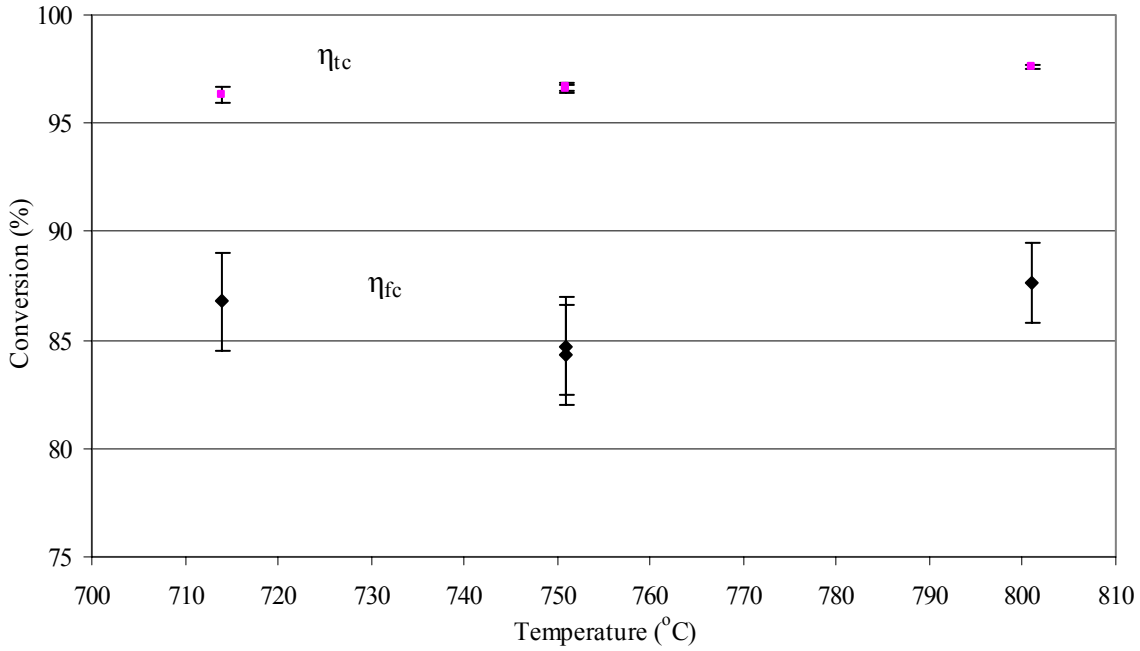

Figure 39. Total carbon and fixed carbon conversion as a function of temperature for gasification of fine ground seed corn at an average ER of 0.27

4.2.4. Effect of the superficial gas velocity

By simultaneously adjusting the flow of air to the gasifier and the biomass feed rate the superficial gas velocity, U, through the reactor can be altered while maintaining the same equivalence ratio. By increasing the superficial gas velocity in this way, the processing capacity of the reactor, the degree of bed mixing, and the elutriation rate, are all likely increased. Carbon conversion analysis was performed on a series of experiments to investigate the impact of the superficial gas velocity on carbon conversion. The analysis facilitated determining whether the potential benefits of enhanced bed mixing realized with increased superficial gas velocity are able to offset the likely increase in elutriation.

A series of three experiments were performed to test the influence of the superficial gas velocity on the gasification of fine ground seed corn and are summarized in Table 17. The k_r and k_e values for the three experiments are plotted in Figure 40 as a function of the superficial gas velocity.

Table 17. Fine ground seed corn gasification data used to analyze the effect of U

Temp (°C)	ER	Steam (mol/mol fc)	U_{fb} (cm/s)	k_r ($x10^6$ s^{-1})	k_e ($x10^6$ s^{-1})	η_{fc} (%)	η_{tc} (%)	Data Sheet Appendix A
750	0.27	0.8±0.15	21±1	370±60	25±2	94±1	98.6±0.1	20061215
750	0.30	0.8±0.15	28±1	370±60	32±2	92±1	98.2±0.1	20061228
750	0.29	0.8±0.15	49±1	460±80	98±6	82±3	96.2±0.2	20061229

Figure 40 shows that within the uncertainty in the results, k_r may not be affected by the value of the superficial gas velocity over the range tested, while k_e increases with increased U. The lack of response in k_r to changes in U demonstrated in the figure suggests that gasification of fine ground seed corn at these conditions is not limited by mass transfer from the bulk fluid to the char particles, which is consistent with the findings of others [11, 28, 35, 37, 60, 66, 77, 89]. The increasing trend of k_e with increasing U shown in Figure 40 is expected [86, 95].

Given the flat response of k_r and the increasing trend in k_e with increased U shown in Figure 40, the decreasing carbon conversion trends of Figure 41 are predictable. Increased superficial gas velocities lead to increased char elutriation rates and in the absence of increased chemical reaction both η_{tc} and η_{fc} suffer as shown in the figure. Conversely, the figure shows that carbon conversion is improved as superficial gas velocities through the reactor are reduced.

From the results of this section, gasification of fine ground seed corn does not appear to be limited by bulk diffusion at 750°C, ER = 0.28. It is also evident that increased carbon conversion can be realized with decreases in the superficial gas velocity. This suggests that for a given biomass processing rate larger diameter reactors should achieve higher carbon conversion. Linear extrapolation of the data of Figure 41 predicts that 99% total carbon conversion can be attained during 750°C gasification of fine ground seed corn at an ER of 0.28 when superficial gas velocities are reduced to approximately 16 cm/s. Therefore, to reach this conversion at these operating conditions while fluidizing with 50 slpm of air, would require enlarging the freeboard of the gasifier used in this study from 6” to 8”.

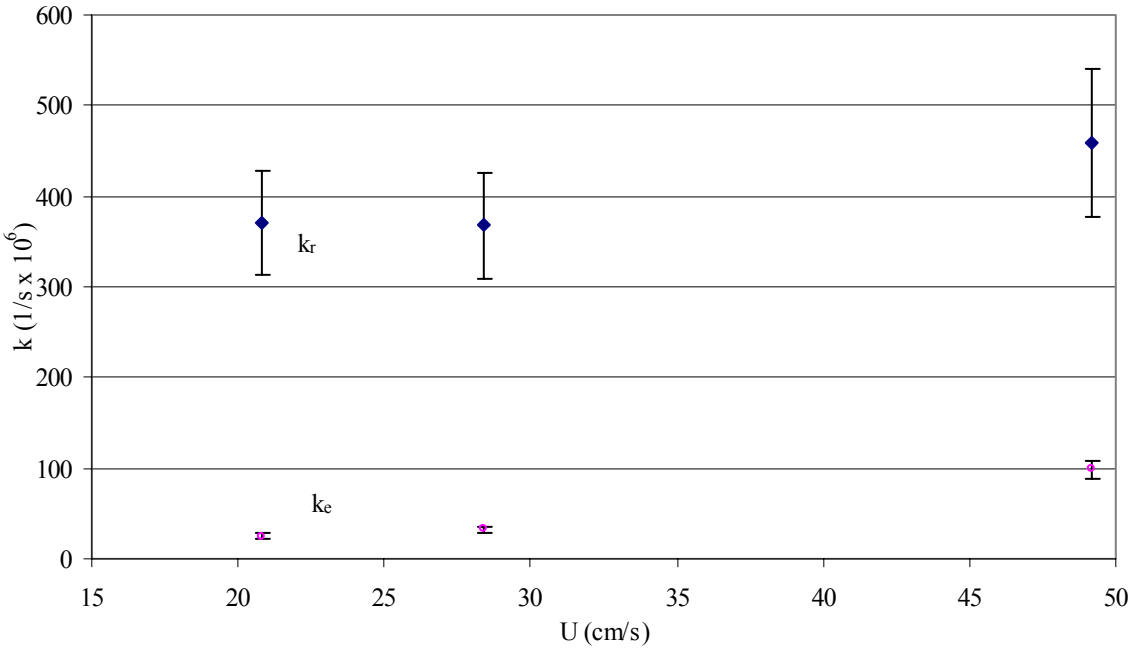

Figure 40. Chemical rate constant and elutriation rate constant as a function of the superficial gas velocity during gasification of ground seed corn at 750°C with an ER of 0.29

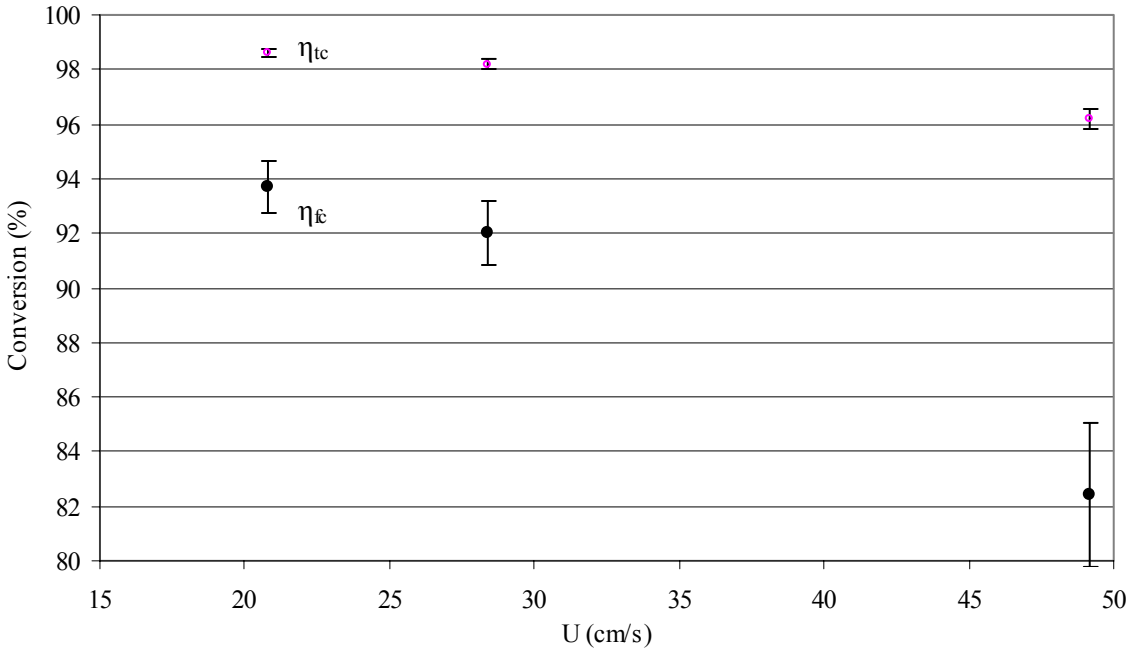

Figure 41. Total carbon and fixed carbon conversion as a function of U during gasification of ground seed corn at 750°C with an ER of 0.29

4.2.5. Effect of biomass particle size

The physical size of the biomass feed stock can influence its gasification rate. When carbon conversion is determined by elutriation, intuition might suggest improving conversion by feeding larger biomass particles because they should yield larger less elutriable char. However, larger fuel particles may also give rise to increased fragmentation [50, 57] and fixed carbon yields [22, 49, 50], both of which could lead to lower carbon conversion. The impact of biomass particle size on gasification rate depends on the balance of these competing factors and is therefore specific to each type of biomass. The role of particle size on the gasification of ground seed corn is explored here. Carbon conversion analysis of these experiments exposed the relative importance of these competing factors and their combined impact on the carbon conversion.

The gasification behavior of two sizes of ground seed corn, fine and coarse, is compared. Figure 30 and Figure 31 give the size distribution of the two grinds as determined by screening. As shown in Table 13 the average mass weighted diameter is 0.96 mm for the fine ground seed corn and 1.9 mm for the coarse while the hydrodynamic diameters are 0.58 mm and 1.0 mm, respectively.

Table 18 summarizes the measured and calculated results for two gasification experiments performed at 750°C and two at 800°C. Coarsely ground seed corn resulted in higher k_e values compared to finely ground at both gasification temperatures. In Sections 4.2.2 and 4.2.3 increases in k_e are directly linked to increases in k_r, indicating the presence of chemically enhanced attrition. However, in this case k_e increases even as k_r remains constant. The increased elutriation rates for coarse corn compared to fine while chemical reaction rates remain constant is consistent with an increase in the primary fragmentation rate experienced by the larger biomass particles. Primary fragmentation is more likely to occur as the size of the fuel particle is increased [50, 57]. Scala and his colleagues [57] studying devolatilization of two different sizes of wood chips observed nearly twice as much fragmentation in 6.35 – 9.50 mm wood chips as compared to 3.35 – 5.0 mm chips. The increase in char surface area realized with increased primary fragmentation does not lead to an increase in the chemical reaction rate constant because the residence time of elutriable char fragments (~ 6s) is much less than the average residence time of the char in the reactor, which is 63 min at 750°C (see data sheet 20060616 in Appendix A) and 37 min at 800°C (see data sheet 20060622 in Appendix A).

Table 18. Ground seed corn gasification data used to analyze the effect of biomass particle size

Temp (°C)	ER	Steam (mol/mol fc)	U_{fb} (cm/s)	Biomass Size	k_r (x10^6 s^{-1})	k_e (x10^6 s^{-1})	η_{fc} (%)	η_{tc} (%)	Data Sheet Appendix A
750	0.28	0.9±0.15	30±1	Fine	230±40	36±2	86±2	97.0±0.2	20060616
750	0.28	0.9±0.15	26±1	Coarse	210±40	46±3	82±3	95.9±0.2	20060715
800	0.27	1.0±0.15	35±1	Fine	400±70	56±4	88±2	97.6±0.1	20060622
800	0.27	1.0±0.15	34±1	Coarse	350±70	97±6	78±3	95.8±0.2	20060713

Carbon conversion data for the 750°C and 800°C gasification experiments is also listed in Table 18. The negative impact on η_{fc} and η_{tc} of the higher elutriation rates in the presences of steady chemical reaction rates for coarse corn is evident in the data and is as expected. At these gasification conditions it is clear that coarsely ground seed corn yields a lower carbon conversion efficiency than does the finely ground.

4.2.6. Effect of the H_2O concentration

Steam gasification of char (Equation 4) is a primary means of converting solid carbon to gas during fluidized bed biomass gasification. Increasing the concentration of a reactant can increase the rate at which a reaction progresses. However, efforts by researchers to enhance carbon conversion by increasing H_2O concentrations in the gasifier have met with limited success [17, 26]. Here, carbon conversion analysis is applied to a series of experiments to discern the relationship between the gasification rate, the carbon conversion, and the concentration of H_2O in the reactor.

Table 19 summarizes the measured and calculated results of a set of three experiments used to analyze the influence of the H_2O concentration on the gasification of fine ground seed corn. These experiments were performed at 800°C and at a low equivalence ratio to magnify the response to changes in the H_2O concentration.

Table 19. Fine ground seed corn gasification data used to analyze the effect of added steam

Temp (°C)	ER	Fuel H_2O (mol/mol fc)	Injected H_2O (mol/mol fc)	k_r ($x10^6$ s^{-1})	k_e ($x10^6$ s^{-1})	η_{fc} (%)	η_{tc} (%)	Data Sheet Appendix A
800	0.24	1.0±0.15	0	290±50	68±4	81±3	96.4±0.2	20060629
800	0.25	1.0±0.15	0.8±0.15	520±90	108±7	83±3	96.7±0.2	20060718
800	0.25	1.0±0.15	2.0±0.15	630±110	110±7	85±2	97.1±0.2	20060721

The moisture content of the ground seed corn averaged 12.4% across this data set. Gasifying at 800°C, this fuel bound moisture provides 1.0 mol H_2O/mol fc as shown in the table. Additional moisture is added to the reaction environment by injecting a measured amount of wet steam into the bed using the method described in Section 3.1.1.4. Any liquid water entering the bed is quickly converted to vapor in the 800°C reactor environment.

The chemical reaction rate coefficient and the elutriation rate coefficient for the four experiments are plotted in Figure 42 as functions of the amount of H_2O entering the gasifier in units of (mol H_2O/mol fc). The amount of H_2O entering the gasifier is the sum of the moisture in the corn and the injected steam listed in Table 19.

Figure 42 shows a significant increase in k_r and k_e as the quantity of moisture in the reactor is nearly doubled beyond the 1 mol H_2O/mol fc provided as fuel moisture. However, a further increase in moisture to nearly 3 mol H_2O/ mol fc does not affect k_r and k_e beyond the uncertainty in the results. As shown in the figure the elutriation response to added steam parallels that of the chemical reaction. Once again it appears that elutriation rates are directly tied to chemical reaction rates through chemically enhanced attrition. As before chemically enhanced attrition here tends to nullify increased chemical reaction leaving carbon conversion essentially unchanged as shown in Figure 43. The figure shows a slight increase in η_{tc} and no significant change in η_{fc} as the moisture content in the reactor is increased from approximately 1 to 3 mol H_2O/mol fc.

Consistent with this study other researchers indicate that the addition of steam to the gasification process has at best a minor impact on carbon conversion [17, 26]. Based on the lack of improved carbon conversion, Kersten *et al.* [17, 26] claim that added steam promoted the water-gas shift reaction (Equation 12) in lieu of increasing gasification rates. However,

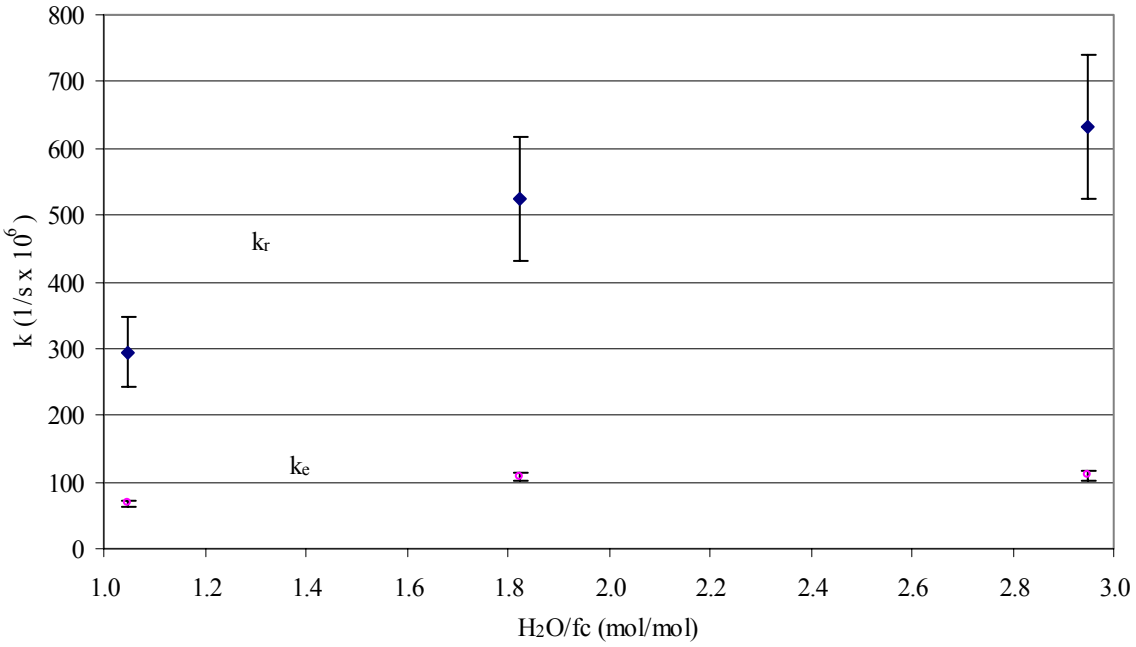

Figure 42. Chemical rate constant and elutriation rate constant as a function of the entering H_2O during gasification of fine ground seed corn at 800°C with an ER of 0.25

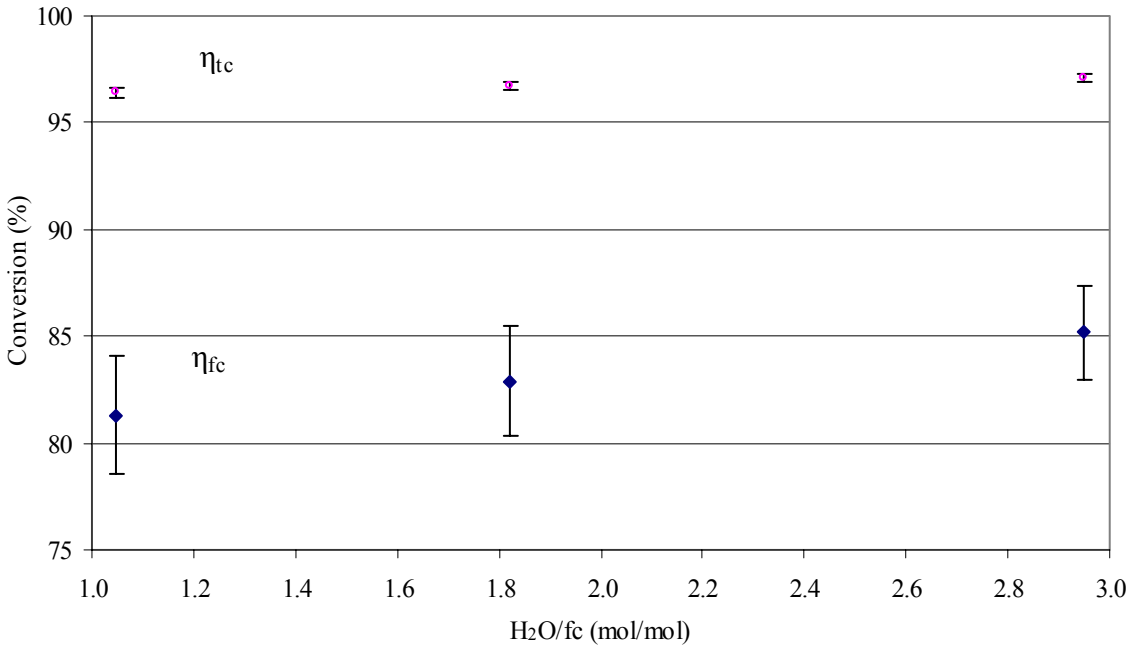

Figure 43. Total carbon and fixed carbon conversion as a function of the entering H_2O for gasification of fine ground seed corn at 800°C and an ER of 0.25

given the observed scatter in their data (see Figure 8 of this document) and the fact that the equivalence ratio varied by ±12% across their data set, it is unclear whether such a statement can be justified. Regardless, if the water-gas shift reaction is active in the current study notable increases in H_2 and CO_2 with a corresponding decrease in CO concentration (see Equation 12) should be realized as steam levels are increased. Figure 44 plots CO, H_2, and CO_2 dry gas concentrations as functions of the H_2O input into the process. Lines connecting the data points have been added to aid in discerning trends in each of the concentrations. Within the uncertainty in the results the figure shows nearly constant trends in the gas concentrations, suggesting that the water-gas shift reaction is not being significantly enhanced with increased H_2O concentrations. Additionally, the significant increase in k_r with increased H_2O demonstrated in Figure 42 gives clear evidence that the shift reaction is certainly not acting as a barrier to solid carbon gasification in these experiments. This conclusion offers an alternate explanation for the lack of improved carbon conversion with added steam witnessed by Kersten *et al.* [17, 26]. While the Kersten *et al.* [17, 26] claim that the water-gas shift reaction prevents steam gasification, the results of these experiments suggest that chemically enhanced attrition plays the dominate role in restraining carbon conversion rather than the shift reaction.

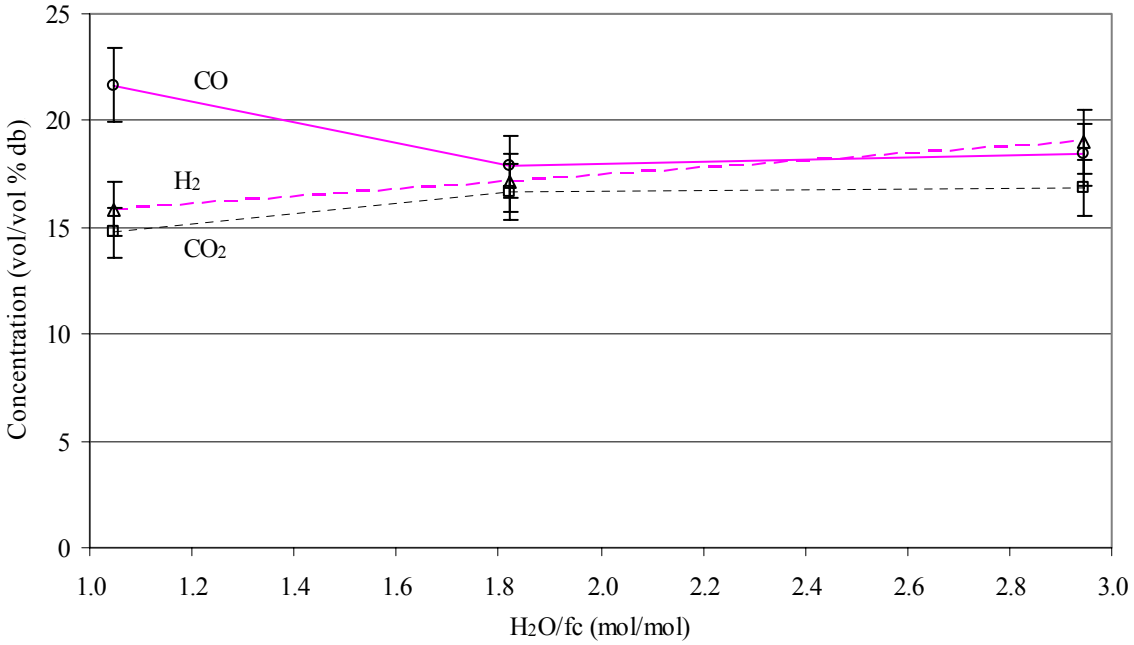

Figure 44. Producer gas concentrations as a function of the entering H_2O (T = 800°C, ER = 0.25)

The results of the present experiments indicate that adding moisture up to approximately 2 mol H_2O/mol fc for ground seed corn encouraged steam gasification of the solid carbon. However, the increased gasification also enhanced char attrition, leading to increased elutriation, and resulting in little gain in the η_{fc} or η_{tc}. So, while the addition of H_2O may be desirable for reforming tar or to increase H_2 concentrations via the water-gas shift reaction, it did not improve carbon conversion in fine ground seed corn gasification.

5. CONCLUSIONS

The carbon conversion efficiency of atmospheric bubbling fluidized bed gasification of biomass was investigated. Equilibrium analysis revealed that carbon conversion is not thermodynamically limited at typical gasification conditions (T > 700°C, ER > 0.2) but published data show it often falling well short of 100%. A thorough review of the literature was used to assemble a picture of the formation of char, its characteristics, and its processing during its time in the reactor. The review served as a foundation for the investigation of the intricacies of carbon conversion in biomass gasification performed for this study.

Using a mass balance on the reactor a transient model was developed which tracks the flow of pyrolytic fixed carbon as it enters and leaves the gasifier. The transient model was compared to a transient model based on a population balance and to experimental data. Reasonable agreement between the population model and the mass balance model was observed with differences highlighting the distinct assumptions on which each model was built. Comparisons of the pyrolytic fixed carbon model to transient experimental data showed very good agreement within measurement uncertainties.

To facilitate a deeper understanding of biomass gasification in a fluidized bed a carbon conversion analysis method was developed. The pyrolytic fixed carbon mass balance on the reactor was combined with steady state experimental measurements to form the carbon conversion analysis methodology. The methodology enables the rate that fixed carbon leaves the reactor by chemical conversion to be distinguished from that leaving by elutriation. The method proved to be a powerful and useful tool for shedding light on the complexities of biomass gasification as evidenced by its application in this study. Applied to the gasification of ground seed corn, the impact of various gasification parameters on pyrolytic fixed carbon removal from the reactor was assessed. Based on this analysis a number of insights regarding the chemical reaction and comminution of the carbon bearing char and their role in determining the carbon conversion were revealed for ground seed corn gasification in a fluidized bed. The impact on ground seed corn gasification was investigated for variations in the equivalence ratio, the gasification temperature, the superficial gas velocity, the biomass particle size, and the concentration of H_2O entering the reactor. The insights gleaned from these experiments suggest that carbon conversion during gasification of ground seed corn is

limited by elutriation of char comminuted by either fragmentation or chemically assisted attrition.

The results of gasifying ground seed corn of varying size (Section 4.2.5) suggest that fragmentation can have a significant impact on the carbon conversion. In those experiments it appeared that feeding larger particles let to an increase in the primary fragmentation rate. The increased fragmentation rate resulted in increased elutriation and a decline in the carbon conversion.

The results of the experiments which varied the ER, the gasification temperature, and the amount of water entering the reactor revealed chemically assisted attrition as an important barrier to carbon conversion during ground seed corn gasification. When carbon conversion is limited by chemically enhanced attrition, increasing gas-solid kinetics increases elutriation through peripheral percolation and results in little or no gain in the conversion efficiency. Therefore hope of improving carbon conversion during biomass gasification limited by chemically assisted attrition, appears to reside with the management of the attrited char. Management strategies can either attempt to deal with attrited char while in the reactor or after it leaves.

One proven means of improving carbon conversion by management of elutriable char within the gasifier is to operate at lower superficial gas velocities. As demonstrated in Figure 41 (Section 4.2.4) carbon conversion is improved as the superficial gas velocity is lowered. U is reduced in this study by decreasing the flow of gas through the fluidized bed but similar gains in carbon conversion may be realized with reductions in the superficial gas velocity in the freeboard only. Reductions in $U_{freeboard}$ can be accomplished by increasing the diameter of the reactor in that section. However, gains in carbon conversion due to increased reactor diameters require a larger capital investment for a given processing rate. The superficial gas velocity in the reactor can also be lowered by fluidizing with O_2 in lieu of air. Eliminating atmospheric N_2 from the reactor not only lowers the superficial velocities but also eliminates its diluting effects on the product steam, increasing the HHV of the produced gas. However, the additional costs associated with O_2 production may offset these benefits.

Given the high volatile content of biomass it may not be surprising that carbon conversion during gasification of ground seed corn in a fluidized bed was found to be limited by the friable nature of its char. What may be striking, however, is that mechanical attrition

of the char appears to play a minor role in limiting carbon conversion. If mechanical attrition were the controlling mechanism, increased chemical reaction rates would tend to increase carbon conversion rates as the fine particles would be preferentially consumed due to their high surface area to volume ratios. By contrast, this research found that increased reaction rates gave rise to increased rates of chemically assisted attrition, leaving carbon conversion substantially unchanged. This revelation is certainly consistent with many published results which show efforts to improve carbon conversion, through enhanced gas-solid kinetics, meeting with limited success.

A carbon conversion analysis methodology has been developed for this project. Application of the method to the gasification of ground seed corn in a bubbling fluidized bed reactor has shown its usefulness as a tool for investigating carbon conversion. The conclusions drawn from the experiments on ground seed corn are expected to be common to other types of biomass but further investigation is required. In addition to investigating other types of biomass, application of the carbon conversion analysis methodology could also be extended to consider the influence of other gasification parameters, such as the alkali content of the bed, and to consider the performance of other types of reactors.

REFERENCES

[1] R. C. Brown, *Biorenewable resources: engineering new products from agriculture*, 1st ed. Ames, Iowa: Iowa State Press, 2003.

[2] D. Kunii and O. Levenspiel, *Fluidization engineering*, 2nd ed. Boston: Butterworth-Heinemann, 1991.

[3] C. Higman and M. van der Burgt, *Gasification*. Amsterdam; Boston: Gulf Professional Pub., 2003.

[4] D. Geldart, *Gas fluidization technology*. Chichester; New York: Wiley, 1986.

[5] C. M. Kinoshita, Y. Wang, and P. K. Takahashi, "Chemical equilibrium computations for gasification of biomass to produce methanol," *Energy Sources*, vol. 13, pp. 361-368, 1991.

[6] X. T. Li, J. R. Grace, A. P. Watkinson, C. J. Lim, and A. Ergudenler, "Equilibrium modeling of gasification: A free energy minimization approach and its application to a circulating fluidized bed coal gasifier," *Fuel*, vol. 80, pp. 195-207, 2001.

[7] X. T. Li, J. R. Grace, C. J. Lim, A. P. Watkinson, H. P. Chen, and J. R. Kim, "Biomass gasification in a circulating fluidized bed," *Biomass and Bioenergy*, vol. 26, pp. 171-193, 2004.

[8] M. J. Prins, K. J. Ptasinski, and F. J. J. G. Janssen, "Thermodynamics of gas-char reactions: First and second law analysis," *Chemical Engineering Science*, vol. 58, pp. 1003-1011, 2003.

[9] M. Ruggiero and G. Manfrida, "Equilibrium model for biomass gasification processes," *Renewable Energy*, vol. 16, pp. 1106-1109, 1999.

[10] G. Schuster, G. Loffler, K. Weigl, and H. Hofbauer, "Biomass steam gasification - an extensive parametric modeling study," *Bioresource Technology*, vol. 77, pp. 71-79, 2001.

[11] T. B. Reed, "Biomass gasification : principles and technology," in *Energy technology review no. 67*. Park Ridge, N.J.: Noyes Data Corp., 1981, pp. xiv, 401 p.

[12] W. C. Reynolds, "STANJAN Version 3," Stanford Department of Mechanical Engineering, 1986.

[13] N. A. Emsick, "Switchgrass derived producer gas as a reburn fuel," Master of Science thesis, Iowa State University, Ames, Iowa, 2004.

[14] L. Zeng and A. R. P. Van Heiningen, "Carbon gasification of kraft black liquor solids in the presence of TiO_2 in a fluidized bed," *Energy and Fuels*, vol. 14, pp. 83-88, 2000.

[15] P. Garcia-Ibanez, A. Cabanillas, and J. M. Sanchez, "Gasification of leached orujillo (olive oil waste) in a pilot plant circulating fluidised bed reactor. Preliminary results," *Biomass and Bioenergy*, vol. 27, pp. 183-194, 2004.

[16] A. Gomez-Barea, R. Arjona, and P. Ollero, "Pilot-plant gasification of olive stone: A technical assessment," *Energy and Fuels*, vol. 19, pp. 598-605, 2005.

[17] S. R. A. Kersten, W. Prins, A. van der Drift, and W. P. M. van Swaaij, "Experimental fact-finding in CFB biomass gasification for ECN's 500 kW_{th} pilot plant," *Industrial and Engineering Chemistry Research*, vol. 42, pp. 6755-6764, 2003.

[18] P. M. Lv, Z. H. Xiong, J. Chang, C. Z. Wu, Y. Chen, and J. X. Zhu, "An experimental study on biomass air-steam gasification in a fluidized bed," *Bioresource Technology*, vol. 95, pp. 95-101, 2004.

[19] F. Miccio, O. Moersch, H. Spliethoff, and K. R. G. Hein, "Generation and conversion of carbonaceous fine particles during bubbling fluidized bed gasification of a biomass fuel," *Fuel*, vol. 78, pp. 1473-1481, 1999.

[20] A. van der Drift and J. van Doorn, "Effect of fuel size and process temperature on fuel gas quality from CFB gasification of biomass," presented at Development in Thermochemical Biomass Conversion, Tyrol, Austria, 2000.

[21] I. Narvaez, A. Orio, M. P. Aznar, and J. Corella, "Biomass gasification with air in an atmosphere bubbling fluidized bed. Effect of six operational variables on the quality of the produced raw gas," *Industrial & Engineering Chemistry Research*, vol. 35, pp. 2110-2120, 1996.

[22] J. Herguido, J. Corella, and J. Gonzalez-Saiz, "Steam gasification of lignocellulosic residues in a fluidized bed at a small pilot scale. Effect of the type of feedstock," *Industrial & Engineering Chemistry Research*, vol. 31, pp. 1274-1282, 1992.

[23] A. van der Drift, J. van Doorn, and J. W. Vermeulen, "Ten residual biomass fuels for circulating fluidized-bed gasification," *Biomass and Bioenergy*, vol. 20, pp. 45-56, 2001.

[24] A. van der Drift, C. M. van der Meijden, and S. D. Strating-Ytsma, "Ways to increase the carbon conversion of a CFB-gasifier," in *12th European Conference and Exhibition on Biomass for Energy and Climate Protection*. Amsterdam, 2002.

[25] C. Franco, F. Pinto, I. Gulyurtlu, and I. Cabrita, "The study of reactions influencing the biomass steam gasification process," *Fuel*, vol. 82, pp. 835-842, 2003.

[26] J. Gil, M. P. Aznar, M. A. Caballero, E. Frances, and J. Corella, "Biomass gasification in fluidized bed at pilot scale with steam-oxygen mixtures. Product distribution for very different operating conditions," *Energy Fuels*, vol. 11, pp. 1109-1118, 1997.

[27] Y. Wang and C. M. Kinoshita, "Kinetic model of biomass gasification," *Solar Energy*, vol. 51, pp. 19-25, 1993.

[28] T. Kojima, P. Assavadakorn, and T. Furusawa, "Measurement and evaluation of gasification kinetics of sawdust char with steam in an experimental fluidized bed," *Fuel Processing Technology*, vol. 36, pp. 201-207, 1993.

[29] P. Mathieu and R. Dubuisson, "Performance analysis of a biomass gasifier," *Energy Conversion and Management*, vol. 43, pp. 1291-1299, 2002.

[30] V. Sricharoenchaikul, W. J. Frederick Jr, and P. Agrawal, "Carbon distribution in char residue from gasification of kraft black liquor," *Biomass and Bioenergy*, vol. 25, pp. 209-220, 2003.

[31] A. van der Drift and J. van Doorn, "Effect of type of fuel, moisture content and particle size on the carbon conversion and fuel gas quality for circulating fluidized bed gasification of biomass," in *1st World Conference and Exhibition on Biomass for Energy and Industry*. Sevilla, Spain, 2000.

[32] J. Gil, J. Corella, M. P. Aznar, and M. A. Caballero, "Biomass gasification in atmospheric and bubbling fluidized bed: Effect of the type of gasifying agent on the product distribution," *Biomass and Bioenergy*, vol. 17, pp. 389-403, 1999.

[33] C. Fushimi, K. Araki, Y. Yamaguchi, and A. Tsutsumi, "Effect of heating rate on steam gasification of biomass. 1. Reactivity of char," *Industrial and Engineering Chemistry Research*, vol. 42, pp. 3922-3928, 2003.

[34] S. T. Chaudhari, S. K. Bej, N. N. Bakhshi, and A. K. Dalai, "Steam gasification of biomass-derived char for the production of carbon monoxide-rich synthesis gas," *Energy and Fuels*, vol. 15, pp. 736-742, 2001.

[35] W. Klose and M. Wolki, "On the intrinsic reaction rate of biomass char gasification with carbon dioxide and steam," *Fuel*, vol. 84, pp. 885-892, 2005.

[36] M. D. Mann, R. Z. Knutson, J. Erjavec, and J. P. Jacobsen, "Modeling reaction kinetics of steam gasification for a transport gasifier," *Fuel*, vol. 83, pp. 1643-1650, 2004.

[37] R. Backman, W. J. Frederick, and M. Hupa, "Basic studies on black-liquor pyrolysis and char gasification," *Bioresource Technology: Biomass, Bioenergy, Biowastes, Conversion Technologies, Biotransformations, Production Technologies*, vol. 46, pp. 153-158, 1993.

[38] T. Hanaoka, S. Inoue, S. Uno, T. Ogi, and T. Minowa, "Effect of woody biomass components on air-steam gasification," *Biomass and Bioenergy*, vol. 28, pp. 69-76, 2005.

[39] A. Olivares, M. P. Aznar, M. A. Caballero, J. Gil, E. Frances, and J. Corella, "Biomass gasification: Produced gas upgrading by in-bed use of dolomite," *Industrial & Engineering Chemistry Research*, vol. 36, pp. 5220-5226, 1997.

[40] S. Q. Turn, C. M. Kinoshita, D. M. Ishimura, and J. Zhou, "The fate of inorganic constituents of biomass in fluidized bed gasification," *Fuel*, vol. 77, pp. 135-146, 1998.

[41] V. Sricharoenchaikul, A. L. Hicks, and W. J. Frederick, "Carbon and char residue yields from rapid pyrolysis of kraft black liquor," *Bioresource Technology*, vol. 77, pp. 131-138, 2001.

[42] D. S. Scott, J. Piskorz, M. A. Bergougnou, R. Graham, and R. P. Overend, "Role of temperature in the fast pyrolysis of cellulose and wood," *Industrial & Engineering Chemistry Research*, vol. 27, pp. 8-15, 1988.

[43] X. Bingyan, W. Chuangzhi, L. Zhengfen, and Z. Xi Guang, "Kinetic study on biomass gasification," *Solar Energy*, vol. 49, pp. 199-204, 1992.

[44] C. Sheng and J. L. T. Azevedo, "Modeling biomass devolatilization using the chemical percolation devolatilization model for the main components," Sapporo, Japan, 2002.

[45] V. Cozzani, C. Nicolella, M. Rovatti, and L. Tognotti, "Modeling and experimental verification of physical and chemical processes during pyrolysis of a refuse-derived fuel," *Industrial & Engineering Chemistry Research*, vol. 35, pp. 90-98, 1996.

[46] W. J. Frederick, Jr and M. Hupa, "Combustion properties of kraft black liquors," U.S. DOE DOE/CE/40936-T1 (DE94007502), 1993.

[47] R. Zanzi, K. Sjostrom, and E. Bjornbom, "Rapid pyrolysis of agricultural residues at high temperature," *Biomass and Bioenergy*, vol. 23, pp. 357-366, 2002.

[48] S. Gaur and T. B. Reed, *Thermal data for natural and synthetic fuels*. New York: Marcel Dekker, 1998.

[49] R. Zanzi, K. Sjostrom, and E. Bjornbom, "Rapid high-temperature pyrolysis of biomass in a free-fall reactor," *Fuel*, vol. 75, pp. 545-550, 1996.

[50] N. Jand and P. U. Foscolo, "Decomposition of wood particles in fluidized beds," *Industrial and Engineering Chemistry Research*, vol. 44, pp. 5079-5089, 2005.

[51] M. Fiorentino, A. Marzocchella, and P. Salatino, "Segregation of fuel particles and volatile matter during devolatilization in a fluidized bed reactor - II. Experimental," *Chemical Engineering Science*, vol. 52, pp. 1909-1922, 1997.

[52] D. Park, O. Levenspiel, and T. J. Fitzgerald, "Plume model for large particle fluidized-bed combustors," *Fuel*, vol. 60, pp. 295-306, 1981.

[53] J. F. Stubington and J. F. Davidson, "Gas-phase combustion in fluidized beds," *AIChE Journal*, vol. 27, pp. 59-65, 1981.

[54] F. Scala and P. Salatino, "Modelling fluidized bed combustion of high-volatile solid fuels," *Chemical Engineering Science*, vol. 57, pp. 1175-1196, 2002.

[55] D. Sutton, B. Kelleher, and J. R. H. Ross, "Review of literature on catalysts for biomass gasification," *Fuel Processing Technology*, vol. 73, pp. 155-173, 2001.

[56] E. Bar-Ziv and I. I. Kantorovich, "Mutual effects of porosity and reactivity in char oxidation," *Progress in Energy and Combustion Science*, vol. 27, pp. 667-697, 2001.

[57] F. Scala, R. Chirone, and P. Salatino, "Combustion and attrition of biomass chars in a fluidized bed," *Energy and Fuels*, vol. 20, pp. 91-102, 2006.

[58] F. Scala, P. Salatino, and R. Chirone, "Fluidized bed combustion of a biomass char (Robinia pseudoacacia)," *Energy and Fuels*, vol. 14, pp. 781-790, 2000.

[59] R. Di Felice, G. Coppola, S. Rapagna, and N. Jand, "Modeling of biomass devolatilization in a fluidized bed reactor," *Canadian Journal of Chemical Engineering*, vol. 77, pp. 325-332, 1999.

[60] P. Ollero, A. Serrera, R. Arjona, and S. Alcantarilla, "The CO_2 gasification kinetics of olive residue," *Biomass and Bioenergy*, vol. 24, pp. 151-161, 2002.

[61] E. Cetin, B. Moghtaderi, R. Gupta, and T. F. Wall, "Influence of pyrolysis conditions on the structure and gasification reactivity of biomass chars," *Fuel*, vol. 83, pp. 2139-2150, 2004.

[62] M. Guerrero, M. P. Ruiz, M. U. Alzueta, R. Bilbao, and A. Millera, "Pyrolysis of eucalyptus at different heating rates: Studies of char characterization and oxidative reactivity," *Journal of Analytical and Applied Pyrolysis*, vol. 74, pp. 307-314, 2005.

[63] E. Cetin, R. Gupta, and B. Moghtaderi, "Effect of pyrolysis pressure and heating rate on radiata pine char structure and apparent gasification reactivity," *Fuel*, vol. 84, pp. 1328-1334, 2005.

[64] S. Rapagna and A. Latif, "Steam gasification of almond shells in a fluidised bed reactor: the influence of temperature and particle size on product yield and distribution," *Biomass and Bioenergy*, vol. 12, pp. 281-288, 1997.

[65] F. Scala, R. Chirone, and P. Salatino, "The influence of fine char particles burnout on bed agglomeration during the fluidized bed combustion of a biomass fuel," *Fuel Processing Technology*, vol. 84, pp. 229-241, 2003.

[66] E. Henrich, S. Buerkle, Z. I. Meza-Renken, and S. Rumpel, "Combustion and gasification kinetics of pyrolysis chars from waste and biomass," *Journal of Analytical and Applied Pyrolysis*, vol. 49, pp. 221-241, 1999.

[67] P. A. Campbell, R. E. Mitchell, and L. Ma, "Characterization of coal char and biomass char reactivities to oxygen," in *Proceedings of the Combustion Institute*, vol. 29, *Proceedings of the Combustion Institute*, 1 ed. Sapporo, Japan: Combustion Institute, 2002, pp. 519-526.

[68] M. P. Kannan and G. N. Richards, "Gasification of biomass chars in carbon dioxide. Dependence of gasification rate on the indigenous metal content," *Fuel*, vol. 69, pp. 747-753, 1990.

[69] P. L. Walker, Jr. and P. A. Thrower, "Chemistry and Physics of Carbon," vol. 16. New York and Basel: Marcel Dekker, Inc., 1981.

[70] F. Marquez-Montesinos, T. Cordero, J. Rodriguez-Mirasol, and J. J. Rodriguez, "CO_2 and steam gasification of a grapefruit skin char," *Fuel*, vol. 81, pp. 423-429, 2002.

[71] D. W. McKee, C. L. Spiro, P. G. Kosky, and E. J. Lamby, "Catalysis of coal char gasification by alkali metal salts," *Fuel*, vol. 62, pp. 217-220, 1983.

[72] R. H. Hurt, A. F. Sarofim, and J. P. Longwell, "Role of microporous surface area in the gasification of chars from a sub-bituminous coal," *Fuel*, vol. 70, pp. 1079-1082, 1991.

[73] A. A. Boateng, L. T. Fan, W. P. Walawender, and C. S. Chee, "Morphological development of rice-hull-derived charcoal in a fluidized-bed reactor," *Fuel*, vol. 70, pp. 995-1000, 1991.

[74] M. J. Wornat, R. H. Hurt, N. Y. C. Yang, and T. J. Headley, "Structural and compositional transformations of biomass chars during combustion," *Combustion and Flame*, vol. 100, pp. 131-143, 1995.

[75] M. J. Wornat, R. H. Hurt, K. A. Davis, and N. Y. C. Yang, "Single-particle combustion of two biomass chars," in *Twenty-Sixth Symposium (International) on Combustion*, vol. 2, *Symposium (International) on Combustion*. Napoli, Italy: Combustion Institute, 1996, pp. 3075-3083.

[76] D. W. McKee, "Mechanisms of the alkali metal catalysed gasification of carbon," *Fuel*, vol. 62, pp. 170-175, 1983.

[77] N. Bettagli, U. Desideri, and D. Fiaschi, "Biomass combustion-gasification model: validation and sensitivity analysis," *Journal of Energy Resources Technology, Transactions of the ASME*, vol. 117, pp. 329-336, 1995.

[78] R. C. Brown, Q. Liu, and G. Norton, "Catalytic effects observed during the gasification of coal and switchgrass," *Proceedings of the Third Biomass Conference of the Americas*, 1997.

[79] R. C. Brown, J. Ahrens, and N. Christofides, "Contributions of attrition and fragmentation to char elutriation from fluidized beds," *Combustion and Flame*, vol. 89, pp. 95-102, 1992.

[80] R. C. Brown and N. Christofides, "Attrition and fragmentation of coal-water mixtures in fluidized beds," in *Processing and Utilization of High Sulfur Coals III*, R. Markuszewski and T. D. Wheelock, Eds. Amsterdam: Elsevier, 1990, pp. 573-583.

[81] F. Scala and R. Chirone, "Fluidized bed combustion of alternative solid fuels," *Experimental Thermal and Fluid Science*, vol. 28, pp. 691-699, 2004.

[82] A. R. Kerstein and S. Niksa, "Fragmentation during carbon conversion: predictions and measurements," in *Twentieth Symposium (International) on Combustion*, vol. 20. Pittsburgh, PA: Combustion Institute, 1984, pp. 941-949.

[83] R. Solimene, A. Marzocchella, and P. Salatino, "Hydrodynamic interaction between a coarse gas-emitting particle and a gas fluidized bed of finer solids," *Powder Technology*, vol. 133, pp. 79-90, 2003.

[84] G. Bruni, R. Solimene, A. Marzocchella, P. Salatino, J. G. Yates, P. Lettieri, and M. Fiorentino, "Self-segregation of high-volatile fuel particles during devolatilization in a fluidized bed reactor," *Powder Technology*, vol. 128, pp. 11-21, 2002.

[85] F. Scala and R. Chirone, "Characterization and early detection of bed agglomeration during the fluidized bed combustion of olive husk," *Energy and Fuels*, vol. 20, pp. 120-132, 2006.

[86] J. F. Davidson, R. Clift, and D. Harrison, *Fluidization*, 2nd ed. London: Academic Press Inc., 1985.

[87] C. Fushimi, K. Araki, Y. Yamaguchi, and A. Tsutsumi, "Effect of heating rate on steam gasification of biomass. 2. Thermogravimetric-mass spectrometric (TG-MS) analysis of gas evolution," *Industrial and Engineering Chemistry Research*, vol. 42, pp. 3929-3936, 2003.

[88] J. Bourke, M. Manley-Harris, C. Fushimi, K. Dowaki, T. Numoura, and J. Michael Jerry Antal, "Do all carbonized charcoals have the same chemical structure? 2. A model of the chemical structure of carbonized charcoal," Published on the web 08/03/2007 by the *American Chemical Society*.

[89] R. H. Hurt, "Stucture, properties, and reactivity of solid fuels," in *Twenty-Seventh Symposium (International) on Combustion*. Boulder, Colorado: The Combustion Institute, 1998, pp. 2887-2904.

[90] M. Asadullah, T. Miyazawa, S.-I. Ito, K. Kunimori, and K. Tomishige, "Demonstration of real biomass gasification drastically promoted by effective catalyst," *Applied Catalysis A: General*, vol. 246, pp. 103-116, 2003.

[91] R. F. Vollaro, "Recommended procedure for sampling traverses in ducts smaller than 12 inches in diameter," U.S. Environmental Protection Agency, Emissions Measurement Branch, Research Triangle Park, NC 1977.

[92] K. W. Junk and R. C. Brown, "Model of coal combustion dynamics in a fluidized bed combustor," *Combustion and Flame*, vol. 95, pp. 219-228, 1993.

[93] G. H. Cunningham, Fuel Laboratory Manager, Hazen Research Inc. Golden, Colorado, Personal communication February 21, 2006.

[94] H. W. Coleman and W. G. Steele, *Experimentation and Uncertainty Analysis for Engineers*. New York: John Wiley & Sons, Inc., 1989.

[95] W.-C. Yang, *Handbook of fluidization and fluid-particle systems*. New York: Marcel Dekker, Inc, 2003.

[96] H. S. Fogler, *Elements of chemical reaction engineering*, 3rd ed. Upper Saddle River, New Jersey: Prentice Hall, 1999.

APPENDIX A: STEADY STATE EXPERIMENT SUMMARY SHEETS

Test: **20060224**

Fuel:	CORN (fine)	
Time Gasifying:	11.55	hr
Feed Rate:	6.01	lb/hr
Fuel H2O:	11.2	% ar
Temp:	714	C
Air Flow:	50	slpm
f :	13.8	%
Steam:	0	mL-H2O/min

feed rate =	5.34	lb df/hr
feed rate =	0.672	g df/s
C feed rate =	0.329	g-C/s
feed rate =	0.02741	mol df/s
O2 feed rate =	0.00778	mol O2/s
H2O feed rate =	0.000	g-H2O/s

Steady State Sample

Collection time:	n/m	min
Sample Vol:	n/m	ft3
Cyclone Catch:	n/m	g-char&ash
C content:	n/m	%
Filter Catch:	n/m	g-char&ash
Filter C Catch:	n/m	g-C
Filter C content:	n/m	%
Producer Gas N2:	46.05	%

Ave sample flow =	n/m	slpm
PG flow rate =	84.78	slpm
Cyclone C =	n/m	g-C/s
Char&ash missed =	n/m	g/s
C missed =	n/m	g-C/s
Char&ash cyclone eff =	n/m	%
C cyclone eff =	n/m	%
Re[1] =	0.01221	g-C/s ± 10%
char&ash loading =	14.40	g/m3

Burnout

Collection time:	n/m	min
Sample Vol:	n/m	ft3
Air flow rate:	50	slpm
C from GC:	394.66	g-C
Cyclone Catch:	84	g-char&ash
C content:	29.5	%
Filter Catch:	n/m	g-char&ash
Filter C Catch:	n/m	g-C
Filter C content:	n/m	%

Ave sample flow =	n/m	slpm
Cyclone C =	24.78	g-C
C missed (estimated)[2] =	3.717	g-C
C missed =	n/m	g-C
Wc(tss) =	423.16	g-C
Char&ash cyclone eff =	n/m	%
C cyclone eff =	n/m	%

Model

ER =	0.271			
Total H2O=	0.126	g-H2O/g df		
Total H2O=	0.609	mol-H2O/mol fixed C		
F =	0.0928	g-C/s	±	14 %
Wc(tss) =	423.2	g-C	±	7 %
kt =	219.3	$x10^{-6}$/s	±	15.7 %
ke =	28.8	$x10^{-6}$/s	±	12.2 %
kr =	190.4	$x10^{-6}$/s	±	18.1 %
Time to 0.99xWc(tss) =	5.83	hr		
Ave char residence time =	76.0	min		
PFCC% =	86.8	%	±	2.61 %
CC% =	96.3	%	±	0.39 %

Notes:

1) Re was measured using a bag house style filter and assumes char is 60% carbon. See Nelson, Nathan, "Hot gas particulate removal from gasification streams", MS Thesis, 2006, Iowa State University, Ames, IA

2) Assumes 85% cyclone carbon collection efficiency.

Test: **20060602**

Fuel:	CORN (fine)				
Time gasifying:	4.33	hr			
Feed Rate:	4.48	lb/hr	feed rate =	3.92	lb df/hr
Fuel H2O:	12.6	% ar	feed rate =	0.493	g df/s
Temp:	805	C	C feed rate =	0.241	g-C/s
Air Flow:	50	slpm	feed rate =	0.02011	mol df/s
f :	9.4	%	O2 feed rate =	0.00778	mol O2/s
Steam:	0	mL-H2O/min	H2O feed rate =	0.000	g-H2O/s

Steady State Sample

Collection time:	60	min	Ave sample flow =	2.16	slpm
Sample Vol:	4.566	ft3	PG flow rate =	82.21	slpm
Cyclone Catch:	39.2	g-char&ash	Cyclone C =	0.00418	g-C/s
C content:	38.4	%	Char&ash missed =	0.00107	g/s
Filter Catch:	0.1013	g-char&ash	C missed =	0.00021	g-C/s
Filter C Catch:	0.0197	g-C	Char&ash cyclone eff =	91.0	%
Filter C content:	19.4	%	C cyclone eff =	95.2	%
Producer Gas N2:	47.49	%	Re =	0.00439	g-C/s ± 5%
			char&ash loading =	8.73	g/m3

Burnout

Collection time:	60	min	Ave sample flow =	1.057	slpm
Sample Vol:	2.24	ft3	Cyclone C =	0.62	g-C
Air flow rate:	50	slpm	C missed (estimated) =	0.030	g-C
C from GC:	70.84	g-C	C missed =	n/m	g-C
Cyclone Catch:	2.6	g-char&ash	Wc(tss) =	71.49	g-C
C content:	24	%	Char&ash cyclone eff =	n/m	%
Filter Catch:	n/m	g-char&ash	C cyclone eff =	n/m	%
Filter C Catch:	n/m	g-C			
Filter C content:	n/m	%			

Model					
ER =	0.370				
Total H2O=	0.144	g-H2O/g df			
Total H2O=	1.022	mol-H2O/mol fixed C			
F =	0.0464	g-C/s	±	14	%
Wc(tss) =	71.5	g-C	±	4	%
kt =	648.7	$x10^{-6}$/s	±	14.6	%
ke =	61.4	$x10^{-6}$/s	±	6.4	%
kr =	587.2	$x10^{-6}$/s	±	16.1	%
Time to 0.99xWc(tss) =	1.97	hr			
Ave char residence time =	25.7	min			
PFCC% =	90.5	%	±	1.55	%
CC% =	98.2	%	±	0.10	%

Notes:

Test: **20060607**

Fuel:	CORN (fine)				
Time Gasifying:	6	hr			
Feed Rate:	4.9	lb/hr	feed rate =	4.28	lb df/hr
Fuel H2O:	12.6	% ar	feed rate =	0.540	g df/s
Temp:	750	C	C feed rate =	0.264	g-C/s
Air Flow:	50	slpm	feed rate =	0.02199	mol df/s
f :	10.6	%	O2 feed rate =	0.00778	mol O2/s
Steam:	0	mL-H2O/min	H2O feed rate =	0.000	g-H2O/s

Steady State Sample

Collection time:	60	min	Ave sample flow =	1.88	slpm
Sample Vol:	3.985	ft3	PG flow rate =	81.79	slpm
Cyclone Catch:	41.1	g-char&ash	Cyclone C =	0.00602	g-C/s
C content:	52.7	%	Char&ash missed =	0.00190	g/s
Filter Catch:	0.1575	g-char&ash	C missed =	0.00054	g-C/s
Filter C Catch:	0.0446	g-C	Char&ash cyclone eff =	85.7	%
Filter C content:	28.3	%	C cyclone eff =	91.8	%
Producer Gas N2:	47.73	%	Re =	0.00656	g-C/s ± 5%
			char&ash loading =	9.77	g/m3

Burnout

Collection time:	75	min	Ave sample flow =	1.01	slpm
Sample Vol:	2.674	ft3	Cyclone C =	1.252	g-C
Air flow rate:	50	slpm	C missed (estimated) =	0.103	g-C
C from GC:	134.39	g-C	C missed =	n/m	g-C
Cyclone Catch:	4	g-char&ash	Wc(tss) =	135.74	g-C
C content:	31.3	%	Char&ash cyclone eff =	n/m	%
Filter Catch:	n/m	g-char&ash	C cyclone eff =	n/m	%
Filter C Catch:	n/m	g-C			
Filter C content:	n/m	%			

Model					
ER =	0.338				
Total H2O=	0.144	g-H2O/g df			
Total H2O=	0.907	mol-H2O/mol fixed C			
F =	0.0572	g-C/s	±	14	%
Wc(tss) =	135.7	g-C	±	4	%
kt =	421.4	$x10^{-6}$/s	±	14.6	%
ke =	48.3	$x10^{-6}$/s	±	6.4	%
kr =	373.1	$x10^{-6}$/s	±	16.5	%
Time to 0.99xWc(tss) =	3.04	hr			
Ave char residence time =	39.6	min			
PFCC% =	88.5	%	±	1.92	%
CC% =	97.5	%	±	0.14	%

Notes:

Test: **20060608**

Fuel:	CORN (fine)				
Time gasifying:	6	hr			
Feed Rate:	4.4	lb/hr	feed rate =	3.85	lb df/hr
Fuel H2O:	12.6	% ar	feed rate =	0.485	g df/s
Temp:	706	C	C feed rate =	0.237	g-C/s
Air Flow:	41.5	slpm	feed rate =	0.01975	mol df/s
f :	14.5	%	O2 feed rate =	0.00645	mol O2/s
Steam:	0	mL-H2O/min	H2O feed rate =	0.000	g-H2O/s

Steady State Sample

Collection time:	60	min	Ave sample flow =	2.04	slpm
Sample Vol:	4.331	ft3	PG flow rate =	70.67	slpm
Cyclone Catch:	31.1	g-char&ash	Cyclone C =	0.00560	g-C/s
C content:	64.81	%	Char&ash missed =	0.00142	g/s
Filter Catch:	0.1476	g-char&ash	C missed =	0.00047	g-C/s
Filter C Catch:	0.0491	g-C	Char&ash cyclone eff =	85.9	%
Filter C content[1]:	33.3	%	C cyclone eff =	92.2	%
Producer Gas N2:	45.85	%	Re =	0.00607	g-C/s ± 5%
			char&ash loading =	8.54	g/m3

Burnout

Collection time:	135	min	Ave sample flow =	0.942	slpm
Sample Vol:	4.492	ft3	Cyclone C =	8.99	g-C
Air flow rate:	41.5	slpm	C missed (estimated) =	0.698	g-C
C from GC:	242.96	g-C	C missed =	n/m	g-C
Cyclone Catch:	19.3	g-char&ash	Wc(tss) =	252.64	g-C
C content:	46.56	%	Char&ash cyclone eff =	n/m	%
Filter Catch:	n/m	g-char&ash	C cyclone eff =	n/m	%
Filter C Catch:	n/m	g-C			
Filter C content:	n/m	%			

Model					
ER =	0.313				
Total H2O=	0.144	g-H2O/g df			
Total H2O=	0.663	mol-H2O/mol fixed C			
F =	0.0703	g-C/s	±	14	%
Wc(tss) =	252.6	g-C	±	4	%
kt =	278.1	$x10^{-6}$/s	±	14.6	%
ke =	24.0	$x10^{-6}$/s	±	6.4	%
kr =	254.1	$x10^{-6}$/s	±	15.9	%
Time to 0.99xWc(tss) =	4.60	hr			
Ave char residence time =	59.9	min			
PFCC% =	91.4	%	±	1.41	%
CC% =	97.4	%	±	0.14	%

Notes: 1) Filter tipped upside down during removal - may have lost collected material
used filter data of 6/7/06 and 6/13/06 to estimate filter catch

Test: **20060616**

Fuel:	CORN (fine)				
Time gasifying:	7.42	hr			
Feed Rate:	5.89	lb/hr	feed rate =	5.17	lb df/hr
Fuel H2O:	12.2	% ar	feed rate =	0.652	g df/s
Temp:	753	C	C feed rate =	0.319	g-C/s
Air Flow:	50	slpm	feed rate =	0.02656	mol df/s
f :	10.5	%	O2 feed rate =	0.00778	mol O2/s
Steam:	0	mL-H2O/min	H2O feed rate =	0.000	g-H2O/s

Steady State Sample

Collection time:	60	min	Ave sample flow =	1.96	slpm
Sample Vol:	4.159	ft3	PG flow rate =	87.75	slpm
Cyclone Catch:	44.6	g-char&ash	Cyclone C =	0.00751	g-C/s
C content:	60.63	%	Char&ash missed =	0.00390	g/s
Filter Catch:	0.3138	g-char&ash	C missed =	0.00189	g-C/s
Filter C Catch:	0.1523	g-C	Char&ash cyclone eff =	76.1	%
Filter C content:	48.5	%	C cyclone eff =	79.9	%
Producer Gas N2:	44.49	%	Re =	0.00940	g-C/s ± 5%
			char&ash loading =	11.14	g/m3

Burnout

Collection time:	105	min	Ave sample flow =	0.947	slpm
Sample Vol:	3.51	ft3	Cyclone C =	9.36	g-C
Air flow rate:	50	slpm	C missed (estimated) =	1.883	g-C
C from GC:	247.87	g-C	C missed =	0.79	g-C
Cyclone Catch:	21.4	g-char&ash	Wc(tss) =	258.02	g-C
C content:	43.74	%	Char&ash cyclone eff =	82.9	%
Filter Catch:	0.0836	g-char&ash	C cyclone eff =	92.2	%
Filter C Catch:	0.01501	g-C			
Filter C content:	18.0	%			

Model					
ER =	0.280				
Total H2O=	0.139	g-H2O/g df			
Total H2O=	0.882	mol-H2O/mol fixed C			
F =	0.0684	g-C/s	±	14	%
Wc(tss) =	258.0	g-C	±	4	%
kt =	265.2	$x10^{-6}$/s	±	14.6	%
ke =	36.4	$x10^{-6}$/s	±	6.4	%
kr =	228.7	$x10^{-6}$/s	±	16.9	%
Time to 0.99xWc(tss) =	4.82	hr			
Ave char residence time =	62.9	min			
PFCC% =	86.3	%	±	2.37	%
CC% =	97.0	%	±	0.16	%

Notes:

Test: **20060620**

Fuel:	CORN (fine)				
Time gasifying:	7.25	hr			
Feed Rate:	6.23	lb/hr	feed rate =	5.47	lb df/hr
Fuel H2O:	12.2	% ar	feed rate =	0.689	g df/s
Temp:	751	C	C feed rate =	0.337	g-C/s
Air Flow:	50	slpm	feed rate =	0.02809	mol df/s
f :	10.5	%	O2 feed rate =	0.00778	mol O2/s
Steam:	0	mL-H2O/min	H2O feed rate =	0.000	g-H2O/s

Steady State Sample

Collection time:	60	min	Ave sample flow =	1.96	slpm
Sample Vol:	4.143	ft3	PG flow rate =	89.19	slpm
Cyclone Catch:	52.1	g-char&ash	Cyclone C =	0.00873	g-C/s
C content:	60.32	%	Char&ash missed =	0.00502	g/s
Filter Catch:	0.396	g-char&ash	C missed =	0.00231	g-C/s
Filter C Catch:	0.1821	g-C	Char&ash cyclone eff =	74.3	%
Filter C content:	46.0	%	C cyclone eff =	79.1	%
Producer Gas N2:	43.77	%	Re =	0.01104	g-C/s ± 5%
			char&ash loading =	13.11	g/m3

Burnout

Collection time:	135	min	Ave sample flow =	0.998	slpm
Sample Vol:	4.758	ft3	Cyclone C =	9.86	g-C
Air flow rate:	50	slpm	C missed (estimated) =	2.061	g-C
C from GC:	312.65	g-C	C missed =	2.46	g-C
Cyclone Catch:	49.1	g-char&ash	Wc(tss) =	324.97	g-C
C content:	20.08	%	Char&ash cyclone eff =	87.0	%
Filter Catch:	0.1463	g-char&ash	C cyclone eff =	80.1	%
Filter C Catch:	0.04905	g-C			
Filter C content:	33.5	%			

Model					
ER =	0.265				
Total H2O=	0.139	g-H2O/g df			
Total H2O=	0.882	mol-H2O/mol fixed C			
F =	0.0724	g-C/s	±	14	%
Wc(tss) =	325.0	g-C	±	4	%
kt =	222.7	$x10^{-6}$/s	±	14.6	%
ke =	34.0	$x10^{-6}$/s	±	6.4	%
kr =	188.7	$x10^{-6}$/s	±	17.2	%
Time to 0.99xWc(tss) =	5.74	hr			
Ave char residence time =	74.8	min			
PFCC% =	84.7	%	±	2.68	%
CC% =	96.7	%	±	0.18	%

Notes:

Test: **20060621**

Fuel:	CORN (fine)				
Time gasifying:	6.87	hr			
Feed Rate:	6.23	lb/hr	feed rate =	5.47	lb df/hr
Fuel H2O:	12.2	% ar	feed rate =	0.689	g df/s
Temp:	751	C	C feed rate =	0.337	g-C/s
Air Flow:	50	slpm	feed rate =	0.02809	mol df/s
f :	10.5	%	O2 feed rate =	0.00778	mol O2/s
Steam:	0	mL-H2O/min	H2O feed rate =	0.000	g-H2O/s

Steady State Sample

Collection time:	45	min	Ave sample flow =	2.04	slpm
Sample Vol:	3.241	ft3	PG flow rate =	91.62	slpm
Cyclone Catch:	37.55	g-char&ash	Cyclone C =	0.00828	g-C/s
C content:	59.54	%	Char&ash missed =	0.00622	g/s
Filter Catch:	0.3737	g-char&ash	C missed =	0.00305	g-C/s
Filter C Catch:	0.1834	g-C	Char&ash cyclone eff =	69.1	%
Filter C content:	49.1	%	C cyclone eff =	73.1	%
Producer Gas N2:	42.61	%	Re =	0.01133	g-C/s ± 5%
			char&ash loading =	13.18	g/m3

Burnout

Collection time:	127	min	Ave sample flow =	0.969	slpm
Sample Vol:	4.345	ft3	Cyclone C =	11.43	g-C
Air flow rate:	50	slpm	C missed (estimated) =	3.077	g-C
C from GC:	301.89	g-C	C missed =	4.97	g-C
Cyclone Catch:	66.9	g-char&ash	Wc(tss) =	318.29	g-C
C content:	17.08	%	Char&ash cyclone eff =	81.0	%
Filter Catch:	0.3044	g-char&ash	C cyclone eff =	69.7	%
Filter C Catch:	0.09632	g-C			
Filter C content:	31.6	%			

Model					
ER =	0.265				
Total H2O=	0.139	g-H2O/g df			
Total H2O=	0.882	mol-H2O/mol fixed C			
F =	0.0724	g-C/s	±	14	%
Wc(tss) =	318.3	g-C	±	4	%
kt =	227.4	$x10^{-6}$/s	±	14.6	%
ke =	35.6	$x10^{-6}$/s	±	6.4	%
kr =	191.8	$x10^{-6}$/s	±	17.3	%
Time to 0.99xWc(tss) =	5.63	hr			
Ave char residence time =	73.3	min			
PFCC% =	84.3	%	±	2.76	%
CC% =	96.6	%	±	0.19	%

Notes:

Test: **20060622**

Fuel:	CORN (fine)				
Time gasifying:	6.75	hr			
Feed Rate:	6.13	lb/hr	feed rate =	5.38	lb df/hr
Fuel H2O:	12.2	% ar	feed rate =	0.678	g df/s
Temp:	801	C	C feed rate =	0.332	g-C/s
Air Flow:	50	slpm	feed rate =	0.02764	mol df/s
f :	9.5	%	O2 feed rate =	0.00778	mol O2/s
Steam:	0	mL-H2O/min	H2O feed rate =	0.000	g-H2O/s

Steady State Sample

Collection time:	45	min	Ave sample flow =	2.06	slpm
Sample Vol:	3.277	ft3	PG flow rate =	98.02	slpm
Cyclone Catch:	31.65	g-char&ash	Cyclone C =	0.00658	g-C/s
C content:	56.14	%	Char&ash missed =	0.00338	g/s
Filter Catch:	0.1921	g-char&ash	C missed =	0.00143	g-C/s
Filter C Catch:	0.0811	g-C	Char&ash cyclone eff =	77.6	%
Filter C content:	42.2	%	C cyclone eff =	82.2	%
Producer Gas N2:	39.83	%	Re =	0.00801	g-C/s ± 5%
			char&ash loading =	9.25	g/m3

Burnout

Collection time:	84	min	Ave sample flow =	0.900	slpm
Sample Vol:	2.67	ft3	Cyclone C =	0.23	g-C
Air flow rate:	50	slpm	C missed (estimated) =	0.041	g-C
C from GC:	141.97	g-C	C missed =	0.00	g-C
Cyclone Catch:	0.8	g-char&ash	Wc(tss) =	142.20	g-C
C content:	28.57	%	Char&ash cyclone eff =	n/m	%
Filter Catch:	0	g-char&ash	C cyclone eff =	n/m	%
Filter C Catch:	0	g-C			
Filter C content:	n/m	%			

Model					
ER =	0.269				
Total H2O=	0.139	g-H2O/g df			
Total H2O=	0.975	mol-H2O/mol fixed C			
F =	0.0644	g-C/s	±	14	%
Wc(tss) =	142.2	g-C	±	4	%
kt =	453.1	$x10^{-6}$/s	±	14.6	%
ke =	56.3	$x10^{-6}$/s	±	6.4	%
kr =	396.7	$x10^{-6}$/s	±	16.7	%
Time to 0.99xWc(tss) =	2.82	hr			
Ave char residence time =	36.8	min			
PFCC% =	87.6	%	±	2.11	%
CC% =	97.6	%	±	0.13	%

Notes:

Test: **20060629**

Fuel:	CORN (fine)				
Time gasifying:	8	hr			
Feed Rate:	6.88	lb/hr	feed rate =	5.99	lb df/hr
Fuel H2O:	13	% ar	feed rate =	0.754	g df/s
Temp:	801	C	C feed rate =	0.369	g-C/s
Air Flow:	50	slpm	feed rate =	0.03074	mol df/s
f :	9.5	%	O2 feed rate =	0.00778	mol O2/s
Steam:	0	mL-H2O/min	H2O feed rate =	0.000	g-H2O/s

Steady State Sample

Collection time:	30	min	Ave sample flow =	2.22	slpm
Sample Vol:	2.353	ft3	PG flow rate =	104.78	slpm
Cyclone Catch:	37.5	g-char&ash	Cyclone C =	0.01102	g-C/s
C content:	52.88	%	Char&ash missed =	0.00477	g/s
Filter Catch:	0.1821	g-char&ash	C missed =	0.00237	g-C/s
Filter C Catch:	0.0904	g-C	Char&ash cyclone eff =	81.4	%
Filter C content:	49.6	%	C cyclone eff =	82.3	%
Producer Gas N2:	37.26	%	**Re =**	**0.01339**	**g-C/s ± 5%**
			char&ash loading =	14.66	g/m3

Burnout

Collection time:	120	min	Ave sample flow =	1.000	slpm
Sample Vol[1]:	4.237	ft3	Cyclone C =	1.73	g-C
Air flow rate:	50	slpm	C missed (estimated) =	0.307	g-C
C from GC:	196.11	g-C	C missed =	0.00	g-C
Cyclone Catch:	11.35	g-char&ash	**Wc(tss) =**	**197.84**	**g-C**
C content:	15.28	%	Char&ash cyclone eff =	98.8	%
Filter Catch:	0.00274	g-char&ash	C cyclone eff =	100.0	%
Filter C Catch:	0	g-C			
Filter C content:	0.0	%			

Model					
ER =	0.242				
Total H2O=	0.149	g-H2O/g df			
Total H2O=	1.048	mol-H2O/mol fixed C			
F =	0.0716	g-C/s	±	14	%
Wc(tss) =	197.8	g-C	±	4	%
kt =	362.1	$x10^{-6}$/s	±	14.6	%
ke =	67.7	$x10^{-6}$/s	±	6.4	%
kr =	294.5	$x10^{-6}$/s	±	18.0	%
Time to 0.99xWc(tss) =	3.53	hr			
Ave char residence time =	46.0	min			
PFCC% =	81.3	%	±	3.42	%
CC% =	96.4	%	±	0.20	%

Notes: 1. Volume meter malfunctioned, calculations assume 1 slpm sample flow

Test: **20060713**

Fuel:	CORN (coarse)				
Time gasifying:	4.833	hr			
Feed Rate:	6.17	lb/hr	feed rate =	5.38	lb df/hr
Fuel H2O:	12.88	% ar	feed rate =	0.677	g df/s
Temp:	801	C	C feed rate =	0.331	g-C/s
Air Flow:	50	slpm	feed rate =	0.02760	mol df/s
f :	9.5	%	O2 feed rate =	0.00778	mol O2/s
Steam:	0	mL-H2O/min	H2O feed rate =	0.000	g-H2O/s

Steady State Sample

Collection time:	30	min	Ave sample flow =	2.50	slpm
Sample Vol[1]:	2.648	ft3	PG flow rate =	95.78	slpm
Cyclone Catch:	38.05	g-char&ash	Cyclone C =	0.01266	g-C/s
C content:	59.89	%	Char&ash missed =	0.00427	g/s
Filter Catch:	0.2004	g-char&ash	C missed =	0.00124	g-C/s
Filter C Catch:	0.0583	g-C	Char&ash cyclone eff =	83.2	%
Filter C content:	29.1	%	C cyclone eff =	91.1	%
Producer Gas N2:	40.76	%	**Re =**	**0.01390**	**g-C/s ± 5%**
			char&ash loading =	15.91	g/m3

Burnout

Collection time:	110	min	Ave sample flow =	1.000	slpm
Sample Vol[1]:	3.884	ft3	Cyclone C =	3.89	g-C
Air flow rate:	50	slpm	C missed (estimated) =	0.347	g-C
C from GC:	139.88	g-C	C missed =	n/m	g-C
Cyclone Catch:	9.6	g-char&ash	**Wc(tss) =**	**144.12**	**g-C**
C content:	40.5	%	Char&ash cyclone eff =	n/m	%
Filter Catch:	n/m	g-char&ash	C cyclone eff =	n/m	%
Filter C Catch:	n/m	g-C			
Filter C content:	n/m	%			

Model					
ER =	0.270				
Total H2O=	0.148	g-H2O/g df			
Total H2O=	1.037	mol-H2O/mol fixed C			
F =	0.0643	g-C/s	±	14	%
Wc(tss) =	144.1	g-C	±	4	%
kt =	446.5	x10^{-6}/s	±	14.6	%
ke =	96.5	x10^{-6}/s	±	6.4	%
kr =	350.0	x10^{-6}/s	±	18.7	%
Time to 0.99xWc(tss) =	2.87	hr			
Ave char residence time =	37.3	min			
PFCC% =	78.4	%	±	4.10	%
CC% =	95.8	%	±	0.24	%

Notes:

Test: **20060715**

Fuel:	CORN (coarse)				
Time gasifying:	6	hr			
Feed Rate:	4.72	lb/hr	feed rate =	4.11	lb df/hr
Fuel H2O:	12.88	% ar	feed rate =	0.518	g df/s
Temp:	746	C	C feed rate =	0.253	g-C/s
Air Flow:	40	slpm	feed rate =	0.02112	mol df/s
f :	11	%	O2 feed rate =	0.00622	mol O2/s
Steam:	0	mL-H2O/min	H2O feed rate =	0.000	g-H2O/s

Steady State Sample

Collection time:	45	min	Ave sample flow =	1.79	slpm
Sample Vol:	2.848	ft3	PG flow rate =	75.44	slpm
Cyclone Catch:	36.95	g-char&ash	Cyclone C =	0.00870	g-C/s
C content:	63.58	%	Char&ash missed =	0.00332	g/s
Filter Catch:	0.213	g-char&ash	C missed =	0.00167	g-C/s
Filter C Catch:	0.1073	g-C	Char&ash cyclone eff =	80.5	%
Filter C content:	50.4	%	C cyclone eff =	83.9	%
Producer Gas N2:	41.4	%	Re =	0.01037	g-C/s ± 5%
			char&ash loading =	13.53	g/m3

Burnout

Collection time:	126	min	Ave sample flow =	1.056	slpm
Sample Vol:	4.699	ft3	Cyclone C =	3.90	g-C
Air flow rate:	50	slpm	C missed (estimated) =	0.629	g-C
C from GC:	218.6	g-C	C missed =	1.11	g-C
Cyclone Catch:	8.7	g-char&ash	Wc(tss) =	223.61	g-C
C content:	44.87	%	Char&ash cyclone eff =	70.2	%
Filter Catch:	0.07784	g-char&ash	C cyclone eff =	77.9	%
Filter C Catch:	0.02346	g-C			
Filter C content:	30.1	%			

Model					
ER =	0.282				
Total H2O=	0.148	g-H2O/g df			
Total H2O=	0.896	mol-H2O/mol fixed C			
F =	0.0570	g-C/s	±	14	%
Wc(tss) =	223.6	g-C	±	4	%
kt =	254.9	$x10^{-6}$/s	±	14.6	%
ke =	46.4	$x10^{-6}$/s	±	6.4	%
kr =	208.5	$x10^{-6}$/s	±	17.9	%
Time to 0.99xWc(tss) =	5.02	hr			
Ave char residence time =	65.4	min			
PFCC% =	81.8	%	±	3.31	%
CC% =	95.9	%	±	0.23	%

Notes:

Test: **20060718**

Fuel:	CORN (fine)				
Time gasifying:	3.5	hr			
Feed Rate:	6.69	lb/hr	feed rate =	5.86	lb df/hr
Fuel H2O:	12.36	% ar	feed rate =	0.739	g df/s
Temp:	798	C	C feed rate =	0.361	g-C/s
Air Flow:	50	slpm	feed rate =	0.03011	mol df/s
f :	9.5	%	O2 feed rate =	0.00778	mol O2/s
Steam:	5.26	mL-H2O/min	H2O feed rate =	0.088	g-H2O/s

Steady State Sample

Collection time:	30	min	Ave sample flow =	2.48	slpm
Sample Vol:	2.632	ft3	PG flow rate =	99.49	slpm
Cyclone Catch:	44.1	g-char&ash	Cyclone C =	0.01156	g-C/s
C content:	47.2	%	Char&ash missed =	0.00204	g/s
Filter Catch:	0.0915	g-char&ash	C missed =	0.00047	g-C/s
Filter C Catch:	0.021	g-C	Char&ash cyclone eff =	92.3	%
Filter C content:	23.0	%	C cyclone eff =	96.1	%
Producer Gas N2:	39.24	%	Re =	0.01203	g-C/s ± 5%
			char&ash loading =	16.00	g/m3

Burnout

Collection time:	123	min	Ave sample flow =	1.158	slpm
Sample Vol:	5.03	ft3	Cyclone C =	3.01	g-C
Air flow rate:	50	slpm	C missed (estimated) =	0.602	g-C
C from GC:	107.34	g-C	C missed =	n/m	g-C
Cyclone Catch:	13.15	g-char&ash	Wc(tss) =	110.95	g-C
C content:	22.89	%	Char&ash cyclone eff =	n/m	%
Filter Catch:	n/m	g-char&ash	C cyclone eff =	n/m	%
Filter C Catch:	n/m	g-C			
Filter C content:	n/m	%			

Model					
ER =	0.247				
Total H2O=	0.260	g-H2O/g df			
Total H2O=	1.822	mol-H2O/mol fixed C			
F =	0.0702	g-C/s	±	14	%
Wc(tss) =	111.0	g-C	±	4	%
kt =	632.5	x10^{-6}/s	±	14.6	%
ke =	108.4	x10^{-6}/s	±	6.4	%
kr =	524.1	x10^{-6}/s	±	17.6	%
Time to 0.99xWc(tss) =	2.02	hr			
Ave char residence time =	26.3	min			
PFCC% =	82.9	%	±	3.08	%
CC% =	96.7	%	±	0.19	%

Notes:

Test: **20060721**

Fuel:	CORN (fine)				
Time gasifying:	3.25	hr			
Feed Rate:	6.56	lb/hr	feed rate =	5.75	lb df/hr
Fuel H2O:	12.39	% ar	feed rate =	0.724	g df/s
Temp:	797	C	C feed rate =	0.354	g-C/s
Air Flow:	50	slpm	feed rate =	0.02951	mol df/s
f :	9.5	%	O2 feed rate =	0.00778	mol O2/s
Steam:	12.1	mL-H2O/min	H2O feed rate =	0.202	g-H2O/s

Steady State Sample

Collection time:	45	min	Ave sample flow =	2.19	slpm
Sample Vol:	3.476	ft3	PG flow rate =	106.55	slpm
Cyclone Catch:	50.65	g-char&ash	Cyclone C =	0.00972	g-C/s
C content:	51.81	%	Char&ash missed =	0.00255	g/s
Filter Catch:	0.1413	g-char&ash	C missed =	0.00045	g-C/s
Filter C Catch:	0.0251	g-C	Char&ash cyclone eff =	88.0	%
Filter C content:	17.8	%	C cyclone eff =	95.5	%
Producer Gas N2:	36.64	%	Re =	0.01017	g-C/s ± 5%
			char&ash loading =	12.00	g/m3

Burnout

Collection time:	74	min	Ave sample flow =	1.196	slpm
Sample Vol:	3.125	ft3	Cyclone C =	0.76	g-C
Air flow rate:	50	slpm	C missed (estimated) =	0.152	g-C
C from GC:	91.85	g-C	C missed =	n/m	g-C
Cyclone Catch:	8.6	g-char&ash	Wc(tss) =	92.76	g-C
C content:	8.83	%	Char&ash cyclone eff =	n/m	%
Filter Catch:	n/m	g-char&ash	C cyclone eff =	n/m	%
Filter C Catch:	n/m	g-C			
Filter C content:	n/m	%			

Model					
ER =	0.252				
Total H2O=	0.420	g-H2O/g df			
Total H2O=	2.947	mol-H2O/mol fixed C			
F =	0.0688	g-C/s	±	14	%
Wc(tss) =	92.8	g-C	±	4	%
kt =	741.6	$x10^{-6}$/s	±	14.6	%
ke =	109.7	$x10^{-6}$/s	±	6.4	%
kr =	632.0	$x10^{-6}$/s	±	17.1	%
Time to 0.99xWc(tss) =	1.72	hr			
Ave char residence time =	22.5	min			
PFCC% =	85.2	%	±	2.58	%
CC% =	97.1	%	±	0.16	%

Notes:

Test: **20061215**

Fuel:	CORN (fine)				
Time gasifying:	4.75	hr			
Feed Rate:	4.81	lb/hr	feed rate =	4.25	lb df/hr
Fuel H2O:	11.66	% ar	feed rate =	0.535	g df/s
Temp:	748	C	C feed rate =	0.262	g-C/s
Air Flow:	40	slpm	feed rate =	0.02182	mol df/s
f :	10.8	%	O2 feed rate =	0.00622	mol O2/s
Steam:	0	mL-H2O/min	H2O feed rate =	0.000	g-H2O/s

Steady State Sample

Collection time:	45	min	Ave sample flow =	1.63	slpm
Sample Vol:	2.597	ft3	PG flow rate =	61.00	slpm
Cyclone Catch:	18.74	g-char&ash	Cyclone C =	0.00349	g-C/s
C content:	50.31	%	Char&ash missed =	0.00124	g/s
Filter Catch:	0.0897	g-char&ash	C missed =	0.00017	g-C/s
Filter C Catch:	0.0123	g-C	Char&ash cyclone eff =	84.8	%
Filter C content:	13.7	%	C cyclone eff =	95.4	%
Producer Gas N2:	51.2	%	Re =	0.00366	g-C/s ± 5%
			char&ash loading =	8.05	g/m3

Burnout

Collection time:	150	min	Ave sample flow =	0.796	slpm
Sample Vol:	4.214	ft3	Cyclone C =	0.36	g-C
Air flow rate:	50	slpm	C missed (estimated) =	0.017	g-C
C from GC:	145.64	g-C	C missed =	n/m	g-C
Cyclone Catch:	2.8	g-char&ash	Wc(tss) =	146.02	g-C
C content:	12.98	%	Char&ash cyclone eff =	n/m	%
Filter Catch:	n/m	g-char&ash	C cyclone eff =	n/m	%
Filter C Catch:	n/m	g-C			
Filter C content:	n/m	%			

Model					
ER =	0.273				
Total H2O=	0.132	g-H2O/g df			
Total H2O=	0.815	mol-H2O/mol fixed C			
F =	0.0578	g-C/s	±	14	%
Wc(tss) =	146.0	g-C	±	4	%
kt =	396.0	$x10^{-6}$/s	±	14.6	%
ke =	25.1	$x10^{-6}$/s	±	6.4	%
kr =	370.9	$x10^{-6}$/s	±	15.6	%
Time to 0.99xWc(tss) =	3.23	hr			
Ave char residence time =	42.1	min			
PFCC% =	93.7	%	±	1.01	%
CC% =	98.6	%	±	0.08	%

Notes:

Test: **20061228**

Fuel:	CORN (fine)				
Time gasifying:	5.5	hr			
Feed Rate:	5.47	lb/hr	feed rate =	4.83	lb df/hr
Fuel H2O:	11.66	% ar	feed rate =	0.609	g df/s
Temp:	748	C	C feed rate =	0.298	g-C/s
Air Flow:	50	slpm	feed rate =	0.02482	mol df/s
f :	10.8	%	O2 feed rate =	0.00778	mol O2/s
Steam:	0	mL-H2O/min	H2O feed rate =	0.000	g-H2O/s

Steady State Sample

Collection time:	30	min	Ave sample flow =	2.10	slpm
Sample Vol:	2.225	ft3	PG flow rate =	83.01	slpm
Cyclone Catch:	16.89	g-char&ash	Cyclone C =	0.00466	g-C/s
C content:	49.65	%	Char&ash missed =	0.00318	g/s
Filter Catch:	0.1449	g-char&ash	C missed =	0.00060	g-C/s
Filter C Catch:	0.0275	g-C	Char&ash cyclone eff =	74.7	%
Filter C content:	19.0	%	C cyclone eff =	88.5	%
Producer Gas N2:	47.03	%	Re =	0.00526	g-C/s ± 5%
			char&ash loading =	9.08	g/m3

Burnout

Collection time:	195	min	Ave sample flow =	0.970	slpm
Sample Vol:	6.677	ft3	Cyclone C =	1.39	g-C
Air flow rate:	50	slpm	C missed (estimated) =	0.159	g-C
C from GC:	162.82	g-C	C missed =	n/m	g-C
Cyclone Catch:	52.32	g-char&ash	Wc(tss) =	164.37	g-C
C content:	2.65	%	Char&ash cyclone eff =	n/m	%
Filter Catch:	n/m	g-char&ash	C cyclone eff =	n/m	%
Filter C Catch:	n/m	g-C			
Filter C content:	n/m	%			

Model					
ER =	0.300				
Total H2O=	0.132	g-H2O/g df			
Total H2O=	0.815	mol-H2O/mol fixed C			
F =	0.0658	g-C/s	±	14	%
Wc(tss) =	164.4	g-C	±	4	%
kt =	400.1	$x10^{-6}$/s	±	14.6	%
ke =	32.0	$x10^{-6}$/s	±	6.4	%
kr =	368.0	$x10^{-6}$/s	±	15.8	%
Time to 0.99xWc(tss) =	3.20	hr			
Ave char residence time =	41.7	min			
PFCC% =	92.0	%	±	1.29	%
CC% =	98.2	%	±	0.10	%

Notes:

Test: **20061229**

Fuel:	CORN (fine)				
Time gasifying:	3.48	hr			
Feed Rate:	9.53	lb/hr	feed rate =	8.42	lb df/hr
Fuel H2O:	11.66	% ar	feed rate =	1.061	g df/s
Temp:	750	C	C feed rate =	0.519	g-C/s
Air Flow:	83	slpm	feed rate =	0.04323	mol df/s
f :	10.6	%	O2 feed rate =	0.01291	mol O2/s
Steam:	0	mL-H2O/min	H2O feed rate =	0.000	g-H2O/s

Steady State Sample

Collection time:	10	min	Ave sample flow =	3.34	slpm
Sample Vol:	1.18	ft3	PG flow rate =	143.79	slpm
Cyclone Catch:	18.15	g-char&ash	Cyclone C =	0.01722	g-C/s
C content:	56.93	%	Char&ash missed =	0.01056	g/s
Filter Catch:	0.1473	g-char&ash	C missed =	0.00261	g-C/s
Filter C Catch:	0.0364	g-C	Char&ash cyclone eff =	74.1	%
Filter C content:	24.7	%	C cyclone eff =	86.8	%
Producer Gas N2:	45.07	%	Re =	0.01983	g-C/s ± 5%
			char&ash loading =	17.03	g/m3

Burnout

Collection time:	165	min	Ave sample flow =	1.068	slpm
Sample Vol:	6.223	ft3	Cyclone C =	3.11	g-C
Air flow rate:	50	slpm	C missed (estimated) =	0.409	g-C
C from GC:	198.36	g-C	C missed =	n/m	g-C
Cyclone Catch:	12.01	g-char&ash	Wc(tss) =	201.87	g-C
C content:	25.86	%	Char&ash cyclone eff =	n/m	%
Filter Catch:	n/m	g-char&ash	C cyclone eff =	n/m	%
Filter C Catch:	n/m	g-C			
Filter C content:	n/m	%			

Model					
ER =	0.286				
Total H2O=	0.132	g-H2O/g df			
Total H2O=	0.830	mol-H2O/mol fixed C			
F =	0.1124	g-C/s	±	14	%
Wc(tss) =	201.9	g-C	±	4	%
kt =	557.0	$x10^{-6}$/s	±	14.6	%
ke =	98.2	$x10^{-6}$/s	±	6.4	%
kr =	458.7	$x10^{-6}$/s	±	17.7	%
Time to 0.99xWc(tss) =	2.30	hr			
Ave char residence time =	29.9	min			
PFCC% =	82.4	%	±	3.18	%
CC% =	96.2	%	±	0.21	%

Notes:

APPENDIX B: UNCERTAINTY ANALYSIS

A detailed description of the uncertainty analysis used to establish 95% confidence bands for the results of this study is given in this appendix. The uncertainty in experimentally measured parameters is conservatively estimated based on the limitations of the equipment and methodologies employed and has been affirmed by repeated measurements made under similar operating conditions. The uncertainty in calculated values is found using error propagation as demonstrated in Reference [94] and in the following example.

B.1 General Uncertainty Analysis

The propagation of error through a data reduction equation is determined using general uncertainty analysis as presented by Coleman and Steele [94]. In this method the estimation of the uncertainty in the calculated parameter, r, which is a function of measured values X_1, X_2, … X_J, is given by:

Equation 74
$$\frac{U_r}{r} = \left[\left(\frac{1}{r} \frac{\partial r}{\partial X_1} U_{X_1} \right)^2 + \left(\frac{1}{r} \frac{\partial r}{\partial X_2} U_{X_2} \right)^2 + \ldots \right]^{1/2}$$

where

U_r = the uncertainty in the calculated value r
U_{Xi} = the uncertainty in the measured parameter X_i

When the data reduction equation is of the form:

Equation 75
$$r = kX_1^a X_2^b X_3^c \ldots$$

where k is a constant then Equation 74 reduces to [94]:

Equation 76
$$\frac{U_r}{r} = \left[a^2 \left(\frac{U_{X_1}}{X_1} \right)^2 + b^2 \left(\frac{U_{X_2}}{X_2} \right)^2 + \ldots \right]^{1/2}$$

And for summations of the form:

Equation 77
$$r = aX_1 + bX_2 + cX_3 + \ldots$$

Equation 74 becomes [94]:

Equation 78 $$\frac{U_r}{r} = \frac{1}{r}\left(U_{X_1}^2 + U_{X_2}^2 + U_{X_3}^2 + \ldots\right)^{1/2}$$

B.2 Uncertainty in F

The pyrolytic fixed carbon feed rate, F, is the product of the pyrolytic fixed carbon fraction, f, and the dry fuel feed rate. A series of batch experiments determined f's dependence on temperature for fine ground seed corn and the results are given in Figure 32. The scatter in the data suggests uncertainties in the measurement of f on the order of ±14%. The dry biomass feed rate is calculated knowing the wet fuel feed rate as determine by a hopper balance (Section 3.2.5) and the moisture content of the fuel (Section 4.1.1). The dry fuel feed rate for a given steady state experiment is determined with reasonable accuracy and is estimated to be ±2%. As the product of f and the dry biomass feed rate, the calculation of F has the form of Equation 75. Therefore the uncertainty in F is calculated by Equation 76:

$$\frac{U_F}{F} = \left[\left(\frac{U_{\dot{m}_{b,dry}}}{\dot{m}_{b,dry}}\right)^2 + \left(\frac{U_f}{f}\right)^2\right]^{1/2} = \left[(0.02)^2 + (0.14)^2\right]^{1/2} = 0.141 \quad (\pm 14\%)$$

As shown in the results, the error introduced with f dominates the estimated uncertainty in F.

B.3 Uncertainty in $W_C(t_{ss})$

The steady state carbon load in the reactor is determined by burning out the bed after steady state gasification has been established. The quantity of carbon in the reactor at a given instant is assessed by measuring the total carbon that leaves the reactor during burnout. As illustrated in Equation 59, the carbon leaving the reactor during burnout is determined in three parts: gaseous carbon, solid carbon recovered by the cyclone, and solid carbon missed by the cyclone as estimated by the isokinetic sample system. The carbon leaving the reactor as a gas is determined by integration over time of the carbonaceous gas concentration profiles as recorded by the micro-GC. During the initial stages of burnout the gas stream is rich in carbon as illustrated in Figure 26. The GC samples the gas stream approximately every four

minutes which makes estimation of the beginning of burnout relative to the GC sample times critical to the accuracy of the carbon integration, as indicated in Section 3.2.4. At the beginning of burnout as much as 24 g of carbon can leave the reactor during a four minute interval, which is equivalent to approximately 0.1 g carbon/s. Estimation of the time that burnout gases begin flowing past the GC can vary by as much as ±15 s, resulting in an uncertainty in the measured carbon mass of ±1.5 g. There is also a ±1.0 g uncertainty in determining the precise end of burnout which gives a total uncertainty in the measured gaseous carbon of ± 2.5 g. The smallest total quantity of carbon leaving the reactor in gaseous form during burnout was approximately 70 g (see data summary sheet 20060602 in Appendix A), which translates to a ±3.6% error in the gaseous carbon measurement. For the steady state experiments of this study in which burnout followed directly after gasification (for experiment 20060224 gasification was quenched with N_2 and burnout occurred the next day) gaseous carbon represents at least 95% of the measured $W_C(t_{ss})$, less than 5% of $W_C(t_{ss})$ was typically collected in the cyclone, leaving less than 1% of the reactor carbon bypassing the cyclone during burnout (see data summary sheets in Appendix A). Uncertainty in the collection and measurement of the carbon removed by the cyclone is estimated to be ±4% due to the potential of char sticking to the inside surface of the cyclone. The uncertainty in the isokinetic collection system is due to occasional light tarring in the thimble filter and deviations from true isokinetic conditions and is estimated to be ±20%. When reactor loadings are small the O_2 introduced during burnout is able to combust most of the carbon before it elutriates. Under these conditions the amount of carbon collected in the thimble filter during burnout becomes much less than 0.5% as the quantity of the total reactor carbon decreases. (For example the carbon bypassing the cyclone, labeled as C_{missed} in the data summary sheets, is equal to 0.3% of the total in the reactor, $W_C(t_{ss})$, in experiment 20060616 Appendix A). Therefore isokinetic sampling during burnout was not employed when small carbon loadings in the reactor were anticipated (see Appendix A: 20060718 for example). Because 95% or more of the reactor carbon was collected as a gas the uncertainty in $W_C(t_{ss})$ is conservatively estimated to be ±4%.

B.4 Uncertainty in $R_e(t_{ss})$

The steady state pyrolytic fixed carbon elutriation rate, $R_e(t_{ss})$, is calculated using Equation 66. Application of Equation 66 requires collection of elutriated char with the

cyclone as well as with the isokinetic probe over a specific time interval during steady state operation. There is very little uncertainty (0.8%) associated with the collection period as times are gauged to within ±5 s and collection periods are all greater than 10 minutes. Assessment of the amount of carbon collected in the cyclone has an uncertainty that is estimated to be less than approximately ±4%. Although the ashing technique used to determine the carbon content of the collected char (Section 3.2.4) is very accurate (±0.5%) the possibility of char sticking in the cyclone leads to the higher uncertainty estimate. Review of the experimental data summary sheets in Appendix A reveals that the cyclone carbon collection efficiency during steady state operation is generally greater than 80%. This leaves approximately 20% of the total $R_e(t_{ss})$ value to be determined using the isokinetic sample system. As described in the previous section the accuracy of isokinetic sampling is estimated to be ±20%. Because the time interval is measured very accurately the uncertainty analysis of Equation 66 centers on the summation of the two mass terms, putting it in the general form of Equation 77. Therefore the uncertainty in $R_e(t_{ss})$ is calculated using

Equation 78. Assuming typical values (40 g of carbon collected in the cyclone and 10 g bypassing the cyclone) the uncertainty in $R_e(t_{ss})$ is found:

$$\frac{U_{R_e(t_{ss})}}{R_e(t_{ss})} = \frac{\left[\left(U_{m_{C,PMC}}\right)^2 + \left(U_{m_{C,PMF}}\right)^2\right]^{1/2}}{R_e(t_{ss})} = \frac{\left[((40g)(0.04))^2 + ((10g)(0.2))^2\right]^{1/2}}{50g} = 0.051 \quad (\pm 5\%)$$

B.5 Sample Uncertainty Calculations

The uncertainties in F, $W_C(t_{ss})$, and $R_e(t_{ss})$ are used to calculate the uncertainties in k_t, k_e, k_r, η_{fc}, and η_{tc}. The uncertainty analysis calculations for each experiment are performed using a spreadsheet and the results are summarized in the experimental summary sheets of Appendix A. Experiment number 20060616 (see Appendix A for data summary sheet) is used as an example below to illustrate these calculations.

Analysis of experimental data using the carbon conversion analysis technique developed in this study begins with the calculation of k_t as given by Equation 34 which can be written in the form shown in Equation 75:

$$k_t = F W_C^{-1}$$

and therefore by Equation 76 yields:

Equation 79
$$\frac{U_{k_t}}{k_t} = \left[(1)^2 \left(\frac{U_F}{F} \right)^2 + (-1)^2 \left(\frac{U_{W_C}}{W_C} \right)^2 \right]^{1/2}$$

Using the uncertainty for F and W_C estimated earlier in this appendix, the uncertainty in k_t is calculated as:

$$\frac{U_{k_t}}{k_t} = \left[(0.141)^2 + (0.04)^2 \right]^{1/2} = 0.146 \quad (\pm 14.6\%)$$

The value of k_e is calculated using Equation 67 which can also be cast into the form given in Equation 75 and therefore the uncertainty in k_e is given by:

$$\frac{U_{k_e}}{k_e} = \left[\left(\frac{U_{R_e}}{R_e} \right)^2 + \left(\frac{U_{W_C}}{W_C} \right)^2 \right]^{1/2}$$

and for experiment 20060616 (Appendix A):

Equation 80
$$\frac{U_{k_e}}{k_e} = \left[(0.05)^2 + (0.04)^2 \right]^{1/2} = 0.06403 \quad (\pm 6.4\%)$$

The value of k_r for a given experiment is found by rearrangement of Equation 25 which has the form given in Equation 77, thus:

Equation 81
$$\frac{U_{k_r}}{k_r} = \frac{1}{k_r} \left[(U_{k_t})^2 + (U_{k_e})^2 \right]^{1/2} = \frac{1}{k_r} \left\{ \left[k_t \left(\frac{U_{k_t}}{k_t} \right) \right]^2 + \left[k_e \left(\frac{U_{k_e}}{k_e} \right) \right]^2 \right\}^{1/2}$$

which for 20060616 yields:

$$\frac{U_{k_r}}{k_r} = \frac{1}{228.7 \times 10^{-6}} \left\{ \left[(265.2 \times 10^{-6})(0.146) \right]^2 + \left[(36.4 \times 10^{-6})(0.064) \right]^2 \right\}^{1/2} = 0.169 \quad (\pm 16.9\%)$$

The pyrolytic fixed carbon conversion efficiency is calculated as stated in Equation 68:

$$\eta_{fc} = 1 - \frac{R_e(t_{ss})}{F} = \frac{1}{F}\left[F - R_e(t_{ss})\right]$$

Application of the general uncertainty expression (Equation 74) yields:

$$\frac{U_{\eta fc}}{\eta_{fc}} = \left[\left(\frac{1}{\eta_{fc}}\frac{\partial \eta_{fc}}{\partial R_e}U_{R_e}\right)^2 + \left(\frac{1}{\eta_{fc}}\frac{\partial \eta_{fc}}{\partial F}U_F\right)^2\right]^{1/2}$$

which equals:

$$= \left\{\left[\frac{F}{(F-R_e)}\left(-\frac{1}{F}\right)\left(\frac{U_{R_e}}{R_e}\right)R_e\right]^2 + \left[\frac{F}{(F-R_e)}\left(\frac{R_e}{F^2}\right)\left(\frac{U_F}{F}\right)F\right]^2\right\}^{1/2}$$

and simplifies to:

Equation 82
$$\frac{U_{\eta fc}}{\eta_{fc}} = \frac{R_e}{(F-R_e)}\left[\left(\frac{U_{R_e}}{R_e}\right)^2 + \left(\frac{U_F}{F}\right)^2\right]^{1/2}$$

For the data of experiment 20060616 this becomes:

Equation 83
$$\frac{U_{\eta fc}}{\eta_{fc}} = \frac{(0.00940)}{(0.0684 - 0.00940)}\left[(0.05)^2 + (0.14)^2\right]^{1/2} = 0.0237 \quad (\pm 2.4\%)$$

Similar to the pyrolytic fixed carbon conversion, the uncertainty in the total carbon conversion is found by application of Equation 74 to Equation 69 giving:

Equation 84
$$\frac{U_{\eta tc}}{\eta_{tc}} = \frac{R_e}{(\dot{m}_{C,b} - R_e)}\left[\left(\frac{U_{R_e}}{R_e}\right)^2 + \left(\frac{U_{\dot{m}C,b}}{\dot{m}_{C,b}}\right)^2\right]^{1/2}$$

The total carbon flow rate into the reactor, C_{fuel}, is a product of the dry fuel feed rate and the carbon fraction of the incoming biomass (Table 11). The uncertainty in the carbon flow rate is that of the dry fuel feed rate which is estimated at ±2% in Section 0. Therefore the uncertainty in the CC for experiment 20060616 is:

Equation 85
$$\frac{U_{\eta tc}}{\eta_{tc}} = \frac{0.0094}{(0.319 - 0.0094)}\left[(0.05)^2 + (0.02)^2\right]^{1/2} = 0.00164 \quad (\pm 0.16\%)$$

The uncertainty values for the other experiments are calculated with a spreadsheet using expressions similar to the above example and are listed in the summary sheets of Appendix A.